

TECHNISCHE UNIVERSITÄT MÜNCHEN

Lehrstuhl für Technische Chemie II

**Selective Oxidation of Propane to Acrylic Acid over  
MoVTe(Sb)NbO<sub>x</sub> Catalysts**

Frederik Nikolaus Naraschewski

Vollständiger Abdruck der von der Fakultät für Chemie  
der Technischen Universität München zur Erlangung des akademischen Grades eines

**Doktors der Naturwissenschaften (Dr. rer. nat.)**

genehmigten Dissertation.

Vorsitzender: Univ.-Prof. Dr. K.-O. Hinrichsen  
Prüfer der Dissertation: 1. Univ.-Prof. Dr. J. A. Lercher  
2. Univ.-Prof. Dr. K. Köhler

Die Dissertation wurde am 07.03.2011 bei der Technischen Universität München eingereicht und durch die Fakultät für Chemie am 11.05.2011 angenommen.



Das große Ziel der Bildung ist nicht Wissen,  
sondern Handeln.

*Herbert Spencer*

Die vorliegende Arbeit entstand in der Zeit von Januar 2006 bis März 2011 unter der Leitung von Prof. Dr. J. A. Lercher am Lehrstuhl für Technische Chemie II der Technischen Universität München.

# *Acknowledgements*

First, I would like to thank Johannes (Prof. J. A. Lercher) for giving me the chance to work in his team on this very exciting project. Thank you for your trust in me to design my own set-up, your support with my publications and your help, guidance and also criticism in all discussions. This time was really an exciting period, I learned very much and enjoyed it (almost) the whole time. Thank you also for giving me the chance to visit and present my results at several national and international conferences.

I would like to thank Andy (PD Dr. A. Jentys) for his advice during the operational work on my thesis, many very helpful discussions and for his support in correcting my paper drafts.

I want to thank the “EliteNetzwerk Bayern” for the possibility to participate in the NanoCat Program and the financial support during my time at TC-II. The meetings and discussions were always helpful and the after-meeting programs were even better. Thanks to Dr. Drees for doing the coordination of this program.

The experimental work would have been very difficult without the help of Xaver. Thank you for your support with handling set-up problems and to ensure the gas supply. Furthermore, I like to thank Martin and Andreas for their help with analytics and electronic stuff.

I would like to thank my diploma student Dani who did a great job in synthesizing the perfect pure Antimony catalysts.

The everyday work would have been much harder without my friends at TC-II. Thank you Jürgen, Matteo, Flo, Stephan and Carsten for being my friends and for many really funny moments. I hope that “Kicker will never be forbidden again”. Thanks to Michael for never ending “Ching-Chang-Chong” playing in various styles (regular, fast, long distance, etc...). I also like to thank Sarah, Dani, Sabine, Sonja, Oliver, Anna, Richard, Manu, Ana and Claudia for many funny evening events, Wies'n - including rollercoaster - and challenging tequila parties. Thank you Manuel for your support with set-up construction and lab-maintenance, countless discussions about the economy, especially the employment market, and optimized

strategies in Travian. Also thanks to Aon, Elvira, Andi, Dechao, Herui, Ben and Virginia for the good atmosphere in our working group.

Very special thanks to Martina, who supported me in various ways at and after work.

Finally I would like to thank my parents for their outsized support during my time at university. Without your help I wouldn't have had the chance to study chemistry in Munich and to write this doctoral thesis. Thank you for everything!

Frederik

March, 2011

# *Table of Contents*

1. General Introduction .....	1
1.1. Economic advantages of selective oxidation processes .....	2
1.1.1. Substitution of alkenes by alkanes for oxygenate production .....	2
1.1.2. Improved handling of methane for fuel applications.....	3
1.2. C-H activation .....	6
1.2.1. C-H activation of alkanes .....	6
1.2.2. Models of C-H bond activation over supported and unsupported oxide clusters...	8
1.2.3. Impact of anions on C-H activation .....	19
1.2.4. Indirect oxidation via electrophilic substitution – chlorination and bromination.....	21
1.2.5. Oxidative C-H activation via activation with non-reducible cations.....	24
1.2.6. Conclusion and outlook .....	28
1.3. Acrylic acid as intermediate in chemical industry.....	29
1.3.1. Usage of acrylic acid.....	29
1.3.2. Historical production of acrylic acid .....	29
1.3.3. Selective oxidation of propene to acrylic acid.....	31
1.3.4. Selective Oxidation of propane to acrylic acid.....	32
1.4. Selective oxidation of propane to acrylic acid.....	36
1.4.1. General mechanism.....	36
1.4.2. Vanadium pyrophosphate oxide catalysts (VPO).....	37
1.4.3. Heteropoly compounds (HPC).....	38
1.4.4. Multi-component metal oxides (MMO) .....	39
1.5. Selective oxidation of propane to acrylic acid over MoVTeNb oxides .....	41
1.5.1. Reaction pathways for selective propane oxidation .....	41
1.5.2. Phases of MoV(Te,Sb)Nb oxide catalysts .....	43
1.5.3. Synthesis routes for MoV(Te,Sb)NbO <sub>x</sub> type catalysts .....	45
1.6. Scope of this thesis .....	47

---

1.7. References .....	49
2. Experimental Section .....	55
2.1. Standard preparation of MoV(Te,Sb)Nb oxides .....	56
2.2. Catalytic testing .....	57
2.2.1. Experimental reactor set-up .....	57
2.2.2. Evaluation of kinetic data .....	60
2.3. Characterization of catalysts.....	63
3. Phase Formation and selective Oxidation of Propane over MoVTeNbO <sub>x</sub> Catalysts with varying Compositions.....	65
3.1. Introduction .....	66
3.2. Experimental.....	69
3.2.1. Catalyst preparation .....	69
3.2.2. Catalyst characterization.....	69
3.2.3. Catalytic activity .....	71
3.3. Results .....	72
3.3.1. Variation of tellurium content in the synthesis gel .....	72
3.3.2. Variation of the vanadium content in the synthesis gel .....	74
3.3.3. Variation of niobium-content in the synthesis gel .....	75
3.4. Discussion.....	76
3.4.1. Influence of chemical composition upon phase concentrations .....	76
3.4.2. Catalytic activity, phase composition and chemical composition .....	78
3.5. Conclusions .....	81
3.6. Acknowledgements .....	82
3.7. References .....	83
3.8. Supplementary material.....	84



---

4. On the Role of the Vanadium Distribution in MoVTeNbO <sub>x</sub> mixed Oxides for the selective catalytic Oxidation of Propane .....	89
4.1. Introduction .....	90
4.2. Experimental.....	93
4.2.1. Catalyst preparation .....	93
4.2.2. Catalyst characterization.....	94
4.2.3. Catalytic activity .....	95
4.3. Results .....	97
4.4. Discussion.....	102
4.5. Conclusions .....	109
4.6. Acknowledgments .....	110
4.7. References .....	111
5. Synthesis and Acid Properties of MoVSb and MoVTeNb Oxides for the selective Oxidation of Propane to Acrylic Acid.....	113
5.1. Introduction .....	114
5.2. Experimental.....	116
5.2.1. Catalyst preparation .....	116
5.2.2. Catalyst characterization.....	117
5.2.3. Catalytic activity .....	118
5.3. Results .....	119
5.4. Discussion.....	126
5.5. Conclusions .....	129
5.6. Acknowledgments .....	130
5.7. References .....	131

6. Summary .....	133
6.1 Summary.....	134
6.2 Zusammenfassung .....	136
Curriculum vitae.....	139
List of publications.....	141

## *List of Abbreviations*

As	Arsenic
at. %	atomic per cent
B	Boron
BET	Brunauer-Emmett-Teller adsorption isotherm
c	Concentration
C	Carbon
°C	Degree Celsius
CNG	Compressed natural gas
d	Day
DFT	Density functional theory
E	Lone electron pair
FID	Flame ionization detector
g	Gram
G	Gibbs energy
Gbbl	Giga Barrel
GC	Gas chromatography
Ge	Germanium
GWP	Global warming potential
h	Hour
H	Hydrogen
HPC	Heteropoly compound
K	Kelvin
kJ	Kilo joule
k <sub>x</sub>	Kinetic constants
l	Liter
LNG	Liquefied natural gas
mg	Milligram
min	Minute
ml	Milliliter
mln	Normal milliliter (defined at 0 °C and 1013.25 mbar)
mm	Millimeter

μm	Micrometer
MMO	Multi-component metal oxide
Mo	Molybdenum
Nb	Niobium
O	Oxygen
P	Phosphorus
PE	Polyethylene
PET	Polyethylene terephthalate
PO	Polypropylene oxide
PP	Polypropylene
PVC	Polyvinylchloride
s	Second
Sb	Antimony
Si	Silicon
T	Temperature
TCD	Thermal conductivity detector
Te	Tellurium
TPD	Temperature Programmed Desorption
THF	Tetrahydrofuran
UCC	Union Carbide Corporation
USD	US-Dollar
V	Vanadium
VPO	Vanadium pyrophosphate oxide
wt. %	weight per cent
XRD	X-ray diffraction

# *Chapter 1*

## *General Introduction*

### *Abstract*

This chapter introduces the general background of selective oxidation processes and in particular in C-H activation over solid oxide catalysts. The industrial usage of acrylic acid is described and historical, common and selective oxidation production processes with MoV(Te,Sb,Nb) oxide catalysts are discussed.

## **1.1. Economic advantages of selective oxidation processes**

### **1.1.1. Substitution of alkenes by alkanes for oxygenate production**

In modern chemical industry polymers, solvents, lacquers and fine chemicals are synthesized starting from small molecules like methanol, formaldehyde, or ethene. These building blocks usually contain between one and four carbon atoms and need a suitable functionality to enable reactions to target molecules. A list of the most important starting materials is shown in Table 1.1. Production of these building blocks starts from carbon sources like crude oil or natural gas that are further processed by steam reforming or steam cracking.<sup>[1]</sup>

The major drawbacks of these processes are the high energy consumption of reforming or cracking steps. Process temperatures between 950 and 1200 K require a high amount of fossil fuel for heat production and the complex product distributions obtained under these conditions demand additional energy intensive separation steps. As a result, these processes are of high costs and therefore reaction routes starting from alkenes are more expensive than the corresponding routes using alkanes that are directly available from natural gas sources. Hence direct oxidations of alkanes to desired oxygenates is one of the „Holy Grails“ of the petro chemistry and would have enormous economic advantage in comparison to the conventional process starting with alkenes.<sup>[2]</sup>

**Table 1.1:** Important intermediates of the chemical industry.<sup>[1]</sup>

Building block	Production	Usage
Methanol	Steam reforming of CH <sub>4</sub> , synthesis from syngas	Acetic acid (Monsanto-process), Methyl ester, Methyl ether, Methylamines, fuel
Formaldehyde	Oxidation of methanol	fine chemicals, polymers
Ethene	Steam cracking of naphtha	Polyethylene (PE), PVC, Acetaldehyde (Wacker-process)
Ethylene oxide	Oxidation of ethene	Ethylene glycol, PET
Propene	Steam cracking of naphtha	Polypropylene (PP), Acrolein, Acrylic acid, Acrylonitril, PO
Acrylic acid	Oxidation of propene	Polymers
Propylene oxide (PO)	Oxidation of propene	Propylene glycol
Maleic anhydride	<i>n</i> -Butane oxidation	Unsaturated Polyester, 1,4-Butanol, THF

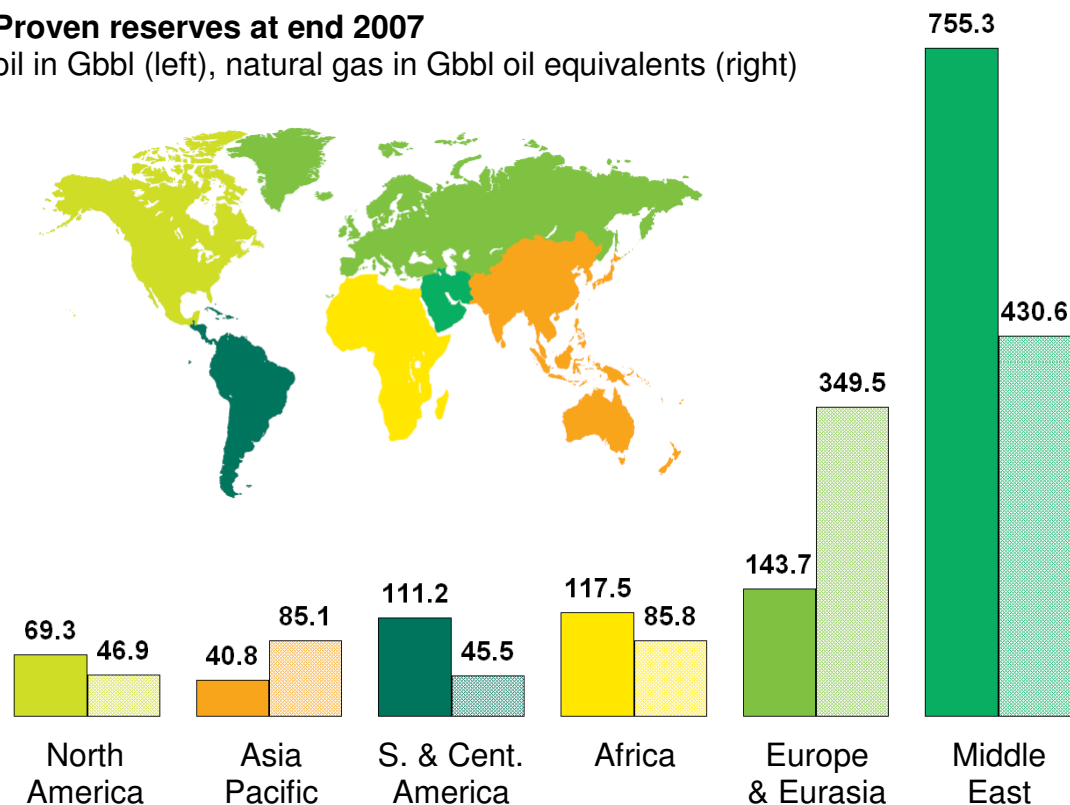
### 1.1.2. Improved handling of methane for fuel applications

One of the biggest challenges for the next decades is the supply with energy for heating and transportation purposes. Nowadays crude oil is used for both applications. Although newer technologies improve exploration and lead to an increase of proven reserves (1987: 910.2 Gbbl; 1997: 1069.3 Gbbl; 2007: 1237.9 Gbbl), the reserves are still limited and new energy sources are needed for the future.

A possible alternative is to cover the demand with natural gas. Natural gas is a mixture of light hydrocarbons consisting mainly of methane. The proven reserves of natural gas are 177.36 trillion cubic meters for 2007,<sup>[3]</sup> whereof 170 cubic meters are the energy equivalent to one barrel of oil (159 liters). Therefore, the reserves of natural gas are equal to 1037 Gbbl of crude oil and are comparable to the oil reserves of 1238 Gbbl. The worldwide distribution of crude oil and natural gas reserves in crude oil equivalents is shown in Figure 1.1.

**Proven reserves at end 2007**

oil in Gbbl (left), natural gas in Gbbl oil equivalents (right)

**Figure 1.1:** Proved reserves of crude oil and natural gas.<sup>[3]</sup>

Natural gas is still underutilized for the applications described above. The main problem is that methane is a gaseous compound and therefore pipeline systems are needed for transportation. Also, gas fields are spread over large areas, making pipeline constructions uneconomic. Transport of compressed methane is not a favorable method either. The energy density of CNG of 1344 kJ/l (at 50 bar and 298 K) is low.<sup>[4]</sup> Furthermore, handling of compressed gas is costly. Another possibility is the liquification of the gas. The energy density of LNG is with 16.128 kJ/l much higher than for CNG, but the low boiling point of methane (111 K) leads to costs of cooling of approximately one quarter of the transported energy. The construction of chiller/condenser units is only practiced for very large gas fields, whereas small fields of methane are not used and the gas is simply burnt off, because methane is also a strong greenhouse gas that has a global warming potential of 21. This means that 1 g methane have the same warming potential as 21 g carbon dioxide. The GWP is calculated respecting efficiency of radiation adsorption over the complete lifetime of the compound. So burning of unused methane makes sense, but usage of the gas would be preferable.<sup>[5]</sup>



An alternative to pipeline construction or liquidation is transformation to methanol. The energy density of methanol of 15.834 kJ/l is comparable to LNG, and with a boiling point of 338 K methanol is liquid at standard conditions and no special cooling dispositions have to be taken. The only inconveniences of methanol are the toxicity and the flammability, which exist also for gasoline and crude oil. Therefore methanol is a perfect form for an energy carrier based on methane.<sup>[4]</sup>

Unfortunately, up to now no direct processes to convert methane into methanol with high yields are available. Methanol is currently produced from methane by a detour over carbon monoxide. In this process methane is reformed with water to carbon monoxide and hydrogen (syngas). In a second reaction step carbon monoxide is hydrogenated to methanol. This conventional process needs large equipment and is therefore immobile. Also, this route over carbon mono oxide leads to high energy demand, so that this process is not economic for large methanol production, used as a gasoline substitute.<sup>[1]</sup>

The most economic solution for converting methane to more convenient methanol is selective methane oxidation. This process is therefore of high economic interest for the usage of natural gas resources.

## 1.2. C-H activation

### 1.2.1. C-H activation of alkanes

Activation of C-H bonds coupled to the functionalization of the carbon atom is one of the most important and challenging elementary reaction steps in organic synthesis. The challenge does not only lie in the homolytic or heterolytic cleavage of the bond itself, in most cases it has to occur under as mild as possible conditions to allow the subsequent reactions to proceed under very controlled conditions. As a result, highly active catalysts are needed and the elementary steps in these reactions are dominated by single electron processes and homolytic C-C bond cleavage, when oxygen is involved, while heterolytic C-H bond breaking is observed only in the minority of cases.

The C-H bond activation and conversion of alkanes in refining processes are somewhat more facile to realize, as the more robust target molecules allow for higher reaction temperatures. Two activation principles dominate, i.e., homolytic cleavage of C-H bonds on metals leading to elimination of hydrogen, a reaction, which is mostly equilibrated under reaction conditions and the acid catalyzed addition of a proton to an alkane leading to a carbonium ion, which decomposes spontaneously to smaller fragments and a carbenium ion as well as the abstraction of a hydride leading directly to the formation of a carbenium ion. Thus, the kinetically dominating C-H activation steps in refining are dominated by processes in which the C-H activation occurs via an ionic bond separation.<sup>[6, 7]</sup>

While it is hardly used for the synthesis of energy carriers, selective oxidation is one of the key reactions in chemical industry. Rough estimated, the worth of chemicals produced by catalytic oxidation processes lies between 20 and 40 billion USD in 1991.<sup>[8]</sup> Especially for the synthesis of intermediates and fine chemicals the pressure to change the feedstock in the chemical industry over the last decade arising from a combination of the limited availability of conventional starting molecules and the pressure to shift to less expensive ones forced the use of alkanes rather than alkenes in many of the selective oxidation routes to functionalized chemicals. This has led in turn to an intense interest in selective oxidation, but has only materialized in few heterogeneously catalyzed reactions among which butane to maleic anhydride<sup>[9-11]</sup> or the oxidation of propane to acrylic acid and the ammoxidation of propane to acrylonitrile<sup>[12-14]</sup> being the most prominent ones.

Understanding the complexity of the catalysts and the multi-step multi-electron processes during selective oxidation at an atomistic and molecular level poses a formidable challenge. More than with any other type of catalytic reaction, it requires that the catalysts are characterized chemically and structurally under realistic reaction conditions in order to be able to draw meaningful conclusions with respect to the surface chemistry (operando investigations). This is related to the fact that the sites active for catalysis are only present in small concentrations and that the catalysts change their oxidation state and surface structure in dependence of exogenic influences such as atmosphere, pressure or temperature. In addition, especially alkanes are rather inactive interacting mostly through dispersion forces with oxide surfaces.<sup>[15]</sup>

The reason for the inertness of alkanes is related to the situation that for carbon and hydrogen the number of valence electrons is equal to the number of valence orbitals and only  $\sigma$ -bonds are present. Reactive modification of these energetically low lying highest occupied molecular orbitals or energetically high lying lowest unoccupied molecular orbitals requires very reactive moieties such as radicals or high temperatures. Additionally, the tetrahedral coordination of the carbons in  $sp^3$ -hybridization efficiently shields the carbon atoms and complicates possible attacks together with the low polarity of the C-H bond. The primary products after activation contain functional groups or hetero atoms and, however, are by far more reactive and susceptible for further chemical reactions.

In consequence, the activation of the first C-H bond is the rate determining step and after addition of the more electronegative substituent to the desired extent the reaction needs to be kinetically stabilized to prevent total oxidation. Thus, achievable yields in these reactions are strictly depending on the ratio of the rate constants for activation to (unwanted) further oxidation ( $k_1:k_2$ ). Maximum yields in a selective oxidation reaction for a model of two consecutive first order reactions are shown as example in Figure 1.2. To reach yields above 70%  $k_1$  needs to be at least one magnitude larger than  $k_2$ , posing a major challenge for the design of catalysts and the process environment.

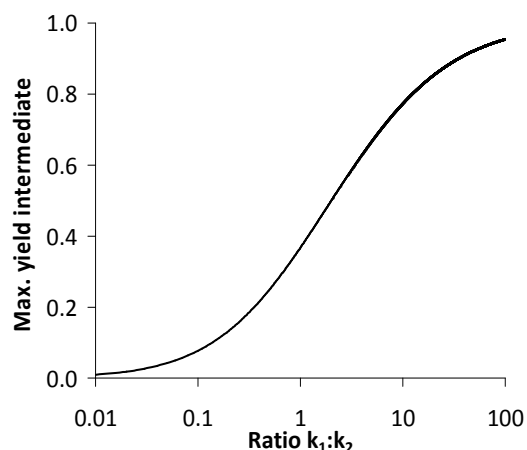


**Figure 1.2:** Maximum achievable yield versus ratio of activation to (unwanted) further oxidation.

For this chapter we will limit ourselves to the discussion of the oxidative activation of the C-H bond in alkanes. Model experiments, kinetic analysis of complex reactions and theoretical studies will be combined to provide an overview on the current state of insight into the processes as well as their potential and limitations. We will first discuss processes on oxide clusters, followed by the influence of anions and cations on the activation mechanism and finally cover bifunctional catalysts used to achieve oxidative functionalization.

### 1.2.2. Models of C-H bond activation over supported and unsupported oxide clusters

We will first discuss the chemistry of small alkanes such as ethane, propane and butane because of the easier C-H activation in these molecules and will treat methane activation as a special point. This is done so as with all these molecules the activated alkanes are able to eliminate hydrogen and may desorb, while this is not possible with methane. It should be emphasized that except for the higher bond strength of the C-H bond of primary carbon atoms, the other principal chemistry will be the same in the initial C-H bond breaking or polarizing step.

#### Vanadium based clusters

C-H activation on catalysts containing vanadium oxide species is certainly the most widely studied elementary reaction related to the wide variety of catalysts based on vanadia. The

catalytic properties of the vanadium moieties are affiliated with the redox properties of vanadium which changes its oxidation states between +III, +IV and +V.<sup>[10, 11, 16-21]</sup> The initial step of the C-H activation is so difficult to assess, because the precursor to the homolytic cleavage does not necessarily involve polarization of the C-H or the V-O bonds. Thus, only the final states of the first reaction would be accessible to the spectroscopic characterization.

Most of the experimental studies initially addressed were focused on supported monolayers of vanadia clusters on oxide surfaces. Pioneering systematic studies came from the groups of Wachs<sup>[22]</sup> and Iglesia and Bell.<sup>[23]</sup> The surface geometry of these clusters was determined with a multitude of indirect spectroscopic characterizations. Overall, it was suggested that monomers, dimers and oligomers are present on the surface (see Figure 1.3) and that the

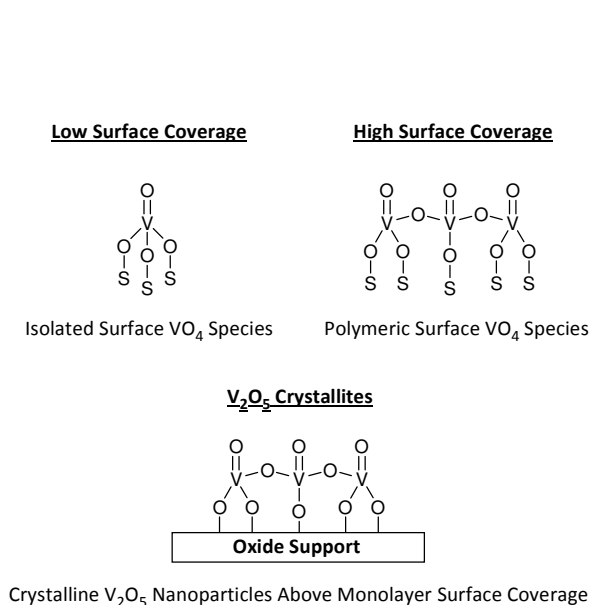


**Figure 1.3:** Supported vanadium oxide catalysts.

catalytic reactivity and the oxidation state depends critically on the size of the surface cluster.<sup>[24]</sup> With increasing cluster size of the surface bound vanadia the reactivity towards alkanes increased. The same trend was observed with decreasing electronegativity of the support (according to Sanderson) indicating that a lower charge at the terminal oxygen facilitates C-H bond breaking in the activation of propane.<sup>[25]</sup> It is interesting to note that the selective oxidation of methanol exhibits the reverse influence of the support oxide, i.e., the catalysts

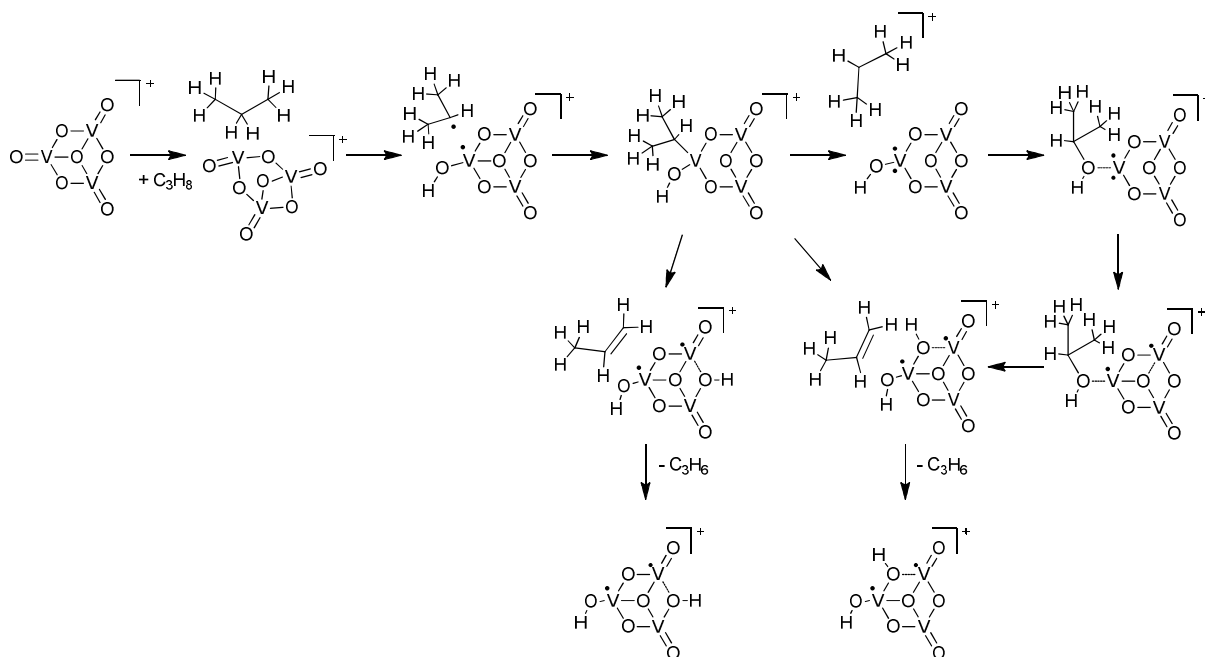
were more active as the charge at the lattice oxygen increased.<sup>[26]</sup>

One of the central issues in these experimental studies concerned questions with respect to the nature of the active oxygen species or more specific the functional group involved in breaking the first C-H bond. In principle three V-O bonds can be distinguished, the terminal V=O bond, the bridging V-O-V bond and the bridging V-O-support bond. For activation of ethane and propane<sup>[27-29]</sup> the V-O-V bond was concluded to be catalytically irrelevant as the turnover frequency did not change with the coverage of the support by vanadia species, which should increase the relative concentration of this species. Also the concentration of the V=O groups

did not influence the observed rate of alkane activation leaving the V-O-support bond to be the only remaining oxygen, which was then also concluded to be catalytically active.

However, as this rationale is based on an indirect elimination following more plausibility than rigorous proof, let us turn to model studies using well defined clusters in the gas phase combined with modeling of the structures and barriers between the intermediates. These clusters may be charged in order to increase their reactivity without changing the relative reactivity of the oxygen atoms in the cluster. The first well defined case of such an approach was a study of the oxidation of propane on a  $[\text{V}_3\text{O}_7]^+$  cluster by the groups of Schwarz and Sauer.<sup>[30, 31]</sup> The cluster was chosen, as it is the smallest polynuclear entity that formally contains only V in +5 oxidation state. The oxidative dehydrogenation of propane involves the reduction of the metal center, brought about by the addition of two hydrogen atoms.

Detailed DFT calculations show that after assuming a quite stable precursor state ( $\Delta G_{298} = -63 \text{ kJ}\cdot\text{mol}^{-1}$ ) the initial reaction of propane with the cluster is the abstraction of a hydrogen atom with an energetic barrier of  $102 \pm 5 \text{ kJ}\cdot\text{mol}^{-1}$ .<sup>[32, 33]</sup> Formally, this sequence is initiated as the double bond between vanadium and oxygen cleaves homolytically and forms radicals in the transition state. In the first step, hydrogen is abstracted from  $\text{C}_3\text{H}_8$  by one of the O=V groups and yields the  $\text{C}_3\text{H}_7\cdot \text{V}_3\text{O}_7\text{H}^+\cdot$  diradical, which recombines and forms a carbon vanadium bond through a rebound mechanism.<sup>[9, 33-38]</sup> From this stable adduct a second hydrogen abstraction by a bridging oxygen is possible and leads directly to propene and  $\text{V}_3\text{O}_7\text{H}_2^+$ . Also a pathway forming a propyl cation that rebinds to a hydroxyl group under formation of *i*-propanol can be found (see also Scheme 1.1).



**Scheme 1.1:** Reaction pathways of propane with  $V_3O_7^+$ .

These experiments demonstrate unequivocally and in agreement with the conclusions by Wachs et al. that V-O-V oxygen does not participate in the initial C-H bond activation. The vanadyl group, however, is indicated in these studies as the decisive reactive oxygen containing group. However, this cluster does not contain bridging oxygen to another oxide, which has been concluded to be the active site. In order to mimic such bridging oxygen between V and a support cation, vanadium substituted silsequioxane cluster has been used (Figure 1.4).<sup>[35]</sup>

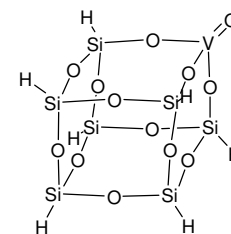
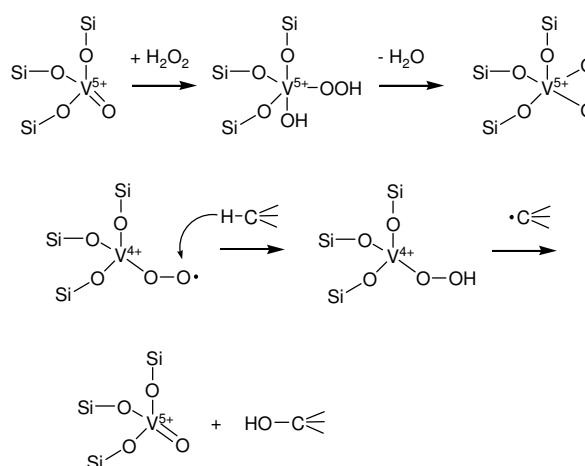


**Figure 1.4:** Vanadium substituted silsequioxane.

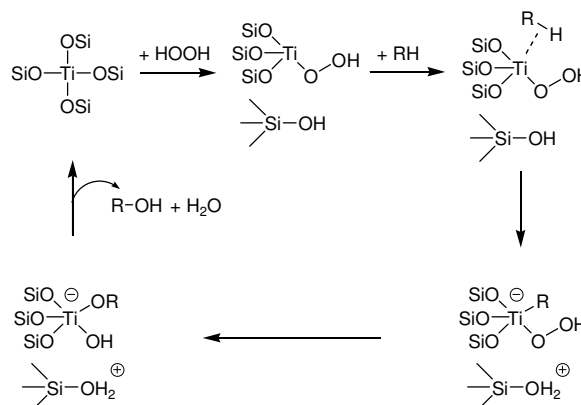
The calculations show that also in this case the first hydrogen abstraction at the vanadyl group is the rate determining step. This practically rules out the involvement of the oxygen link to the surface as the oxygen initiating the overall reaction sequence. In passing it is interesting to note that in a recent contribution also the generation of a peroxovanadate has been proposed that could explain the much higher reactivity of oxygen compared to  $N_2O$  (which cannot form a peroxovanadate) in pulse experiments.<sup>[39]</sup>

This is in line with observation that vanadium substituted zeolites are able to activate the C-H bond at the primary carbon atom in light alkanes, while this is not possible with titanium substituted materials.<sup>[40, 41]</sup> In this case the peroxo- $V^{5+}$  site has been identified by EPR spectroscopy. Alcohols are formed in the presence of both substituents together with  $H_2O_2$  (Scheme 1.2).<sup>[42]</sup>



**Scheme 1.2:** Formation of peroxo- $V^{5+}$  sites.

It is presently unclear, why titanium substituted zeolites are only able to activate and oxidize (hydroxylate) alkanes at the secondary carbon atom, while vanadium substituted materials oxidize the alkane at the primary carbon atom. The catalytic cycle proposed is described in Scheme 1.3.



**Scheme 1.3:** Possible mechanism for alkane activation of TS-1.

One possibility to explain the high selectivity for the activation of the C-H bond at the secondary carbon atom with Ti substituted zeolites could be the fact that the alkane is dehydrogenated in a first step in analogy to the dehydrogenation observed with  $La^{3+}$  exchanged zeolites<sup>[43]</sup> and that subsequently the olefin is hydroxylated with the  $TiO_2$  site as discussed extensively in the literature. In this case the primary dehydrogenation will occur at a C-H bond of a secondary (or tertiary) carbon atom and will determine so the selectivity of hydroxylation. It is remarkable that in recently reported titanium rich MFI type zeolites, the activity towards *n*-hexane was even higher than towards 1-hexene again only forming products that are oxidized at the secondary carbon atom.<sup>[44]</sup> Indeed, a detailed study with Ti-MFI shows that activation at the primary carbon atom is about 100 times lower than that at the secondary carbon position.<sup>[45]</sup> The mechanism speculated by Davis et al. would offer a reasonable explanation that has not been contemplated, however, in the paper. It could be that



the synergetic interaction between the (basic) oxygen at the SiOH group and the accessible Ti leads to a heterolytic cleavage of the C-H bond (which is significantly easier at the secondary carbon atom) and the formation of a Ti-C bond as postulated. The subsequent  $\beta$ -hydride elimination leads to the formation of an olefin, which in turn is rapidly hydroxylated on the titanium sites.<sup>[46]</sup>

### Molybdenum and Tungsten oxide clusters

While vanadium based transition metal oxide clusters are the most studied, other transition metal oxides and in particular those based on molybdenum and tungsten also show remarkable catalytic activity. It is interesting to compare in this case the differences in the particular surface chemistry induced by the metal cation and by the surface structure.

Similar to vanadium, molybdenum based oxides activate the C-H bond also via a homolytic cleavage at a molybdenyl group. This is concluded from experimental and computational studies linking the presence of the Mo=O group to the activity of the catalytic material.<sup>[47, 48]</sup> As much as these results seem to emphasize the similarities to the supported vanadia catalysts, important differences between the two systems exist. The rate normalized to the accessible Mo at the surface increases drastically as the surface concentration of Mo increases (note the contrast to the equal catalytic activity in a similar relation for vanadia clusters). However, what is even more striking is the fact that the ratio of the rate constants between the initial oxidative elimination of hydrogen from propane increases, while that of total oxidation either from propane or from propene decreases. This suggests that the sites for the unselective reactions have to be related to sites at the interface between the support ( $\text{Al}_2\text{O}_3$  in the study cited<sup>[47]</sup>) and the molybdenum oxide species on the surface. The molybdenum oxide species show overall a higher reducibility in  $\text{H}_2$  with increasing surface concentration. The rate of the supported molybdenum oxide species reducibility (at 673 K) is directly proportional to the rate of oxidative dehydrogenation and hence to the rate of C-H activation, which constitutes the rate determining step in oxidative dehydrogenation. DFT calculations of the C-H activation in propane on trimeric Mo oxide clusters indicate that the lowest barrier exists for the hydrogen abstraction from the secondary carbon atom of propane by one of the terminal oxygen atoms in a one electron process (Figure 1.5).

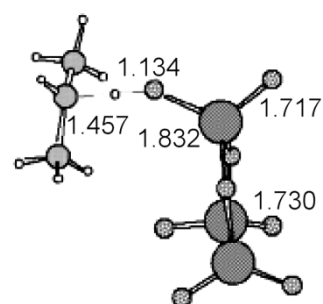


**Figure 1.5:** Hydrogen abstraction on Mo oxide cluster.

Reaction steps involving two electrons and acid-base type interactions have energetic barriers, which are more than  $50 \text{ kJ}\cdot\text{mol}^{-1}$  higher emphasizing the unlikelihood of such reaction pathways.<sup>[48]</sup> Also pathways involving the simultaneous cleavage of two C-H bonds are highly unlikely. Comparing the C-H activation of propane with that in methane one notes that again the one electron process has the lowest energetic barrier, but that this barrier (according to experiments and DFT calculations) is at least  $60 \text{ kJ}\cdot\text{mol}^{-1}$  higher than in case of propane emphasizing the difficulty to break the C-H bond of methane on these catalysts.<sup>[49]</sup>

These experiments suggest that the cleavage of the C-H bond is a one electron process also for Mo oxides and is the more facile the weaker the C-H bond is. Given the weaker C-H bond in propene (compared to propane) one might ask if propene formed will not be immediately consumed in a sequential activation/oxidation leading to very low selectivities. Let us analyze the situation in this respect by comparing the simplest oxidative activation, the oxidative dehydrogenation of propane with the further reaction of propene, the dominating primary product. For the former reaction, the relative activities for between  $\text{ZrO}_2$  supported vanadium, molybdenum and tungsten oxides decrease in the order  $\text{VO}_x/\text{ZrO}_2 < \text{MoO}_x/\text{ZrO}_2 < \text{WO}_x/\text{ZrO}_2$ , while the corresponding apparent energies of activation increase in that order.<sup>[50]</sup> This indicates that the activities are inversely proportional to the C-H bond cleavage energies. The activation energies of propane oxidative dehydrogenation are higher than for further total oxidation of propene. The difference in the activation energies ( $48\text{-}61 \text{ kJ}\cdot\text{mol}^{-1}$ ) is larger than between bond dissociation enthalpies for the weakest C-H bond in propane and propene ( $40 \text{ kJ}\cdot\text{mol}^{-1}$ ). It increases in the sequence  $\text{VO}_x/\text{ZrO}_2 < \text{MoO}_x/\text{ZrO}_2 < \text{WO}_x/\text{ZrO}_2$  suggesting that relative rates also depend on the differences in the heat of sorption between propane and propene, which will increase as the Lewis acidity ( $\text{V}^{5+} < \text{Mo}^{6+} < \text{W}^{6+}$ ) increases.

### Complex mixed oxides

So far the impact of different oxides and supports on the activity for C-H bond activation has been discussed. In this context it has been noted that the primary activity for the one electron cleavage depends on the ability of the oxide to be reduced and the strength of the C-H bond involved. Any component of a complex oxide that would enhance the strength of the metal oxygen bond is expected to decrease the activity of the reducible species.

This has been shown for zirconia supported molybdenum oxide clusters upon addition of alkali metals.<sup>[51]</sup> The presence of alkali cations (Cs, K, Li) did not affect the structure of MoO<sub>x</sub> domains, but influenced their electronic and catalytic properties. Propane C-H activation decreased monotonically with increasing concentration of the alkali cation and for a given concentration with increasing base strength of the corresponding alkali oxide. Also in this case the subsequent oxidation of propene was slightly suppressed by weakening the acid strength of Mo<sup>6+</sup> though the formation of a mixed oxide.<sup>[52]</sup>

The positive influence of the presence of a bridging oxygen between the active vanadium cluster and the support on the selectivity of the oxidative dehydrogenation and the observation that two vanadium atoms form an active site leads to the question whether it is possible to positively influence the catalytic properties by combining two cations in the active phase.

The simplest conceptual scenario is given by the deposition of a vanadium oxide cluster on a polymolybdate monolayer surface supported on alumina.<sup>[53]</sup> Without changing the mechanism of the C-H bond activation, the combination enhances the rate of C-H bond activation, by increasing the reducibility of the vanadium oxide clusters. The initial rate of oxidative dehydrogenation (equivalent to the rate of C-H activation) increased proportional nearly up to a monolayer of vanadium indicating a low sensitivity to the particular structure of the vanadia, but was significantly higher if vanadia was supported on alumina. Most remarkably the ratio of the rate constant for the further oxidation and of the primary formation of propene decreased with increasing concentration of vanadia and was for the best catalyst drastically lower than the corresponding ratio in the case of VO<sub>x</sub>/Al<sub>2</sub>O<sub>3</sub>. In line with the arguments used above the presence of molybdenum are speculated to have reduced the interactions of propene with the accessible cations. The retention of propene is concluded to be critical for the further oxidation.

This effect is not confined to the system vanadia/molybdena though. A positive effect was also observed for chromia decorated surfaces although the surface chemistry is more complex.<sup>[54]</sup> In a similar strategy it was reported recently that the addition of oxides of varying acid base properties could tune the selectivity and activity of a NiO catalyst for oxidative dehydrogenation. The reasons for his positive effects were explained by a modification of the reducibility of NiO, but neither the site of activity nor the detailed kinetics are currently understood in the same detail as with the vanadia and molybdena systems.<sup>[55]</sup>

Very complex oxides based on  $\text{MoVTeNbO}_x$  are currently used for more demanding reactions such as the conversion of propane to acrylic acid.<sup>[18, 56, 57]</sup> The active phase in these materials is a complex structure consisting of octahedra with Mo and V oxides building up five, six and seven membered channels in which Nb and Te oxides are coordinated. A (0 0 1) surface of such a material is displayed in Figure 1.6.

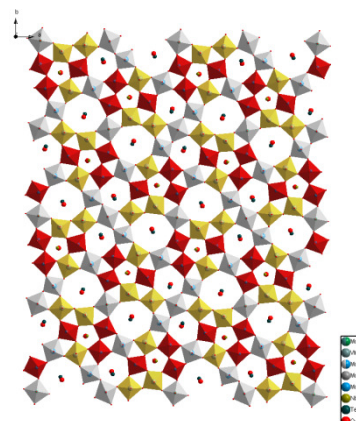


**Figure 1.6:** Structural model of  $\text{MoVTeNbO}_x$  M1 phase.

In these oxides the substitution of V for Mo leads to a situation similar to the one described by the layered material described above, i.e., single or paired vanadia units are embedded in a molybdenum matrix. These vanadia octahedra have been identified as the active sites<sup>[18, 58-60]</sup> and the catalytic activity is proportional to the concentration of vanadium. However, the dependence is not straightforward and substantial differences in catalytic activity of the vanadia units seem to exist depending on the location of the substitution. Using the oxidative dehydrogenation of ethane one notes a unique and unparalleled selectivity to ethene with very low rate constants of the oxidation of ethane.<sup>[61]</sup> Also in this case the specific catalytic chemistry does not seem to be confined to this particular structure, although a related structure the so called M2 phase is not active for C-H bond activation (see Figure 1.7).

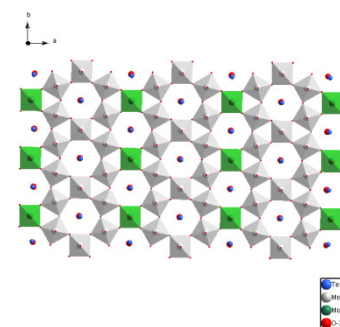


**Figure 1.7:** Structural model of  $\text{MoVTeNbO}_x$  M2 phase.

It is interesting to note that in this structure vanadium is only present in isolated sites, which would be in line with the experimental and theoretical observation that pairs of vanadium oxide units are needed for the initial C-H activation. Indeed several of such materials have been reported to very active and selective for the oxidative dehydrogenation of propane.<sup>[62]</sup> Alternatively, the distortion of the V-O octahedron has been claimed to be responsible for its high activity.<sup>[59, 63]</sup> It should be noted that the intense discussion on the site for the multi electron oxidation process of propane to acrylic acid is not decisive for the current contribution, as almost all authors agree that solely the vanadia unit is responsible for the oxidative dehydrogenation of propane, which constitutes the first and in many cases also the rate determining step.<sup>[64]</sup>

Transition metal species in zeolites

The catalytic sites activating the C-H bond in the oxides discussed so far were primarily terminal oxygen atoms (such as vanadyl groups), which are ideally suited for one electron oxidation steps. Enzymes,<sup>[65, 66]</sup> but also designed catalytic sites such as reducible cation pairs at ion exchange sites in zeolites are able to activate alkanes via a bridging oxygen groups.<sup>[67]</sup> Only few cations, such as Fe, Cu and Co show catalytic activity in such environment for oxidation reactions. The reason for the existence of only few cations is related to the steric limitations by the size of the hydrated metal cations (hindering larger cations to be exchanged) during the ion exchange procedure and the probability that at least two aluminum cations must be substituted in the zeolites structure at such close distances that the di- or trivalent cation can bridge that distance forming e.g., a Cu-O-Cu moiety.<sup>[68]</sup>

There is a quite intense debate on the nature of these complexes involving  $\text{Fe}^{+3}$  and  $\text{Cu}^{+2}$  cations which ended quite indecisive as seen in the recent example for Cu exchanged ZSM-5.<sup>[69]</sup> The site depicted in Figure 1.8 has been deduced from evidence using primarily spectroscopy. Diffraction results that would allow for a complete structural analysis are not available and will be very difficult to obtain as all as faults in the zeolite structure impede a precise structure determination. This situation brings attention to the point that the structural information on Cu monooxygenase begins only now to reach a level that would permit to start to address the mechanism of the oxygen activation. The current understanding is that a single Cu cation site is located about 2 nm away from a Cu ion pair. The oxidation state of the three cations is not unequivocally settled yet.<sup>[65]</sup>

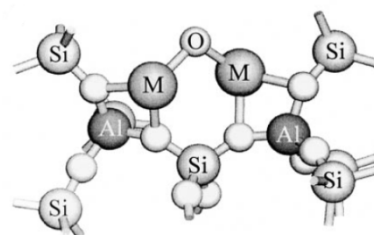


**Figure 1.8:** Bridging oxygen between two divalent metal cations at exchange sites in zeolites.

Recent DFT calculations on the mechanism of the oxidative C-H activation in Cu-ZSM5 suggest a possible way in which methane and higher alkanes can be activated.<sup>[69]</sup> Via this route even methane can be converted at around 200 °C forming methoxy and hydroxy groups with the simultaneous reduction from  $\text{Cu}^{+2}$  to  $\text{Cu}^{+}$ . The constraints in the zeolite and the strong bonding hinder, however, desorption of the formed methoxy groups or methanol. Similar to the surface chemistry described above the hydrogen of, e.g., methane is being cleaved from methane in a one electron oxidation step. The resulting diradical will bind at the newly formed bridging hydroxy group forming methanol. With respect to the inability to

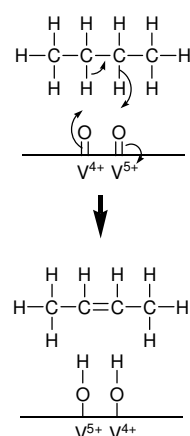
desorb this species one needs to emphasize that supported CuO oxide is an excellent steam reforming catalyst that most likely decomposes the desorbing methanol.<sup>[70]</sup> Interestingly, Fe exchanged zeolites need N<sub>2</sub>O to generate the active oxygen, while Cu and Co exchanged can be activated in oxygen.

### 1.2.3. Impact of anions on C-H activation

#### *Vanadium pyrophosphate as catalyst for butane activation*

Vanadium phosphates are currently the only large scale catalyst employed for the selective oxidative process of alkanes, in specific for the oxidation of butane to maleic anhydride.<sup>[9]</sup> With vanadium as the main redox active element in the catalyst, it is critical to ask whether or not the surface chemistry proceeds analogous to the activation discussed so far for supported vanadia and complex mixed oxide catalysts.

Two interesting facts have been established early on. The catalysts develop readily the (1 0 0) surface in the process of drying and conditioning for the reaction.<sup>[71]</sup> This specific surface has been claimed to be responsible for catalytic action. While such a complex reaction involves a wide variety of sites, promoters and variants of catalysts (see e.g.,<sup>[72, 73]</sup>), the principal chemistry of the C-H activation from *n*-butane seems to be closely related to the vanadyl groups as discussed above.<sup>[74, 75]</sup> Scheme 1.4 shows the proposed mechanism for the formation of 2-butene in this first step. One notes the schematic nature of the proposed transition state along this route (a second pathway involving alkoxy groups has also been proposed in ref.<sup>[75]</sup> above), but formally two vanadyl groups are involved, as discussed also later as the probably dominating active site. It is striking that a kinetic analysis does not indicate butene as an intermediate with marked concentration in the gas phase. This indicates that at least the interaction between butene and the surface must be very strong.



**Scheme 1.4:**  
Proposed mechanism  
for the formation of 2-  
butene.

If one explores the (1 0 0) surface of vanadium pyrophosphate using DFT calculations, the termination by P=O and V=O groups, but also the existence of P-O-V bonds is notable.<sup>[76]</sup> In line with the arguments used above to explain the effect of metal cations on the catalytic activity and selectivity of V=O groups we would like to speculate that the presence of the highly electronegative phosphorus enhances the reducibility of vanadium. Moreover the top view in Figure 1.9 shows that neighboring V=O groups exist, well separated by P=O groups indicating that the surface site that has been identified as required for the alkane activation is also present on this material. As a word of caution though it should be mentioned, however,

that the surface structure may quite disordered and may form over a much longer period during operation as it had been thought originally.<sup>[77]</sup> This is indeed reflected in the marked influence the relative concentrations of vanadium and phosphorus have on the catalytic activity.<sup>[78]</sup> A dynamic equilibrium between several phases exists on the surface of the vanadium pyrophosphates making it very difficult to identify more than the principal features of the atoms involved. There has been, however, a recent elegant in situ study by  $^{31}\text{P}$  and  $^{51}\text{V}$  solid state NMR spectroscopy to probe the phosphorus and vanadium species involved in the oxidation reactions.  $\delta\text{-VOPO}_4$  has been identified to be the phase most important for the overall conversion of *n*-butane to maleic anhydride. Cycling through oxidation and reduction it could be shown that  $\text{P}/\text{V}^{5+}$  were pairs which were active for the overall reaction. Note that this, unfortunately, does not provide the insight with respect to the initial C-H bond activation.

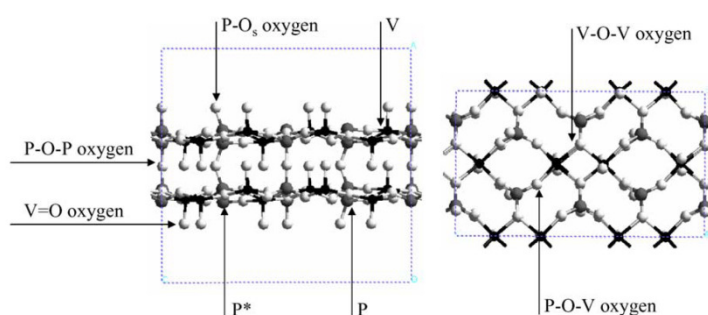


**Figure 1.9:** Model of  $(\text{VO})_2\text{P}_2\text{O}_7$  (1 0 0) surface.

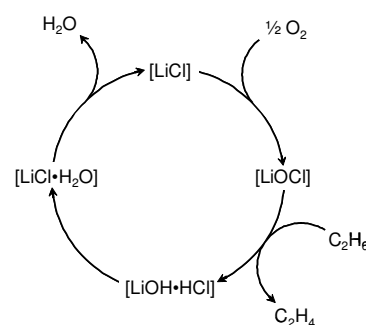
### Supported LiCl as catalyst for oxidative dehydrogenation of ethane to ethene

So far anions and cations were used and discussed as promoting species changing the properties of the redox element to activate the C-H bond. In principle, however the anion itself can undergo the redox step and is able to catalyze the oxidative dehydrogenation of ethene (e.g. <sup>[79-81]</sup>).

The most remarkable catalysts in this respect are MgO supported alkali chlorides, which form at reaction temperatures a melt covering the support surface.  $\text{Dy}_2\text{O}_3$  has been found to be an excellent promoter that is not interfering with the chemistry, but helps to maintain a reasonably large specific surface area. The active sites are speculated to be hypochlorite anions, which are formed only transiently in the presence of oxygen at the surface of the liquid layer or dissolved in the catalysts. The catalyst is regenerated by eliminating water (see Scheme 1.5).



Mechanistic details are not evaluated, because of the transient nature of the catalytically active sites. The presence of oxygen leads to the formation of positively charged chlorine. It is speculated that the reaction proceeds via the electrophilic substitution of hydrogen for chlorine followed by an immediate elimination of HCl. Concerted elimination of HCl would be very rapid under these conditions, as the reaction temperature is typically above 823 K. Elimination of water would complete the catalytic reaction cycle and reconstitute LiCl as catalyst. The catalytic reactivity is not limited to LiCl. Several pure and mixed alkali and alkali earth chlorides showed promising catalytic properties. It should be noted that the selectivity of the catalysts increased with decreasing melting point indicating that the mobility at the surface leads to a dynamically restructuring material that avoids in this way the formation of undercoordinated metal cations. Such accessible metal cations had been identified as the key sites to adsorb olefins and to provide the required sorption locations for total oxidation.



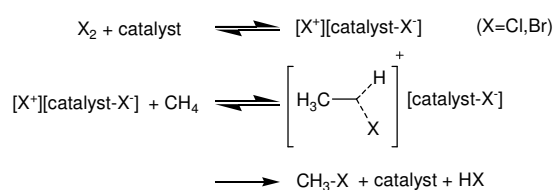
**Scheme 1.5:** Catalytic cycle of oxidative dehydrogenation over LiCl catalysts.

#### 1.2.4. Indirect oxidation via electrophilic substitution – chlorination and bromination

In the surface chemistry described so far, the C-H bond was activated by a homolytic cleavage leading to a diradical species that can rebind. In case in which the cation may polarize the C-H bond so far that the C-H bond is cleaved the hydrocarbon moiety will bind to the metal cation and eventually form a carbon-metal bond (vide infra). The oxidative elimination of the alkene via  $\beta$ -hydride elimination will then lead to the olefin. Here we will describe an alternative approach using polarization and electrophilic substitution. Once substituted the highly electronegative substituent will rearrange the electron distribution at the carbon atom and lead so to oxidation. This is usually achieved via halogenation (chlorination or bromination) of alkanes.

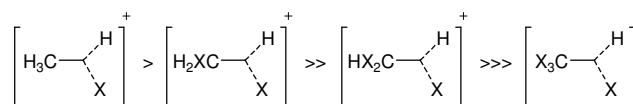
FeO<sub>x</sub>Cl<sub>y</sub>/Al<sub>2</sub>O<sub>3</sub>, TaOF<sub>3</sub>, NbOF<sub>3</sub>/Al<sub>2</sub>O<sub>3</sub>, ZrOF<sub>2</sub>/Al<sub>2</sub>O<sub>3</sub>, SbOF<sub>3</sub>/Al<sub>2</sub>O<sub>3</sub>, SbF<sub>5</sub>/graphite and Nafion-H/TaF<sub>5</sub> are known as catalysts for selective chlorination and bromination of methane.<sup>[82]</sup> The

activation of methane is achieved under relatively mild conditions (543 K). The mechanism is shown in Scheme 1.6. In the first step a Lewis acid site of the catalyst polarizes chlorine leading to  $\text{Cl}^-$  and  $\text{Cl}^+$  bound to the catalyst. In the next step  $\text{Cl}^+$  is transferred into methane by an electrophilic insertion. In the transition state carbon is five-coordinated by four methane-hydrogen and one  $\text{Cl}^+$  in a cationic complex and finally  $\text{Cl}^+$  replaces hydrogen to form methyl chloride together with hydrogen chloride from the negative polarized chloride. This is also the rate determining step and the energy barrier and also the rate of the reaction is dependent on the stability of the five-coordinated transition state.



**Scheme 1.6:** Mechanism of selective methane chlorination over solid acids and  $\text{Cl}_2$ .

In the direct radical chlorination the chlorinated products react as readily as methane leading to unwanted multiple chlorination steps. In the



**Scheme 1.7:** Stability of transition states of selective methane chlorination.

electrophilic insertion the already chlorinated products pass also over a multi-chlorinated transition state. In case of reaction with methyl chloride two chlorine will be incorporated in the five-coordinated transition state and due to the electron drawing effect of chlorine, the stability of this cationic complex is lower than the corresponding transition state of the mono-chlorinated reactant. In consequence, the energy barrier is higher for the second chlorine insertion compared to the first insertion and the rate will be slower. The decreasing stability of multiply chlorinated products (compare Scheme 1.7) leads to an order of reaction rates, in which rate of formation decreases in parallel to the degree of substitution. If only one equivalent of the chlorine is used, the mono chlorination is in this reaction strongly preferred. Conversions of 34% and 96% selectivity to mono chlorinated product were realized in that way. Thus, the role of the catalyst in the electrophilic substitution is to polarize chlorine and stabilize the formed electrophilic chlorine. Indirectly the lower reactivity towards electrophilic substitution leads to the decreased rates for higher substituted products.

Catalytic activity for C-H activation reactions has also been reported for Lanthanum oxides ( $\text{La}_2\text{O}_3$ ) and chlorides ( $\text{LaOCl}$ ,  $\text{LaCl}_3$ ), if  $\text{HCl}$  is used for the chlorination under oxidizing conditions at 400 – 500 °C. This would be a dramatic commercial benefit, as one mol of  $\text{HCl}$  is generated for each  $\text{Cl}$  inserted, which has to be reoxidized to  $\text{Cl}_2$  in a separate process.<sup>[83-85]</sup> It is interesting to note that the catalytic materials,  $\text{La}_2\text{O}_3$  and  $\text{LaOCl}$ , have been reported as active catalysts for oxidative methane coupling,<sup>[86-89]</sup> and for ethane oxidative dehydrogenation.<sup>[90, 91]</sup>  $\text{LaCl}_3$  is known as a promoter in catalysts for the oxydehydrochlorination and ethane conversion to vinyl chloride<sup>[92]</sup> and is also used in selective chlorination of methane.

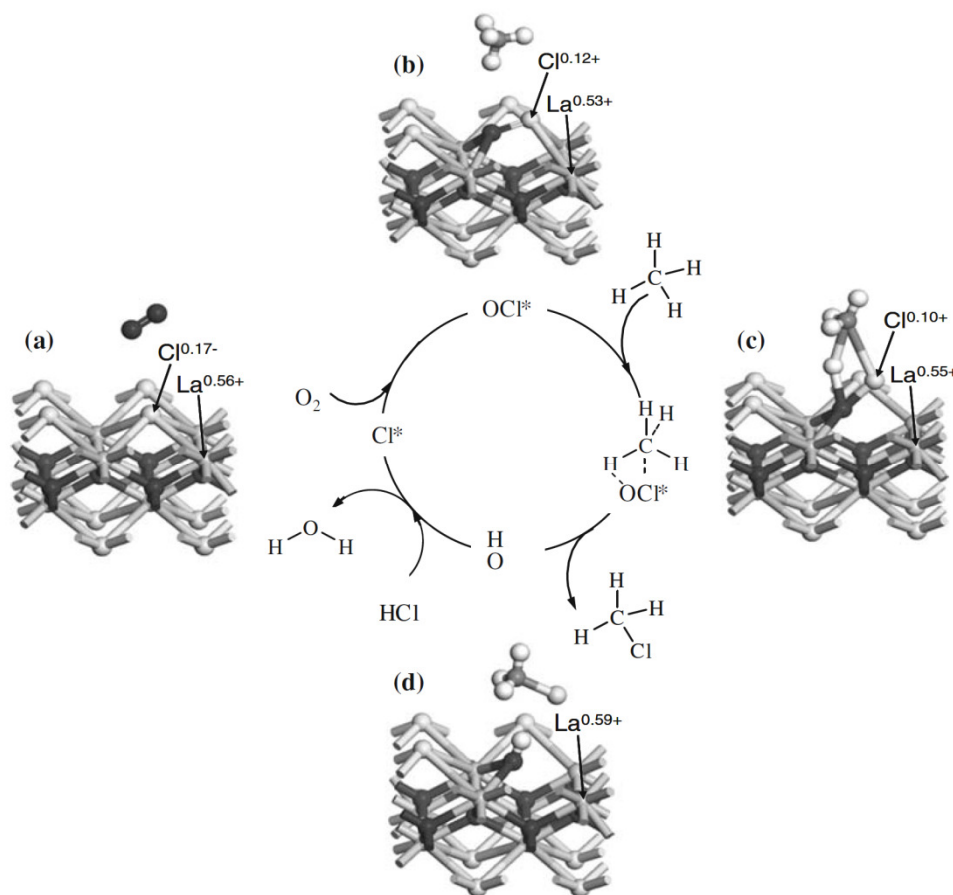


**Figure 1.10:** Mechanism of selective methane chlorination over  $\text{LaOCl}$ .

The active sites are hypochlorite  $\text{OCl}^-$  surface species having a formal oxidation state of +1.<sup>[83-85]</sup> The active site is formed from  $\text{LaCl}_3$  by the reaction with molecular oxygen (see Figure 1.10). In the next step methane forms a five-coordinated transition state with the positive charged chlorine, which decomposes and leaves a surface hydroxyl group and methyl chloride after decomposition. To close the catalytic cycle the catalyst hydrogen chloride forms

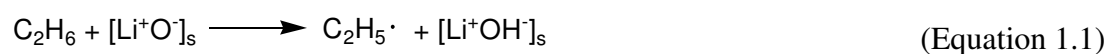
water and a surface chloride that is oxidized with molecular oxygen to the original active hypochloride species.<sup>[83]</sup>

Similarities of the two reaction mechanisms are obvious. Also in the latter case the rate determining step proceeds over a five-coordinated carbon and the stability of this transition state should also decrease with higher number of chlorine bound to carbon, increasing the selectivity of the mono chlorinated product, but catalytic tests with stoichiometric mixtures of CH<sub>4</sub> : HCl : O<sub>2</sub> 2:2:1 at 475 °C showing 65% methyl chloride and 25% methylene dichloride (rest are oxidation products CO and CO<sub>2</sub>) at 27% conversion. Thus, this reaction is not as selective as the previous described catalysts and reasons for this are still under discussion. Even changes in temperature between 450 – 550 °C showed no significant influence on the selectivity of the methyl chloride, but it should also be noted that these temperatures are still much higher than the temperature of the selective FeO<sub>x</sub>Cl<sub>y</sub>/Al<sub>2</sub>O<sub>3</sub> catalysts (270 °C).

### 1.2.5. Oxidative C-H activation via activation with non-reducible cations

#### C-H Activation of alkanes by Li promoted MgO

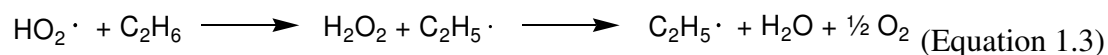
Li<sub>2</sub>O/MgO is one of the most prominent examples for oxidative C-H activation relying on defect sites at surfaces, well exemplified by the pioneering work of Lunsford et al.<sup>[93, 94]</sup> The active sites have been originally proposed to be [Li<sup>+</sup>O<sup>-</sup>]<sub>s</sub> sites, which are generated in an MgO host lattice by substitution of divalent magnesium cation by Li<sup>+</sup>. This oxygen radical site<sup>[79, 95, 96]</sup> catalyzes the abstraction of hydrogen from, e.g., ethane with formation of [Li<sup>+</sup>OH<sup>-</sup>]<sub>s</sub> and an ethyl radical (Equation 1.1) in the rate determining step.



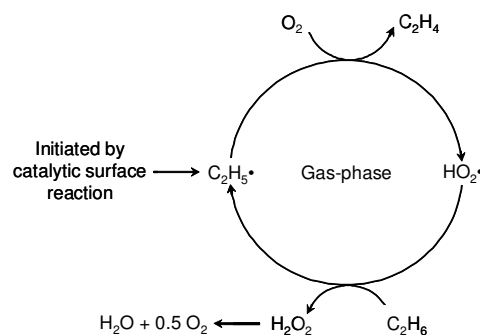
The initially formed ethyl radical is desorbed into gas phase, where free radical reactions proceed. In the gas phase molecular oxygen abstracts a second hydrogen leading to ethane and a hydroperoxy radical (Equation 1.2)



This hydroperoxy radical can again remove a hydrogen atom from ethane under recreation of an ethyl radical, forming a separate catalytic cycle in the gas phase. The formed hydrogen peroxide decomposes to water and oxygen (Equation 1.3), but formation of two hydroxyl radical by homolytic cleavage is also possible, also enabling the start of a new chain reaction.

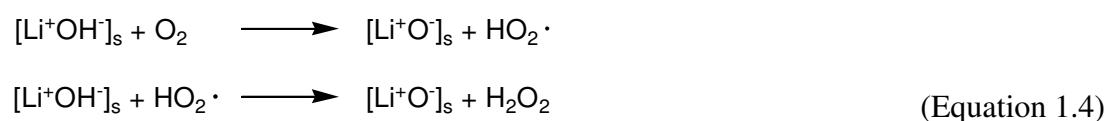


Overall, ethane is oxidized to ethene by molecular oxygen. The role of the catalysts is to catalytically supply of ethyl radicals needed in the radical cycle of the gas phase reaction (Scheme 1.8).



**Scheme 1.8:** Catalytic cycle in gas-phase after activation by  $[\text{Li}^+\text{O}^-]$ .

After initiation of the catalytic gas phase reaction, the active center on the surface of the catalysts needs to be regenerated by reaction with oxygen. At high temperatures ( $700^\circ\text{C}$ ), regeneration of the surface  $[\text{Li}^+\text{OH}^-]$  occurs under removal of lattice oxygen. At lower temperature gas phase oxygen is needed for the regeneration, forming a hydroperoxy radical under recreation of the active center  $[\text{Li}^+\text{O}^-]$ . The hydroperoxy radical can react to hydrogen peroxide under regeneration of a second active center and finally after scission to two hydroxyl radical regenerate two more active centers (Equation 1.4). Overall one oxygen molecule is able to regenerate four active centers.



In contrast to the original proposal, surface science studies by the group of Goodman showed that the concentration of  $[\text{Li}^+\text{O}^-]$  sites does not correlate with the activity for methane activation.<sup>[97]</sup> Instead,  $\text{F}^0$  centers (oxygen vacancies containing two electrons) at or near the surface of MgO have been established to be the sites inducing the C-H bond breaking. One should note that such sites would correspond to such surface sites of low coordination, which are in equilibrium with the near surface F centers. The presence of  $\text{Li}^+$  substituted into the MgO lattice induces a higher concentration of such sites. It is interesting to note also that the  $[\text{Li}^+\text{O}^-]$  sites are mostly found in the bulk and not at the surface. A recent study of  $\text{F}^0$  centers on MgO (0 0 1) showed for the first time the quantitative measure of the high strength of interaction between the tip of an AFM microscope and these sites giving reference to their unusual reactivity.<sup>[98]</sup>

It should be noted at this point that C-H activation can be also achieved on a wide variety of non-reducible oxides (for an excellent review see ref. <sup>[99]</sup>). Most notable, C-H bond cleavage can also be achieved over non-reducible oxides such as alumina on highly defect sites. In contrast to the chemistry discussed above, the C-H bond cleavage involves the heterolytic cleavage into a proton coordinating in the final state to oxygen at the site and a carbanion which interacts with the metal cation.<sup>[100]</sup> Also several cases of cations in zeolites, such  $\text{Ga}^{3+}$ ,  $\text{La}^{3+}$  and  $\text{Zn}^{2+}$  exchanged zeolites have been found to activate C-H bonds in an analogous way. In these cases a very high strength of interaction of the exposed cations <sup>[101]</sup> with the C-H bonds leads to the heterolytic dissociation.<sup>[43, 102]</sup> While the final product, i.e., olefins in the simplest case, represent an oxidation step with respect to the starting molecule, we will not discuss this chemistry in detail here, as the C-H activation step is not typical for C-H activation involving oxygen.

#### *Bifunctional oxidative catalysis with main group cations at zeolite exchange sites*

So far, we have discussed the role of specific catalytic sites involving also the metal oxygen bonds and anionic species catalyzing the C-H bond separation. However, surprisingly only the coordinating effect of a cation in a large electrostatic field is sufficient to induce C-H bond transfer. This requires the confined space of, e.g., a zeolite that enforces the proximity between an alkane and molecular oxygen. Exchangeable cations provide the high local field apparently necessary to reduce the energy needed to excite the hydrocarbon oxygen charge-transfer.<sup>[103]</sup> It is remarkable, that for reactions in the gas phase the energy to perform such charge transfer lies energetically much higher <sup>[104]</sup> than when both reaction partners are

confined to a zeolite cage. The source of the energy to stimulate seems not to be critical, i.e., the reaction can be induced by visible light <sup>[105]</sup> as well as by thermal energy. <sup>[106]</sup>

It appears, however, that the local geometry of the arrangement between oxygen the alkane and the cation is critical and is strongly determined by the size and equilibration of ion exchange of the cation.

This is best seen in the comparison between  $\text{Ca}^{2+}$  and  $\text{Mg}^{2+}$  and their interactions with the alkane. The direct importance and accessibility of the alkaline earth metal cations has been established by a series of ion exchange experiments which in essence showed that the catalyst activity drastically increased, once the ion exchange level led to cations accessible by the reacting molecules. <sup>[107]</sup> A more subtle local arrangement is important for the type of interaction with the alkane (see Figure 1.11). <sup>[108]</sup> The small difference in the ionic radius of

$\text{Mg}^{2+}$  and  $\text{Ca}^{2+}$  leads to a deeper embedding of the former into the plane of the six-ring of the SII site in zeolite Y. In consequence, the DFT calculations indicate that  $\text{Mg}^{2+}$  interacts with alkanes mainly in  $\eta^2$  mode, while with  $\text{Ca}^{2+}$  interaction with methane and ethane leads preferentially to the  $\eta^3$  mode, while for propane even indications for adsorption in  $\eta^4$  mode have been found. The larger cation

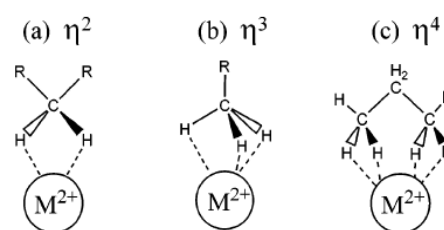


**Figure 1.11:** Schematic representation of possible conformations of light alkanes to the exchanged cation.

leads to more electrostatic contributions of the bonding, while the shielding of  $\text{Mg}^{2+}$  induces contributions of directed hydrogen bonding to the oxygen of the zeolite lattice.

In situ IR spectroscopy reveals that indeed not only the alkane interacts with the cations, but that also molecular oxygen forms an adsorption complex, the stretching frequency of which is observable in the adsorbed state, because of the induction of a dipole by these interactions. <sup>[109]</sup>

It should be noted that the interaction with the better shielded  $\text{Mg}^{2+}$  is significantly weaker than with  $\text{Ca}^{2+}$  cations. Molecular oxygen and alkanes compete for the adsorption sites, but indirect evidence exists that both are indeed adsorbed in the proximity of the cation. This geminal adsorption on one cation would lead to a charge transfer intermediate, which would take the form  $[\text{C}_3\text{H}_8^+\text{O}_2^-]$ . <sup>[110]</sup> Proposed to be aided by protons, it rearranges eventually to hydroperoxide, which decomposes for the case of propane to propan-2-ol or acetone.

### 1.2.6 Conclusion and outlook

The discussed examples show that the catalyzed oxidative C-H activation proceeds in the dominant number of cases via single electron processes induced, however, by a surprisingly wide variety of catalytically active sites. These span from classic transition metal terminal or bridging oxygen groups, exemplified best by vanadia, over transiently formed terminal oxygen, such as in the Cu exchanged zeolite based catalysts, to the  $F^0$  centers in MgO type catalysts and the facilitation of the formation of charge transfer complexes in zeolites by exposed cations. Despite the homolytic cleavage of the C-H bond, the lability of the metal oxygen bond and the polarizability of the C-H bond facilitate the reaction and appear to lower the energies involved in the reaction pathways. The achievable selectivity remains a great challenge, because most of the materials contain accessible metal cations and labile oxygen providing also polar pathways to the subsequent oxidation of the intermediate once the C-H bond has been cleaved in the first (rate determining) activation step. Certainly, less defects and undercoordinated cations would help to improve the selectivity for a particular catalyst.

While impressive progress has been made in the characterization of such catalysts, the sites active in the C-H bond cleavage are frequently minority sites constituting only a very small fraction of the surface. Together with the fact that the surface of the oxides and the active sites in zeolites are very sensitive to the reactive environment, this poses a formidable challenge to characterize the sites. Such insight together with well-targeted synthesis approaches are, however, the key to the next generation of catalysts for C-H activation and selective functionalization.



### 1.3. Acrylic acid as intermediate in chemical industry

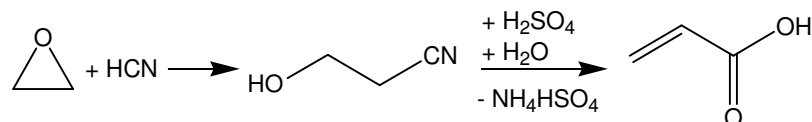
#### 1.3.1. Usage of acrylic acid

Acrylic acid is an important intermediate in chemical industry with a world production capacity of 3.4 million tons per year in 2004.<sup>[1]</sup> Acrylic acid is mainly used in form of acrylic esters in polymers for lacquers, colorings and additives in paper and textile production. Superabsorbent polymers are a relatively new product based on acrylate polymers. The application varies from filtration and diapers to fire-retardant gels, and therefore the annual growth rate of acrylic acid production of 5% is the highest of all unsaturated acids.

#### 1.3.2. Historical production of acrylic acid

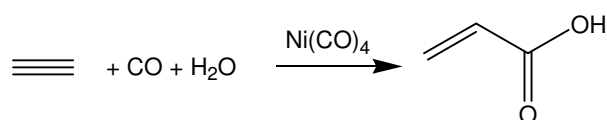
The first commercial process for acrylic acid production was the so called Ethylenecyan-hydrin process which was developed by Röhm & Haas in Darmstadt in 1901. Ethylene oxide and hydrogen cyanide are converted to hydroxyl propionitril in alkaline medium and further hydrolyzed with diluted sulfuric acid to acrylic acid.<sup>[1]</sup>

This process shown in Scheme 1.9 was used until 1971.



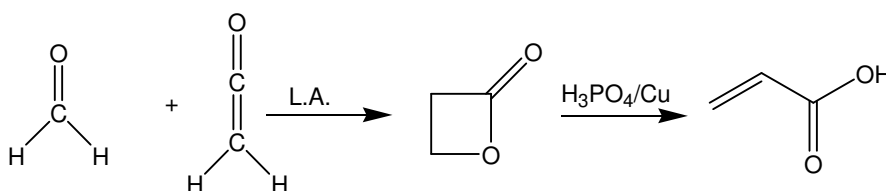
**Scheme 1.9:** Ethylenecyan-hydrin process for acrylic acid production.

In the 1960's and 1970's the Reppe process was favored, where the catalyzed carbonylation of acetylene takes place in the presence of water as shown in Scheme 1.10. As catalyst nickel tetra carbonyl is usually used at conditions of about 100 bar and temperature between 490 to 510 K. A few modifications exist which are different in type and amount of the used catalyst. The Reppe process was used by BASF until the 1990s.<sup>[111]</sup>



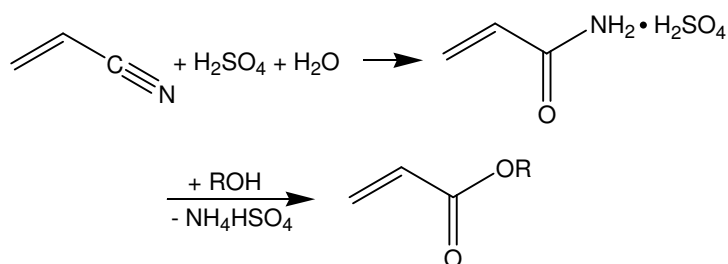
**Scheme 1.10:** Reppe process for acrylic acid production.

The third commercial process starts with formaldehyde that is reacted with ketene in the presence of a lewis acid ( $\text{AlCl}_3$ ,  $\text{ZnCl}_2$ ,  $\text{BF}_3$ ) to  $\beta$ -propion lactone. In a second step  $\beta$ -propion lactone is decomposed at 410 – 450 K and 25 – 250 bar with phosphoric acid and copper as catalyst (Scheme 1.11).<sup>[1]</sup>



**Scheme 1.11:** Acrylic acid production from formaldehyde and ketene.

The last historical process that was used for industrial acrylic acid production based on the hydrolysis of acrylonitrile with sulfuric acid and water. It is possible to gain directly an acryl ester by using an alcohol instead of water in the second step. In this process stoichiometric amounts of ammonium bisulfate are formed (Scheme 1.12).<sup>[1]</sup>

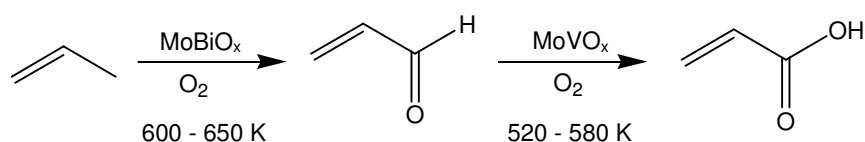


**Scheme 1.12:** Acrylonitrile hydrolysis for acrylic acid production.

All historical processes have in common that they use expensive starting materials (ethylene oxide, acetylene, ketene or acrylonitrile) and also involve toxic chemicals for the reaction (hydrogen cyanide, carbon monoxide, formaldehyde). Therefore the high expenses of these procedures promoted the development of a more economic and environmentally friendly process. With the increasing popularity of crude oil at the end of the oil crisis in 1979, propene became more available through steam reforming and therefore the price of propene was low compared to acetylene. As a result the selective oxidation of propylene to acrylic acid became more and more interesting.

### 1.3.3. Selective oxidation of propene to acrylic acid

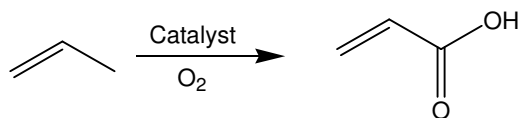
Currently, acrylic acid is produced by a two step oxidation from propene in a multi tubular fixed bed reactor. In the first step a mixture of propene, steam and air is converted to acrolein at a temperature of 600 – 650 K. The exothermic reaction is catalyzed by molybdenum based metal oxides. The reaction products of the first step are transferred directly into the second reactor, where further oxidation to acrylic acid takes place at temperatures between 520 and 580 K. Again, Molybdenum metal oxides are used to catalyze this step. The yield of the first and second step is up to 90% and 97% respectively, resulting in an overall yield of 87% for this process based on propene. Both reactions are shown in Scheme 1.13.<sup>[112]</sup>



**Scheme 1.13:** Selective two step oxidation of propene to acrylic acid.

Furthermore, acrylic acid can be obtained from a one step oxidation of propylene as described in Scheme 1.14. In this case the oxidation of propylene to acrolein and the second oxidation of acrolein to acrylic acid take place in the same reactor. But the yields of acrylic acid via this process are significantly lower than that of the two step process. This can be explained by the differences in the composition of the used catalysts in the two step process, which can be optimized for each reaction. Furthermore, the different temperatures used for each step play an important role. The activation of propene requires a higher reaction temperature than for

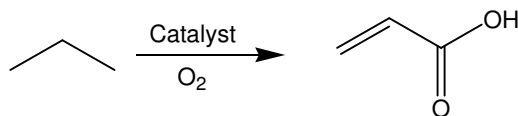
acrolein. 600 – 630 K are necessary to obtain a sufficient propene conversion. At this temperature acrolein is not only oxidized to acrylic acid. Total oxidation of acrolein and acrylic acid takes place, leading to lower yields of the desired product and following to a large amount of carbon oxides.<sup>[113]</sup>



**Scheme 1.14:** One step oxidation of propene to acrylic acid.

### 1.3.4. Selective oxidation of propane to acrylic acid

Propane is a component of natural gas with an up to 10% fraction (compare chapter 1.1.1.). Therefore it would be an economical preferred raw material based on its availability for the oxidation to acrylic acid (Scheme 1.15).



**Scheme 1.15:** Selective oxidation of propane to acrylic acid.

In Figure 1.12 the development of propane and propene prices are shown between January 2007 and December 2008. The prices for the second term of 2008 are not representative due to massive distortions of the financial markets and commodities prices. Therefore average prices for propane and propene were calculated between January 2007 and July 2008. In this period the average price per ton of propane and propene are 567 USD and 1093 USD, resulting in a price difference of 526 USD per ton. From this data it is possible to estimate minimum yields required for the selective oxidation of propane to acrylic acid, to be competitive within the selective oxidation of propene on an economic level.

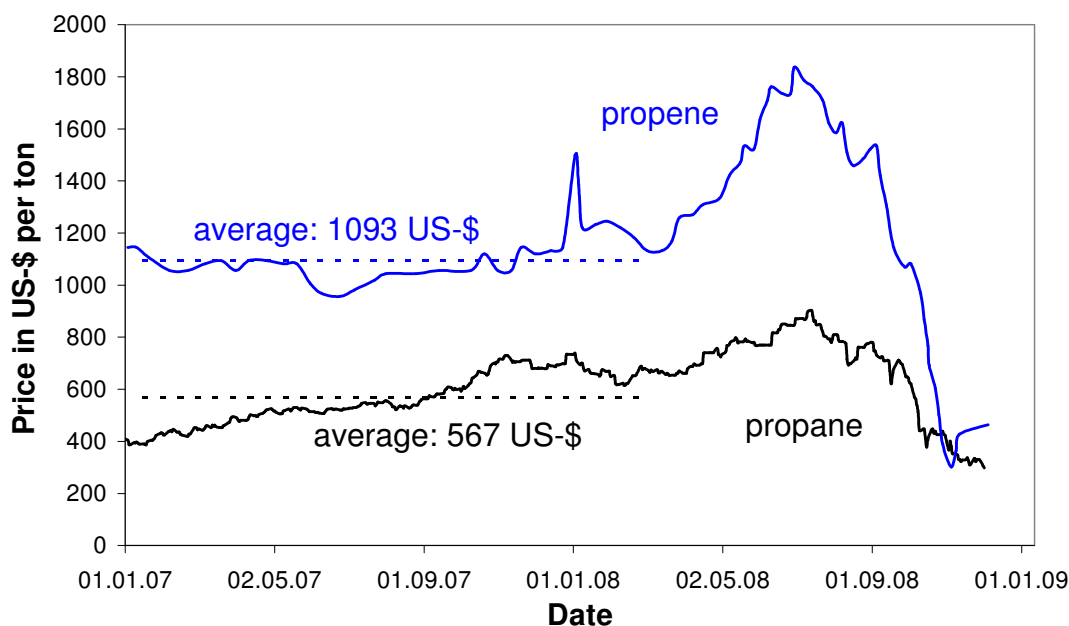
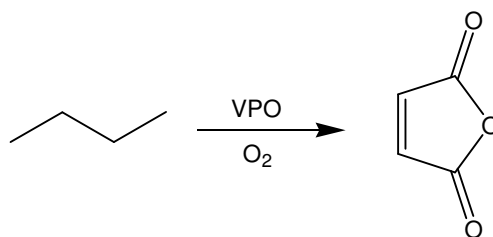


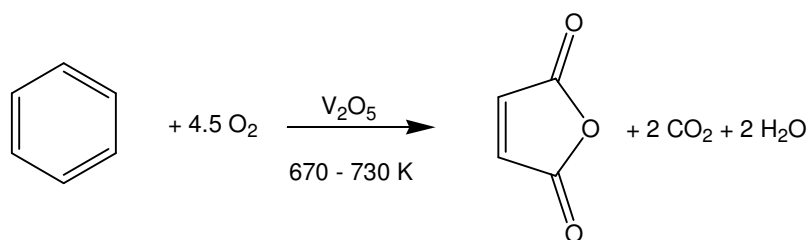
**Figure 1.12:** Development propane and propene price for 2007 – 2008.

Starting from one ton propene 1.54 tons of acrylic acid are produced (for 90% yield), so feedstock costs for one ton acrylic acid are 710 USD. The calculation based on propane revealed that 49% yield is needed, to have similar feedstock costs. It should be noted that processes are only changed if the profit opportunities exceed the expenses of operational change and risk and therefore the yield of acrylic acid has to be higher than 49% to compensate the change and additional risk. Therefore when yields exceed the range of 60 – 70%, the usage of propane for acrylic acid production would be preferred. Up to now highest reported yield for selective oxidation of propane is 48%.<sup>[114-116]</sup>

Nowadays selective oxidation of alkanes is realized only in case of *n*-butane oxidation to maleic anhydride over VPO catalysts (Scheme 1.16). The yields for this process range between 45 and 61% and further developments in reaction technology that separate the oxygen from the substrate lead to yields higher 70%. Since the 1970's this process is used commercially and it replaced the oxidation of benzene to maleic anhydride (Scheme 1.17). For a short time the oxidation of butene was also used, but rising prices for butene accelerated the development of the *n*-butane oxidation.<sup>[1, 117, 118]</sup>



**Scheme 1.16:** Selective oxidation of n-butane to maleic anhydride.<sup>[1]</sup>



**Scheme 1.17:** Oxidation of benzene to maleic anhydride.<sup>[1]</sup>

Yields reachable in selective oxidation reactions can be estimated, based on a concept upon the stability of the desired product. If the product is in relation to the reactant a very stable molecule high selectivity is easy to reach, whereas for a very instable product high selectivity is impossible, due to decomposition and further oxidation (compare also chapter 1.2.1). For stability quantification the difference of the bond strength between the weakest C-H bond in the reactant and the weakest C-H or C-C bond in the product molecule ( $\Delta^0 H_{C-H \text{ reactant}} - \Delta^0 H_{C-H \text{ or C-C product}}$ ) is calculated.<sup>[119]</sup>

A plot of the bond energy difference and observed selectivity for 23 selective oxidation reactions shows a clear correlation (Figure 1.13). Reactions with highly stable products like ethylbenzene to styrene or 1-butene to butadiene are in Figure 1.13 in the upper left corner, indicating high selectivities, whereas reactions with instable products like methane to formaldehyde or isobutene to methacrolein are in the lower right corner.

If the bond energy difference is less than  $30 \text{ kJ}\cdot\text{mol}^{-1}$  very high product selectivity is possible, whereas higher energy difference leads to a fast decrease of the selectivity. For differences greater than  $70 \text{ kJ}\cdot\text{mol}^{-1}$  near zero product selectivity is observed.

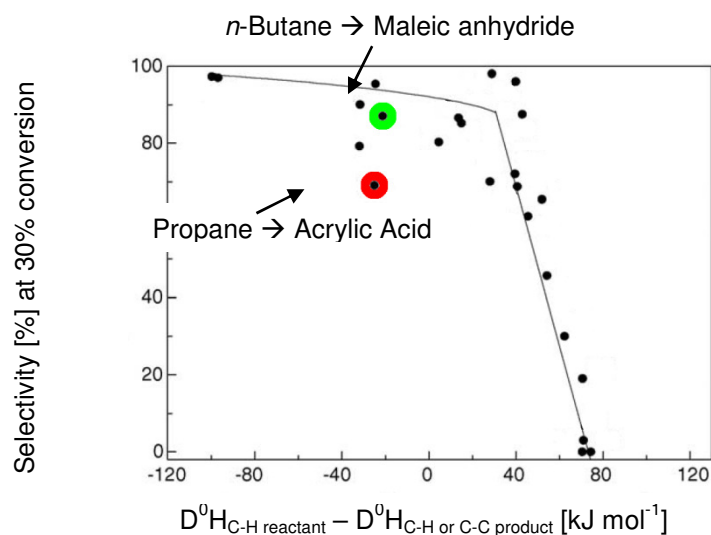


**Figure 1.13:** Correlation between bond energies and selectivity in oxidation reactions.

The selective oxidations of *n*-butane to maleic anhydride and propane to acrylic acid both possess the fabulous situation that all bonds in the product molecule are stronger than the weakest C-H bond of *n*-butane or propane. In this situation high selectivity should be possible. The potential of the *n*-butane oxidation (green dot in Figure 1.13) is already developed, indicated by the position near to the trend line, whereas for propane oxidation the observed selectivity is heavily below the trend line. From this model further improvements for the selective oxidation of propane to acrylic acid should be possible and might lead to a catalyst that is capable for industrial usage.

## 1.4. Selective oxidation of propane to acrylic acid

### 1.4.1. General mechanism

Today acrylic acid is prepared by selective oxidation of propene. Since complete oxidation of organic compounds to  $\text{CO}_2$  and water is extremely exothermic, deep oxidation is thermodynamically favored. The production of partially oxidized hydrocarbons requires precise kinetic control. “Achieving only partial oxidation of hydrocarbons is like toasting marshmallows on a campfire. The trick is to find the perfect conditions near the red hot coals and to allow just enough time to reach a nice gold-brown without burning them to a tasteless black crisp”,<sup>[120]</sup> such catalyst is needed which activates the inert propane molecule (compare chapter 1.2.) and still keeps the selectivity of oxygenates high.<sup>[121]</sup>

Selective oxidation reactions on heterogeneous oxide catalysis proceed usually through a Mars-van-Krevelen mechanism. In such mechanism, the active sites oxidize the reactant molecules by creating lattice oxygen vacancies. In a second step the catalyst is re-oxidized by gas phase oxygen.<sup>[122, 123]</sup>

The selective oxidation of an alkane through the Mars-van-Krevelen mechanism is given in Figure 1.14 a-e. In the first step propane is adsorbed on the surface of the catalyst and is oxidized from lattice oxygen to propene and water (Figure 1.8 b). This C-H activation is the rate determining step in this reaction (compare also with chapter 1.2.).

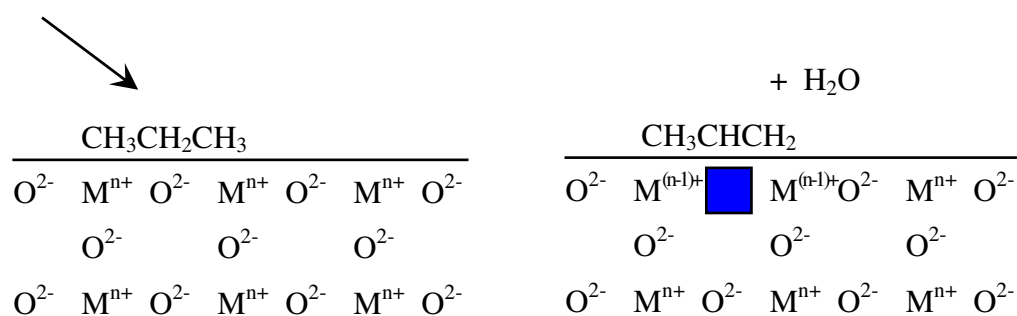
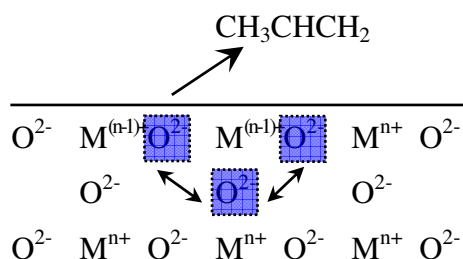


Figure 1.14 a: Adsorption of propane.

Figure 1.14 b: Oxidation of propane to propene and water.



The oxidation product propene desorbs, leaving an oxygen vacancy that can migrate through the catalysts (Figure 1.14 c). The re-oxidation occurs from oxygen from the gas phase (Figure 1.14 d) and finally leads to a recovered catalyst (Figure 1.14 e).



**Figure 1.14 c:** Desorption of propene and migration of oxygen vacancy.

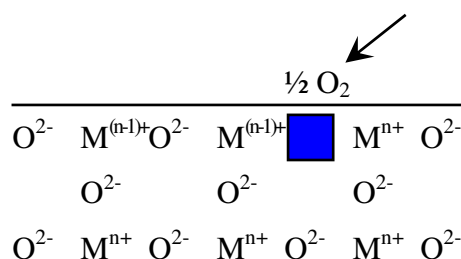


**Figure 1.14 d:** Reoxidation from gaseous oxygen.

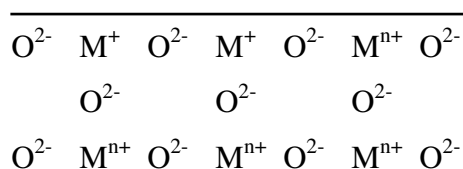


**Figure 1.14 e:** Recovered catalyst.

### 1.4.2. Vanadium pyrophosphate oxide catalysts (VPO)

For selective oxidation of propane to acrylic acid three different catalysts systems are described in literature.<sup>[121]</sup> One of them are vanadium pyrophosphate type catalysts (VPO), which have been used successfully in the industrial process of *n*-butane oxidation to maleic anhydride. The VPO system shows high activity and selectivity in *n*-butane oxidation. Reported yields of maleic anhydride vary from 45 to 61% with *n*-butane conversion of about 65% and selectivity to maleic anhydride ranging from 65% to 97%. However, VPO catalysts are not very effective in propane selective oxidation to acrylic acid. Some examples for VPO catalysts are given in Table 1.2. The low yields of acrylic acid, contrary to the maleic anhydride yields in *n*-butane oxidation, may suggest that VPO type catalysts are rather specific towards the length of hydrocarbon chain. Moreover the stability of

the partial oxidation products could play a role. Maleic anhydride is more stable than acrolein and acrylic acid regarding to further oxidation.<sup>[124-126]</sup>

**Table 1.2:** Results for selective propane oxidation with VPO catalysts.

<i>Catalyst composition</i>	<i>T</i> [K]	<i>Propane conversion</i> [%]	<i>Acrylic acid yield</i> [%]	<i>Selectivity</i> [%]
VP <sub>1,15</sub> Te <sub>0,1-0,15</sub> O <sub>x</sub>	663	30	10.5	30 <sup>[124]</sup>
VP <sub>1,05</sub> O <sub>x</sub>	658	37	14.4	39 <sup>[126]</sup>
VP <sub>1,1</sub> O <sub>x</sub>	693	46	14.7	32 <sup>[125]</sup>

### 1.4.3. Heteropoly compounds (HPC)

A further system for selective propane oxidation are heteropoly compounds (HPC). HPC refer to inorganic, heteropoly acids and their corresponding salts. They have well defined cage-like structures with a central cation and surrounding polyanions. The central cation are heteroatoms like P, As, Si, Ge or B. The polyanions are often oxoanions of Mo or W. The best known cage-like structures used as oxidation catalysts are the Keggin type compounds with the general formula  $[X^{n+}M_{12}O_{40}]^{(8-n)-}$ . Here,  $X^{n+}$  is the central cation surrounded by  $MO_6$  octahedral polyanions. The negative charge of the HPC can be neutralized by protons, giving HPC a strong acidity. Due to this property they have been used as acid catalysts in solution for dehydration, esterification and alkylation. Table 1.3 shows examples of HPCs and their conversions, selectivities and yields in propane oxidation to acrylic acid. While the simple form of the Keggin compound  $H_3PMO_{12}O_{40}$  is inactive in propane oxidation, the conversion can be improved by structural modification, such as treatment with ammonia or pyridine.<sup>[127-130]</sup>

**Table 1.3:** Examples for HPC catalysts for selective oxidation of propane to acrylic acid.

<b>Catalyst composition</b>	<b>Feed</b>	<b>T [K]</b>	<b>Propane conversion [%]</b>	<b>Acrylic acid yield [%]</b>	<b>Selectivity [%]</b>
H <sub>3</sub> PMO <sub>12</sub> O <sub>40</sub>	C <sub>3</sub> /O <sub>2</sub> /H <sub>2</sub> O/N <sub>2</sub>	613	0	0	0 [127, 129]
H <sub>1,26</sub> Cs <sub>2,5</sub> Fe <sub>0,08</sub> PVMO <sub>11</sub> O <sub>40</sub>	C <sub>3</sub> /O <sub>2</sub> /N <sub>2</sub>	653	47	13	28 [128]
(NH <sub>4</sub> ) <sub>3</sub> PMO <sub>12</sub> O <sub>40</sub>	C <sub>3</sub> /O <sub>2</sub> /H <sub>2</sub> O/N <sub>2</sub>	613	4.5	0	6 [127, 129]
(PyH) <sub>3</sub> PMO <sub>12</sub> O <sub>40</sub>	C <sub>3</sub> /O <sub>2</sub> /H <sub>2</sub> O/N <sub>2</sub>	613	7.5	2	29 [127, 129]

Note: C<sub>3</sub> = propane

#### 1.4.4. Multi-component metal oxides (MMO)

The third class of catalysts for selective oxidation of propane to acrylic acid are multi-component metal oxides (MMO), also known as complex mixed oxides (compare chapter 1.2.2.). These materials contain a mix of multiple crystal and amorphous phases and do not have a well-defined primary structure, but MMOs are generally prepared through calcination methods at high temperatures and thus have excellent thermal stability. MoVNb mixed oxides were developed in the 1970s [131] and used for the oxidation of ethane to ethene and acetic acid. These catalysts are also capable to activate propane with acetic acid, acetaldehyde and carbon oxides as the only products. The application of MMOs in selective propane oxidation started in the 1990s. All known MMO type catalysts contain molybdenum and the most of them include also vanadium. The best results were achieved on catalysts which also contain tellurium and niobium. Well known is the catalyst system of the type MoVTeNbO<sub>x</sub> which is most promising regarding to propane conversion and acrylic acid selectivity. Recently studies are attended to MMOs containing antimony instead of tellurium. The results of some MoV(Te,Sb,Nb)O<sub>x</sub> catalysts are shown in Table 1.4. Further description of the MoVTeNbO<sub>x</sub> system is in chapter 1.5.. [114, 115, 132-138]

**Table 1.4:** Multi component metal oxide catalysts for selective oxidation of propane.

<b>Catalyst composition</b>	<b>Feed</b>	<b>T [K]</b>	<b>Propane conversion [%]</b>	<b>Acrylic acid yield [%]</b>	<b>Selectivity [%]</b>
MoV <sub>0,3</sub> Te <sub>0,23</sub> Nb <sub>0,12</sub> O <sub>x</sub>	C <sub>3</sub> /air/H <sub>2</sub> O	653	80	48	60 <sup>[114]</sup>
MoV <sub>0,3</sub> Te <sub>0,23</sub> Nb <sub>0,12</sub> O <sub>x</sub>	C <sub>3</sub> /O <sub>2</sub> /H <sub>2</sub> O/He	623	23	14	61 <sup>[132]</sup>
MoV <sub>0,3</sub> Sb <sub>0,16</sub> Nb <sub>0,05</sub> O <sub>x</sub>	C <sub>3</sub> /air/H <sub>2</sub> O	653	50	16	32 <sup>[134]</sup>
MoV <sub>0,3</sub> Sb <sub>0,25</sub> Nb <sub>0,11</sub> O <sub>x</sub>	C <sub>3</sub> /O <sub>2</sub> /H <sub>2</sub> O/N <sub>2</sub>	673	21	12	61 <sup>[133]</sup>

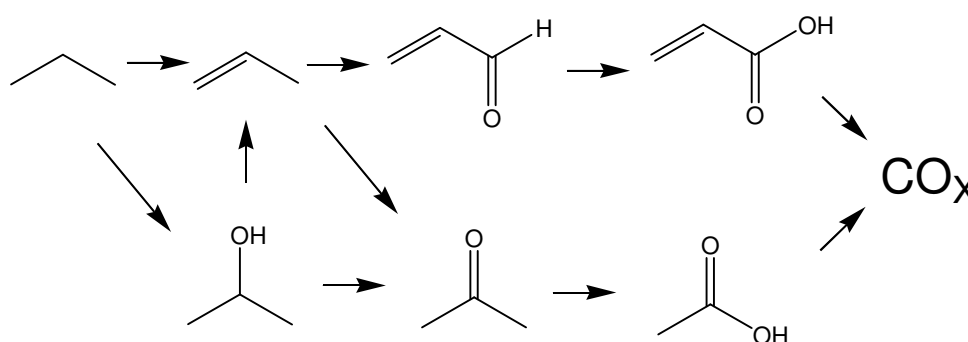
Note: C<sub>3</sub> = propane

## 1.5. Selective oxidation of propane to acrylic acid over MoVTeNb oxides

### 1.5.1. Reaction pathways for selective propane oxidation

The oxidation of propane can be described by a complex reaction network that starts with propane and ends with the deep oxidation product carbon dioxide. In the following model and also in most literature carbon monoxide and carbon dioxide will not be distinguished. For simplification reasons the sum of both components is described with  $\text{CO}_x$ .

The reaction network for the oxidation of propane is shown in Scheme 1.18. The activation of propane leads to propene or iso-propanol. Elimination of iso-propanol opens a path to propene, whereas the oxidation forms acetone. Propene can either be oxidized in allylic position to acrolein or by oxo-insertion to acetone. Oxidation of acrolein leads to the wanted product acrylic acid. Acetone reacts under C-C bond cleavage to acetic and finally both acids can be further oxidized to carbon oxides.<sup>[139-144]</sup>



**Scheme 1.18:** Reaction network for the selective oxidation of propane.

A third pathway from propane over 1-propanol, propanal and 1-propionic acid to carbon oxides is also proposed, but it is only of low relevance and therefore it is in Scheme 1.18 neglected.<sup>[121]</sup>

This reaction network is proposed for catalysts of the type  $\text{MoVTeNbO}_x$ , but due to the comparable structure it is postulated that this system is also valid for similar catalyst systems like  $\text{MoVSb(Nb)O}_x$ .<sup>[145]</sup> The development of standard formation enthalpies for the reaction steps is shown in Figure 1.15. Each reaction step is exothermic. The dehydration of propane to propene is in this reaction network exothermic ( $\Delta H_R^0 = -117 \text{ kJ}\cdot\text{mol}^{-1}$ ), due to the coupling

with the strong exothermic water formation ( $\Delta H_{\text{R}}^0 = -242 \text{ kJ}\cdot\text{mol}^{-1}$ ). In contrast the dehydrogenation of propane without water formation is endothermic with  $\Delta H_{\text{R}}^0 = +125 \text{ kJ}\cdot\text{mol}^{-1}$  and therefore suffers under poor conversions in chemical equilibrium [121].

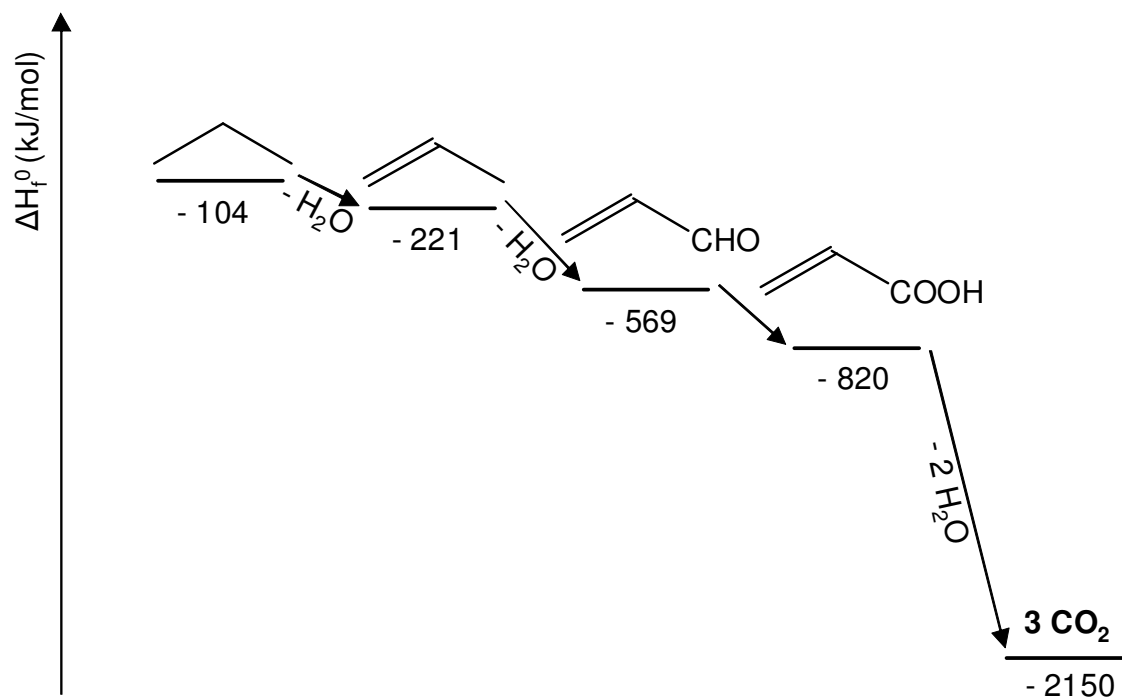


**Figure 1.15:** Standard formation enthalpies of intermediates and products for propane oxidation. [121]

The relative reactivities increase in the order: propane < acetic acid  $\approx$  acrylic acid < propylene < acetone < acrolein  $\approx$  isopropanol. This sequence is based on the nature of the radical mechanism and the decrease of C–H bonds strength for the oxygenates. [141]

### 1.5.2. Phases of MoV(Te,Sb)Nb oxide catalysts

Two phases containing all four metals are known. These two phases were found by Mitsubishi Chemical Corporation in the early 1990's and were named *M1* and *M2* by Ushikubo et al..<sup>[114, 115, 134-136]</sup> The *M1* phase crystallizes in an orthorhombic system and can be described as a corner sharing MO<sub>6</sub> octahedron arranged periodically in *c* axis, where M can be molybdenum or vanadium. The octahedron form channels perpendicular to the *ab* plane. The channels are formed from five, six or seven octahedra (see also Figure 1.6).<sup>[146-152]</sup> The tellurium cations are located in the hexagonal and heptagonal channels, whereas the niobium cations occupy pentagonal bipyramidal sites in the channels formed from five octahedron.<sup>[137, 146, 153]</sup> The existence of different oxidation states of molybdenum (+V and +VI) and the formation of channels with seven octahedron appears to be essential for the activity in propane activation, due to distortion of the octahedron, resulting in a higher reactivity. It was shown, that a *M1* phase consisting of only molybdenum and vanadium is able to activate propane.<sup>[154]</sup>

The *M2* phase is a hexagonal layered structure formed from octahedron with molybdenum, vanadium and niobium centers (see also Figure 1.7.). Tellurium occupies in this structure the hexagonal channels.<sup>[148]</sup> The stoichiometric composition of the *M1* phase is Te<sub>2</sub>OM<sub>20</sub>O<sub>56</sub> (M = Mo, V, Nb) and of the *M2* phase TeM<sub>3</sub>O<sub>9</sub> (M = Mo, V, Nb)<sup>[155]</sup>. Molybdenum, vanadium and niobium can partly be exchanged against each other under preservation of the structure. The synthesis procedure and most suitable reactants are still under discussion and the specific effect of each preparation step on catalyst properties is debated.<sup>[156-160]</sup> The catalytic properties of the different phases *M1* and *M2* are still under discussion, especially effects that result from mixtures from *M1* and *M2* phases.<sup>[161]</sup> Also the exact nature of active sites as well their reactivities are still under discussion.<sup>[140, 153, 162, 163]</sup>

In the case of antimony containing catalysts also a phase is formed that is analogous to the tellurium containing *M1* phase, formed by corner sharing MO<sub>6</sub> octahedron. M corresponds to molybdenum and vanadium in the same way as the tellurium containing catalysts. Antimony like tellurium presents a lone pair of electrons and should be able to accommodate the same types of coordination. The valence of antimony is three or five but the mainly present form is Sb (V) as reported by Millet et al..<sup>[164]</sup> The Sb (V) entities correspond to SbO<sub>4</sub> trigonal bipyramids and form infinite chains of the type [Sb-O]<sub>∞</sub> in the hexagonal channels. The Sb

(III) cations in the *M1* phase should form  $\text{SbO}_3\text{E}$  trigonal pyramid groups which correspond to  $[\text{Sb-O-Sb}]$  dimers. The antimony cations and oxygen anions are occupying hexagonal channels formed by the octahedron. Analogous to the tellurium containing catalysts there are also pentagonal channels which are occupied by molybdenum and vanadium and heptagonal channels which are empty. The formal stoichiometries can be written as  $(\text{SbO})_2\text{M}_{20}\text{O}_{56}$ . M can be molybdenum, vanadium and niobium.<sup>[164-166]</sup>

Also *M2* phase can be formed from antimony containing materials. The mainly valence state of antimony is III and following the Sb (III) cations should form  $\text{SbO}_3\text{E}$  trigonal pyramid groups. This result in  $[\text{Sb-O-Sb}]$  dimers formed in the hexagonal channels. Additionally Sb (V) cations are present in the *M2* phase, which cannot adopt a three-fold coordination. They have at least four oxygen neighbours forming  $\text{SbO}_4$  groups resulting in  $[\text{Sb-O}]_\infty$  entities in the hexagonal channels.<sup>[164]</sup>



### 1.5.3. Synthesis routes for MoV(Te,Sb)NbO<sub>x</sub> type catalysts

Several methods exist to prepare multi-component metal oxides of the type MoV(Te,Sb)NbO<sub>x</sub>. All methods have in common, that a precursor is obtained from metal salts, which is further calcined to obtain the final catalyst. The most common metal salts for catalyst preparation are ammonium para molybdate ((NH<sub>4</sub>)<sub>6</sub>Mo<sub>7</sub>O<sub>24</sub>), telluric acid (H<sub>6</sub>TeO<sub>6</sub>), vanadyl sulfate (VOSO<sub>4</sub> · x H<sub>2</sub>O), ammonium niobate oxalate ((NH<sub>4</sub>)NbO(C<sub>2</sub>O<sub>4</sub>)<sub>2</sub>) and antimony (III) sulfate (Sb<sub>2</sub>(SO<sub>4</sub>)<sub>3</sub>).<sup>[137, 138, 167-172]</sup> Further used metal oxides are tellurium dioxide (TeO<sub>2</sub>), vanadium (V) oxide (V<sub>2</sub>O<sub>5</sub>) and antimony (III) oxide (Sb<sub>2</sub>O<sub>3</sub>) and metallic tellurium.<sup>[158, 159, 173-175]</sup>

The different synthesis methods are described in the following:

#### Dry-up (evaporation) method<sup>[157, 160, 176]</sup>

For the dry-up method all precursors are dissolved in water followed by the removal of water by evaporation under decreased pressure (30 - 50 kPa) to obtain a precursor, that is calcined at 873 K in an inert atmosphere. Catalysts produced by this method often have phase impurities that decrease the catalytic performance.

#### Freeze drying / Spray drying<sup>[177, 178]</sup>

The freeze drying and spray drying are synthesis methods similar to the dry-up method. The water from the metal salt solution is in this case removed by freeze drying or by a spray dryer. In both cases a solid precursor is obtained that is calcined to the final catalyst. Catalysts obtained by both methods range from phase pure materials to materials with high fractions of different phases depending on the exact parameters for the synthesis. Accordingly the catalysts performances range from very good to no acrylic acid yield observable.

Hydrothermal synthesis <sup>[156, 160]</sup>

For the hydrothermal synthesis metal salts are dissolved in water and brought into a Teflon lined autoclave. The autoclave is exposed to hydrothermal conditions (448 K) for a specific time (1 – 10 days). The residue is separated with a suction filter and dried (353 K). The so obtained precursor is calcined as described in the previous methods. Catalysts synthesized by hydrothermal method have the advantage of very good phase purity. The disadvantage is the effort in preparation and due to material loss in precursor separation is the yield of catalyst lower than with the other methods.

Solid state synthesis <sup>[146, 160, 179]</sup>

The solid state synthesis is done by grinding metal salts to a homogeneous mixture that is calcined. This procedure needs the smallest effort for preparation, but good phase compositions are rarely obtained.

The hydrothermal reaction method is the best synthesis route to prepare phase pure mixed metal oxides for selective propane oxidation. Unfortunately it is also the most extensive method, which is undesirable for industrial production.

## **1.6. Scope of this thesis**

Multi component mixed metal oxides are of great interest for the selective oxidation of propane to acrylic acid. Up to now the yield for this reaction does not exceed 50% and therefore this process is not competitive with the today's used propene oxidation process.

The alkane C-H activation of the catalysts is also very low, complicating the use on an industrial scale. Also the formations of side products like acetic acid or deep oxidation to carbon dioxide lower the yields of acrylic acid. Understanding the effects of catalytic activity of the different phases and the reaction pathways that lead to the observable product distribution would be of great interest to synthesize catalysts that are competitive the today's propene oxidation systems on an economical base.

In this thesis the selective oxidation of propane to acrylic acid was investigated. The focus was a profound understanding of the macrokinetics of the catalyst. Therefore detailed kinetic measurements are the bases for developed models. Characterization was supplemented by a variety of physicochemical techniques. From these results the conclusions were drawn and a macrokinetic model was developed to describe the different processes on the catalyst. From this model further conclusions on the nature of active site could be drawn. The experimental specifications are described in chapter 2.

The phase formation of MoVTeNb oxides depending on the metal composition is described in chapter 3. Catalysts with variation of the metal composition in the synthesis mixture were synthesized and tested in the selective oxidation. Further characterization was done by XRD for phase determination, ICP-AES for metal composition of the final catalysts and nitrogen sorption for surface area determination.

Chapter 4 deals with the macrokinetics of the selective oxidation of propane over MoVTeNb oxide catalysts. For this purpose the reaction kinetics of each intermediate in the reaction network were determined and a macrokinetic model for the propane oxidation was developed that explains the product distribution at different contact times. This model can also be used to identify changes of the reaction kinetics caused by variations in synthesis. Together with further characterization by XRD, ICP-AES and BET and conclusions on the active centers of MoVTeNb oxides for oxidation reaction could be drawn.

Chapter 5 focuses on the exchange of tellurium by antimony in the multi component metal oxides. For this purpose catalysts of the composition  $\text{MoVSbO}_x$  were synthesized and tested for the selective oxidation of propane. In addition to the previous described characterization  $\text{NH}_3$ -TPD were done to determine acid site concentrations to explain changes of the in the reaction network of MoVSb oxides in contrast to MoVTeNb oxide catalysts.

Chapter 6 gives a summary of the most important results and conclusions.

## 1.7. References

- [1] H.-J. Arpe, *Industrielle Organische Chemie*, 6. ed., Wiley-VCH, Weinheim, **2007**.
- [2] M. Baerns, O. Buyevskaya, *Catalysis Today* **1998**, *45*, 13.
- [3] *BP Statistical Review of World Energy June 2008*, **2008**.
- [4] R. A. Periana, D. J. Taube, E. R. Evitt, D. G. Loffler, P. R. Wentrcek, G. Voss, T. Masuda, *Science* **1993**, *259*, 340.
- [5] V. Koß, *Umweltchemie: Eine Einführung für Studium und Praxis*, 1. ed., Springer, Berlin, **2008**.
- [6] T. F. Narbeshuber, H. Vinek, J. A. Lercher, *J. Catal.* **1995**, *157*, 388.
- [7] J. A. Lercher, R. A. v. Santen, H. Vinek, *Catal. Lett.* **1994**, *27*, 91.
- [8] G. Centi, F. Cavani, F. Trifiro, *Selective Oxidation by Heterogeneous Catalysis*, Kluwer Academic / Plenum Publishers, New York, Boston, Dordrecht, London, Moscow, **2001**.
- [9] J. M. M. Millet, *Top. Catal.* **2006**, *38*, 83.
- [10] F. Cavani, F. Trifiro, *Catal. Today* **1999**, *51*, 561.
- [11] B. Grzybowska-Swierkosz, *Top. Catal.* **2000**, *11*, 23.
- [12] T. Ushikubo, K. Oshima, A. Kayou, M. Vaarkamp, M. Hatano, *J. Catal.* **1997**, *169*, 394.
- [13] J. Holmberg, R. K. Grasselli, A. Andersson, *Top. Catal.* **2003**, *23*, 55.
- [14] R. K. Grasselli, *Catal. Today* **1999**, *49*, 141.
- [15] F. Eder, J. A. Lercher, *J. Phys. Chem.* **1997**, *101*, 1273.
- [16] P. Botella, J. M. L. Nieto, B. Solsona, A. Mifsud, F. Marquez, *J. Catal.* **2002**, *209*, 445.
- [17] J. M. M. Millet, H. Roussel, A. Pigamo, J. L. Dubois, J. C. Jumas, *Appl. Catal. A* **2002**, *232*, 77.
- [18] W. Ueda, D. Vitry, T. Katou, *Catal. Today* **2005**, *99*, 43.
- [19] M. M. Lin, *Appl. Catal. A* **2003**, *250*, 305.
- [20] M. M. Lin, *Appl. Catal. A* **2003**, *250*, 287.
- [21] W. A. Goddard, K. Chenoweth, S. Pudar, A. C. T. v. Duin, M. J. Cheng, *Top. Catal.* **2008**, *50*, 2.
- [22] I. E. Wachs, *Catal. Today* **2005**, *100*, 79.
- [23] M. D. Argyle, K. Chen, E. Iglesia, A. T. Bell, *J. Phys. Chem. B* **2005**, *109*, 2414.
- [24] M. D. Argyle, K. Chen, C. Resini, C. Krebs, E. Iglesia, A. T. Bell, *J. Phys. Chem. B* **2004**, *108*, 2345.
- [25] D. E. Keller, S. M. K. Airaksinen, A. O. Krause, B. M. Weckhuysen, D. C. Koningsberger, *J. Am. Chem. Soc.* **2007**, *129*, 3189.
- [26] G. Deo, I. E. Wachs, *J. Catal.* **1994**, *146*, 323.
- [27] X. Gao, M. A. Banares, I. E. Wachs, *J. Catal.* **1999**, *188*, 325.
- [28] X. Gao, J.-M. Jehng, I. E. Wachs, *J. Catal.* **2002**, *209*, 43.
- [29] Z. Zhao, X. Gao, I. E. Wachs, *J. Phys. Chem. B* **2003**, *107*, 6333.
- [30] S. Feyel, D. Schröder, X. Rozanska, J. Sauer, H. Schwarz, *Angew. Chem., Int. Ed.* **2006**, *45*, 4677.
- [31] S. Feyel, D. Schröder, H. J. Schwarz, *J. Phys. Chem. A* **2006**, *110*, 2647.
- [32] X. Rozanska, J. Sauer, *J. Phys. Chem. A* **2009**, *113*, 11586.
- [33] X. Rozanska, J. Sauer, *Int. J. Quantum Chem.* **2008**, *108*, 2223.

- [34] S. Feyel, D. Schröder, X. Rozanska, J. Sauer, H. Schwarz, *Angew. Chem.* **2006**, *118*, 4793.
- [35] X. Rozanska, R. Fortrie, J. Sauer, *J. Phys. Chem. C* **2007**, *111*, 6041.
- [36] M. J. Cheng, K. Chenoweth, J. Oxgaard, A. v. Duin, W. A. Goddard, *J. Phys. Chem. C* **2007**, *111*, 5115.
- [37] X. Xu, F. Faglioni, W. A. Goddard, *J. Phys. Chem. A* **2002**, *106*, 7171.
- [38] H. Fu, Z. P. Liu, Z. H. Li, W. N. Wang, K. N. Fan, *Journal of the American Chemical Society* **2006**, *128*, 11114.
- [39] X. Rozanska, E. V. Kondratenko, J. Sauer, *J. Catal.* **2008**, *256*, 84.
- [40] V. N. Shetti, M. J. Rani, D. Srinivas, P. Ratnasamy, *J. Phys. Chem. B* **2006**, *110*, 677.
- [41] D. Srinivas, P. Ratnasamy, *Stud. Surf. Sci. Catal.* **2007**, *170*, 1205.
- [42] A. V. Ramaswamy, S. Sivasanker, P. Ratnasamy, *Microporous Mesoporous Mater.* **1994**, *2*, 451.
- [43] C. Sievers, A. Onda, A. Guzman, K. S. Ollinger, R. Olindo, J. A. Lercher, *J. Phys. Chem. C* **2007**, *111*, 210.
- [44] W. Fan, R. G. Duan, T. Yokoi, P. Wu, Y. Kubota, T. Tatsumi, *J. Am. Chem. Soc.* **2008**, *130*, 10150.
- [45] G. B. Shul'pin, T. Sooknoi, V. B. Romakh, G. Süß-Fink, L. S. Shul'pina, *Tetrahedron Lett.* **2006**, *47*, 3071.
- [46] C. B. Kouw, C. B. Dartt, J. A. Labinger, M. E. Davis, *J. Catal.* **1994**, *149*, 195.
- [47] K. Chen, S. Xie, A. T. Bell, E. Iglesia, *J. Catal.* **2001**, *198*, 232.
- [48] G. Fu, X. Xu, X. Lu, H. Wan, *J. Phys. Chem. B* **2005**, *109*, 6416.
- [49] G. Fu, X. Xu, X. Lu, H. Wan, *J. Am. Chem. Soc.* **2005**, *127*, 3989.
- [50] K. D. Chen, A. T. Bell, E. Iglesia, *J. Phys. Chem. B* **2000**, *104*, 1292.
- [51] K. Chen, S. Xie, A. T. Bell, E. Iglesia, *J. Catal.* **2000**, *195*, 244.
- [52] J. A. Lercher, H. Noller, *J. Catal.* **1982**, *77*, 152.
- [53] H. Dai, A. T. Bell, E. Iglesia, *J. Catal.* **2004**, *221*, 491.
- [54] S. Yang, E. Iglesia, A. T. Bell, *J. Phys. Chem. B* **2006**, *110*, 2732.
- [55] E. Heracleous, A. A. Lemonidou, *J. Catal.* **2010**, *270*, 67.
- [56] M. M. Lin, *Appl. Catal. A* **2001**, *207*, 1.
- [57] P. Beato, A. Blume, F. Girgsdies, R. E. Jentoft, R. Schlögl, O. Timpe, A. Trunschke, G. Weinberg, Q. Basher, F. A. Hamid, S. B. A. Hamid, E. Omar, L. M. Salim, *Appl. Catal. A* **2006**, *307*, 137.
- [58] J. M. Oliver, J. M. L. Nieto, P. Botella, *Catal. Today* **2004**, *96*, 241.
- [59] P. Botella, E. Garcia-Gonzalez, J. M. L. Nieto, J. M. González-Calbet, *Solid State Sci.* **2005**, *7*, 507.
- [60] R. K. Grasselli, D. J. Buttrey, J. D. Burrington, A. Andersson, J. Holmberg, W. Ueda, J. Kubo, C. G. Lugmair, A. F. V. Jr, *Top. Catal.* **2006**, *38*, 7.
- [61] P. Botella, E. García-González, A. Dejoz, J. M. L. Nieto, M. I. Vázquez, J. González-Calbet, *J. Catal.* **2004**, *225*, 428.
- [62] T. Katou, D. Vitry, W. Ueda, *Catal. Today* **2004**, *96*, 235.
- [63] T. Katou, D. Vitry, W. Ueda, *Catal. Today* **2004**, *91-92*, 237.
- [64] R. K. Grasselli, D. J. Buttrey, P. D. Jr., J. D. Burrington, C. G. Lugmair, A. F. V. Jr., T. Weingand, *Catal. Today* **2004**, *91-92*, 251.
- [65] R. Balasubramanian, A. C. Rosenzweig, *Acc. Chem. Res.* **2007**, *40*, 573.
- [66] S. I. Chan, V. C.-C. Wang, J. C.-H. Lai, S. S.-F. Yu, P. P.-Y. Chen, K. H.-C. Chen, C.-L. Chen, M. K. Chan, *Angew. Chem., Int. Ed.* **2007**, *46*, 1992.
- [67] G. I. Panov, A. K. Uriarte, M. A. Rodkin, V. I. Sobolev, *Catal. Today* **1998**, *41*, 365.
- [68] M. J. Rice, A. K. Chakraborty, A. T. Bell, *J. Catal.* **2000**, *194*, 278.

- [69] J. S. Woertink, P. J. Smeets, M. H. Groothaert, M. A. Vance, B. F. Sels, R. A. Schoonheydt, E. I. Solomon, *Proc. Natl. Acad. Sci. U. S. A.* **2009**, *106*, 18909.
- [70] M. H. Groothaert, P. J. Smeets, B. F. Sels, P. A. Jacobs, R. A. Schoonheydt, *J. Am. Chem. Soc.* **2005**, *127*, 1394.
- [71] V. V. Guliants, S. A. Holmes, J. B. Benziger, P. Heaney, D. Yates, I. E. Wachs, *J. Mol. Catal. A: Chem.* **2001**, *172*, 265.
- [72] B. K. Hodnett, *Catal. Rev. Sci. Eng.* **1985**, *27*, 373.
- [73] G. Centi, F. Trifiro, J. R. Ebner, V. M. Franchetti, *Chem. Rev.* **1988**, *88*, 55.
- [74] Y. Zhang-Lin, M. Froissier, R. P. Sneed, J. C. Vedrine, J. C. Volta, *J. Catal.* **1994**, *145*, 256.
- [75] Y. Zhang-Lin, M. Froissier, J. C. Vedrine, J. C. Volta, *J. Catal.* **1994**, *145*, 267.
- [76] D. J. Thompson, I. M. Ciobica, B. K. Hodnett, R. A. v. Santen, M. O. Fanning, *Catal. Today* **2004**, *91-92*, 177.
- [77] M. Hävecker, R. W. Mayer, A. Knop-Gericke, H. Bluhm, E. Kleimenov, A. Liskowski, D. Su, R. Follath, F. G. Requejo, D. F. Ogletree, M. Salmeron, J. A. Lopez-Sanchez, J. K. Bartley, G. J. Hutchings, R. Schlögl, *J. Phys. Chem. B* **2003**, *107*, 4587.
- [78] F. Cavani, S. Luciani, E. D. Esposti, C. Cortelli, R. Leanza, *Chem. Eur. J.* **2010**, *16*, 1646.
- [79] S. Gaab, J. Find, T. E. Müller, J. A. Lercher, *Top. Catal.* **2007**, *46*, 101.
- [80] B. Tope, Y. Zhu, J. A. Lercher, *Catal. Today* **2007**, *123*, 113.
- [81] C. P. Kumar, S. Gaab, T. E. Müller, J. A. Lercher, *Top. Catal.* **2008**, *50*, 156.
- [82] G. A. Olah, B. Gupta, M. Farina, J. D. Felberg, W. M. Ip, A. Husain, R. Karpeles, K. Lammertsma, A. K. Melhotra, N. J. Trivedi, *J. Am. Chem. Soc.* **1985**, *107*, 7097.
- [83] S. G. Podkolzin, E. E. Stangland, M. E. Jones, E. Peringer, A. A. Lemonidou, J. A. Lercher, *J. Am. Chem. Soc.* **2007**, *129*, 2569.
- [84] E. Peringer, C. Tejuja, M. Salzinger, A. A. Lemonidou, J. A. Lercher, *Appl. Catal. A* **2008**, *350*, 178.
- [85] E. Peringer, S. G. Podkolzin, M. E. Jones, R. Olindo, J. A. Lercher, *Top. Catal.* **2006**, *38*, 211.
- [86] J. H. Lunsford, *Angew. Chem., Int. Ed.* **1995**, *34*, 970.
- [87] A. H. Kaddouri, N. D. Blasio, R. D. Rosso, *React. Kinet. Catal. Lett.* **2001**, *72*, 309.
- [88] K. D. Campbell, H. Zhang, J. H. Lunsford, *J. Phys. Chem.* **1988**, *92*, 750.
- [89] C. T. Au, H. He, S. Y. Lai, C. F. Ng, *Appl. Catal. A* **1997**, *159*, 133.
- [90] S. Sugiyama, K. Sogabe, T. Miyamoto, H. Hayashi, J. B. Moffat, *Catal. Lett.* **1996**, *42*, 127.
- [91] P. Ciambelli, L. Lisi, R. Pirone, G. Ruoppolo, G. Russo, *Catal. Today* **2000**, *61*, 317.
- [92] A. E. Schweizer, M. E. Jones, D. A. Hickman, WO Pat. 6 452 058, **2002**.
- [93] S. J. Conway, J. H. Lunsford, *J. Catal.* **1991**, *131*, 513.
- [94] S. J. Conway, D. J. Wang, J. H. Lunsford, *Appl. Catal. A* **1991**, *79*, L1.
- [95] S. Fuchs, L. Leveles, K. Seshan, L. Lefferts, A. Lemonidou, J. A. Lercher, *Top. Catal.* **2001**, *15*, 169.
- [96] S. Gaab, M. Machli, J. Find, R. K. Grasselli, J. A. Lercher, *Top. Catal.* **2003**, *23*, 151.
- [97] M. C. Wu, C. M. Truong, K. Coulter, D. W. Goodman, *J. Catal.* **1993**, *140*, 344.
- [98] T. König, G. H. Simon, U. Martinez, L. Giordano, G. Pacchioni, M. Heyde, H.-J. Freund, *ACS Nano* **2010**, *4*, 2150.
- [99] C. Copéret, *Chem. Rev.* **2010**, *110*, 656.
- [100] J. Joubert, A. Salameh, V. Krakoviack, F. Delbecq, P. Sautet, C. Copéret, J. M. Basset, *J. Phys. Chem. B* **2006**, *110*, 23944.

- [101] E. A. Pidko, R. A. v. Santen, E. J. M. Hensen, *Phys. Chem. Chem. Phys.* **2009**, *11*, 2893.
- [102] E. A. Pidko, E. J. M. Hensen, R. A. v. Santen, *J. Phys. Chem. C* **2007**, *111*, 13068.
- [103] H. Frei, *Science* **2006**, *313*, 309.
- [104] H. Tsubomura, R. S. Mulliken, *J. Am. Chem. Soc.* **1960**, *82*, 5966.
- [105] F. Blatter, H. Frei, *J. Am. Chem. Soc.* **1993**, *115*, 7501.
- [106] J. Xu, B. L. Mojet, J. G. v. Ommen, L. Lefferts, *J. Phys. Chem. B* **2004**, *108*, 15728.
- [107] J. Xu, B. L. Mojet, J. G. v. Ommen, L. Lefferts, *J. Catal.* **2005**, *232*, 411.
- [108] E. A. Pidko, J. Xu, B. L. Mojet, L. Lefferts, I. R. Subbotina, V. B. Kazansky, R. A. v. Santen, *J. Phys. Chem. B* **2006**, *110*, 22618.
- [109] J. Xu, B. L. Mojet, J. G. v. Ommen, L. Lefferts, *J. Phys. Chem. B* **2005**, *109*, 18361.
- [110] P. Li, Y. Xiang, V. H. Grassian, S. C. J. Larsen, *J. Phys. Chem. B* **1999**, *103*, 5058.
- [111] W. Reppe, *Neue Entwicklungen auf dem Gebiet der Chemie des Acetylen und Kohlendoxyds*, Springer, Berlin, Göttingen, Heidelberg, **1949**.
- [112] W. Nojiri, Y. Sakai, Y. Watanabe, *Catalysis Reviews Science and Engineering* **1995**, *37*, 145.
- [113] F. Cavani, F. Trifiro, *Applied Catalysis A* **1992**, *88*, 115.
- [114] T. Ushikubo, H. Nakamura, Y. Koyasu, S. Wajiki, US Patent 5,380,933, **1995**.
- [115] T. Ushikubo, H. Nakamura, Y. Koyasu, S. Wajiki, EP Patent 608.838 A2, **1994**.
- [116] J. J. Siegfried, *Journal of Political Economy* **1970**, *78*, 1378.
- [117] G. Landi, L. Lisi, G. Russo, *Journal of Molecular Catalysis A* **2005**, *239*, 172.
- [118] G. Landi, L. Lisi, J. C. Volta, *Journal of Molecular Catalysis A* **2004**, *222*, 175.
- [119] A. Costine, B. K. Hodnett, *Applied Catalysis A* **2005**, *290*, 9.
- [120] C. H. Bartholomew, R. J. Farrauto, *Fundamentals of industrial catalytic processes*, 2 ed., John Wiley & Sons, **2005**.
- [121] M. M. Lin, *Applied Catalysis A* **2001**, *207*, 1.
- [122] P. Mars, D. W. van Krevelen, *Chemical Engineering Science* **1954**, *3 supp.*, 41.
- [123] K. D. Chen, A. Khodakov, J. Yang, A. T. Bell, E. Iglesia, *Journal of Catalysis* **1999**, *186*, 325.
- [124] M. Ai, *Journal of Catalysis* **1989**, *101*, 389.
- [125] Z. Wang, W. Wei, G. Liu, G. Mao, D. Kuang, *Acta Petroleum Sinica* **1998**, *14*, 21.
- [126] R. Zhao, Z. Wu, Z. Wang, *Shiyu Huagong* **1995**, *24*, 157.
- [127] W. Li, K. Oshihara, W. Ueda, *Applied Catalysis A* **1999**, *182*, 357.
- [128] N. Mizuno, M. Tateishi, M. Iwamoto, *Applied Catalysis A* **1995**, *128*, L165.
- [129] W. Ueda, Y. Suzuki, *Chemistry Letters* **1995**, 541.
- [130] K. Nomiya, T. Takahashi, T. Shirai, M. Miwa, *Polyhedron* **1987**, *6*, 213.
- [131] R. K. Grasselli, *Journal of Chemical Education* **1986**, *63*, 216.
- [132] L. Luo, J. Labinger, M. Davis, in *Catalysis and Surface Science, Poster, 219th ACS Meeting*, **2000**.
- [133] M. Takahashi, S. To, S. Hirose, JP Patent 98,118,491, **1998**.
- [134] T. Ushikubo, Y. Koyasu, H. Nakamura, S. Wajiki, JP Patent 98,045,664, **1998**.
- [135] T. Ushikubo, K. Oshima, A. Kayo, T. Umezawa, K. Kiyono, I. Sawaki, EP Patent 529.853 A2, **1992**.
- [136] T. Ushikubo, I. Sawaki, K. Oshima, K. Inumaru, S. Kobayakawa, K. Kiyono, US Patent 5,422,328, **1995**.
- [137] P. Botella, J. M. L. Nieto, B. Solsona, *Catalysis Letters* **2002**, *78*, 383.
- [138] K. Oshihara, T. Hisano, W. Ueda, *Topics in Catalysis* **2001**, *15*, 153.
- [139] E. Balcells, F. Borgmeier, I. Grissted, H. G. Lintz, *Catalysis Letters* **2003**, *87*, 195.
- [140] E. Balcells, F. Borgmeier, I. Grissted, H. G. Lintz, F. Rosowski, *Applied Catalysis A* **2004**, *266*, 211.



- [141] M. H. Lin, T. B. Desai, F. W. Kaiser, P. D. Klugherz, *Catalysis Today* **2000**, *61*, 223.
- [142] L. Luo, J. A. Labinger, M. E. Davis, *Journal of Catalysis* **2001**, *200*, 222.
- [143] D. L. Stern, R. K. Grasselli, *Journal of Catalysis* **1997**, *167*, 560.
- [144] S. R. Logan, *Fundamentals of Chemical Kinetics*, Longman, Essex, **1996**.
- [145] E. K. Novakova, J. C. Vedrine, E. G. Derouane, *Journal of Catalysis* **2002**, *211*, 226.
- [146] P. Botella, E. Garcia-Gonzalez, J. M. L. Nieto, J. M. Gonzalez-Calbet, *Solid State Sciences* **2005**, *7*, 507.
- [147] P. DeSanto, D. J. Buttrey, R. K. Grasselli, C. G. Lugmair, A. F. Volpe, B. H. Toby, T. Vogt, *Topics in Catalysis* **2003**, *23*, 23.
- [148] P. DeSanto, D. J. Buttrey, R. K. Grasselli, C. G. Lugmair, A. F. Volpe, B. H. Toby, T. Vogt, *Zeitschrift Für Kristallographie* **2004**, *219*, 152.
- [149] H. Murayama, D. Vitry, W. Ueda, G. Fuchs, M. Anne, J. L. Dubois, *Applied Catalysis A* **2007**, *318*, 137.
- [150] J. N. Al-Saedi, V. K. Vasudevan, V. V. Guliants, *Catalysis Communications* **2003**, *4*, 537.
- [151] M. Aouine, J. L. Dubois, J. M. M. Millet, *Chemical Communications* **2001**, 1180.
- [152] H. Hibst, F. Rosowski, G. Cox, *Catalysis Today* **2006**, *117*, 234.
- [153] R. K. Grasselli, J. D. Burrington, D. J. Buttrey, P. DeSanto, C. G. Lugmair, A. F. Volpe, T. Weingand, *Topics in Catalysis* **2003**, *23*, 5.
- [154] W. Ueda, D. Vitry, T. Katou, *Catalysis Today* **2005**, *99*, 43.
- [155] J. M. M. Millet, H. Roussel, A. Pigamo, J. L. Dubois, J. C. Jumas, *Applied Catalysis A* **2002**, *232*, 77.
- [156] P. Botella, B. Solsona, A. Martinez-Arias, J. M. L. Nieto, *Catalysis Letters* **2001**, *74*, 149.
- [157] M. M. Lin, *Applied Catalysis A* **2003**, *250*, 287.
- [158] J. M. L. Nieto, P. Botella, B. Solsona, J. M. Oliver, *Catalysis Today* **2003**, *81*, 87.
- [159] X. L. Tu, N. Furuta, Y. Sumida, M. Takahashi, H. Niiduma, *Catalysis Today* **2006**, *117*, 259.
- [160] H. Watanabe, Y. Koyasu, *Applied Catalysis A* **2000**, *194*, 479.
- [161] M. Baca, M. Aouine, J. L. Dubois, J. M. M. Millet, *Journal of Catalysis* **2005**, *233*, 234.
- [162] R. K. Grasselli, *Catalysis Today* **2005**, *99*, 23.
- [163] R. K. Grasselli, D. J. Buttrey, J. D. Burrington, A. Andersson, J. Holmberg, W. Ueda, J. Kubo, C. G. Lugmair, A. F. Volpe, *Topics in Catalysis* **2006**, *38*, 7.
- [164] J. M. M. Millet, M. Baca, A. Pigamo, D. Vitry, W. Ueda, J. L. Dubois, *Applied Catalysis A* **2003**, *244*, 359.
- [165] M. Baca, J. M. M. Millet, *Applied Catalysis A* **2005**, *279*, 67.
- [166] O. V. Safonova, B. Deniau, J. M. M. Millet, *Journal of Physical Chemistry B* **2006**, *110*, 23962.
- [167] W. Ueda, D. Vitry, T. Katou, *Catalysis Today* **2004**, *96*, 235.
- [168] V. V. Guliants, R. Bhandari, J. N. Al-Saedi, V. K. Vasudevan, R. S. Soman, O. Guerrero-Perez, M. A. Banares, *Applied Catalysis A* **2004**, *274*, 123.
- [169] M. M. Lin, *Applied Catalysis A* **2003**, *250*, 305.
- [170] P. Botella, J. M. L. Nieto, B. Solsona, A. Mifsud, F. Marquez, *Journal of Catalysis* **2002**, *209*, 445.
- [171] E. K. Novakova, J. C. Vedrine, E. G. Derouane, *Journal of Catalysis* **2002**, *211*, 235.
- [172] W. Ueda, K. Oshihara, D. Vitry, T. Hisano, Y. Kayashima, *Catalysis Surveys from Japan* **2002**, *6*, 33.
- [173] P. Botella, P. Concepcion, J. M. Lopez Nieto, Y. Moreno, *Catalysis Today* **2005**, *99*, 51.

- 
- [174] F. Ivars, P. Botella, A. Dejoz, J. M. L. Nieto, P. Concepcion, M. I. Vazquez, *Topics in Catalysis* **2006**, 38, 59.
- [175] G. Y. Popova, T. V. Andrushkevich, G. I. Aleshina, L. M. Plyasov, M. I. Khramov, *Applied Catalysis A* **2007**, 328, 195.
- [176] B. C. Zhu, H. B. Li, W. S. Yang, L. W. Lin, *Catalysis Today* **2004**, 93-95, 229.
- [177] P. Beato, A. Blume, E. Girgsdies, R. E. Jentoft, R. Schlogel, O. Timpe, A. Trunschke, G. Weinberg, Q. Basher, F. A. Hamid, S. B. A. Hamid, E. Omar, L. M. Salim, *Applied Catalysis A* **2006**, 307, 137.
- [178] A. Celaya Sanfiz, T. W. Hansen, A. Sakthivel, A. Trunschke, R. Schlogel, A. Knoester, H. H. Brongersma, M. H. Looi, S. B. A. Hamid, *Journal of Catalysis* **2008**, 258, 35.
- [179] S. A. Holmes, J. Al-Saeedi, V. V. Guliants, P. Boolchand, D. Georgiev, U. Hackler, E. Sobkow, *Catalysis Today* **2001**, 67, 403.

# *Chapter 2*

## *Experimental Section*

## **2.1. Standard preparation of MoV(Te,Sb)Nb oxides**

MoV(Te,Sb)Nb oxide catalysts were prepared with a hydrothermal method (compare chapter 1.5.3.). Used metal salts were ammonium para molybdate  $(\text{NH}_4)_6\text{Mo}_7\text{O}_{24} \cdot 4 \text{H}_2\text{O}$ , telluric acid  $\text{H}_6\text{TeO}_6$ , vanadyl sulfate  $\text{VOSO}_4 \cdot x \text{H}_2\text{O}$  and ammonium niobium oxalate  $(\text{NH}_4)\text{NbO}(\text{C}_2\text{O}_4)_2 \cdot x\text{H}_2\text{O}$ . All chemicals were from Aldrich or Fluka and were used as received. For the calculation of stoichiometries the molecular weights of ammonium para molybdate and telluric acid were used, whereas for vanadyl sulfate and ammonium niobium oxalate this method was not possible, due to the unknown amount of water. For calculation of the needed amount of vanadium and niobium salt the information of the metal content from analysis available from the vendor was used.

The synthesis was done in a Teflon lined tube. In this way decanting of the synthesis gel was not required. The tube was heated in an oil bath to 353 K. 50 ml ultra pure water was filled into the teflon tube and the calculated amount of ammonium para molybdate was added under magnetic stirring. Telluric acid was dissolved in approximately 10 ml water and was added to the molybdate solution drop wise, resulting in a clear solution. Vanadylsulfate  $\text{VOSO}_4 \cdot x \text{H}_2\text{O}$  was dissolved in 10 ml water. To improve solubility the solution was heated on a hotplate to 353 K and then slowly (30 min) added into the teflon tube. In result the color of the solution becomes black. The ammonium niobium oxalate  $(\text{NH}_4)\text{NbO}(\text{C}_2\text{O}_4)_2 \cdot x\text{H}_2\text{O}$  was also added as a heated solution (353 K) within 5 minutes followed by 10 minutes stirring. The solution turned from black over dark purple to olive green during this time. Dissolved oxygen was removed by bubbling nitrogen for 2 minutes through the solution. Then the Teflon tube was closed by a teflon cap (the magnetic stir bar was left in the tube during hydrothermal treatment), mounted into a steel autoclave and heated to 448 K under autogenous pressure. After a defined time, the autoclave was removed from the oven and cooled with water to room temperature (approx. 15 min). The residue was filtrated, washed five times with ultra pure water and dried at 353 K for 16 h. The material was calcined 2 h at 523 K in static air and then 2 h at 873 K in nitrogen (heating rate 10 K/min).

Before testing the sample in the reaction set-up it was ground to powder and afterwards pressed with 61 MPa (using a round stainless steel pressing device with a diameter of 2.5 cm with a hydraulic press at 3 tons) and sieved to a particle size of 150 – 212  $\mu\text{m}$ .

Variations of this standard procedure are described in the particular chapter.

## 2.2. Catalytic testing

### 2.2.1. Experimental reactor set-up

Selective oxidation of propane was performed in a six-fold parallel continuous plug flow reactor at atmospheric pressure. The reactors consist of steel tubes with an inner diameter of 4 mm and 18 cm length and were connected to the set-up by VCR screwings with copper sealings. The reactors were equipped with a mantle of aluminum to enhance heat transfer between reactor and oven.

The feed consist of propane, oxygen, steam and nitrogen as balance and were controlled by Bronkhorst mass flow controllers. The evaporation of water was done with a commercial available Wagner CEM system (controlled evaporator mixer). The flow in each reactor was controlled by individual mass flow controllers, operated at elevated temperature. To stabilize the inlet pressure of the reactor MFCs a buffer of 250 ml volume was mounted between the feed system and the reactor MFCs. The reactor MFCs were calibrated at elevated temperature to nitrogen. The flow of feed can be calculated from the density and heat capacity of the relevant feed composition. Results for a feed composition of 5 / 10 / 65 / 25 (propane / O<sub>2</sub> / N<sub>2</sub> / H<sub>2</sub>O) are shown in Table 2.1 (mln are defined at 1013.25 hPa and 273.15 K).

**Table 2.1:** Conversion of N<sub>2</sub> - Feed flow: 5 / 10 / 65 / 25 (propane / O<sub>2</sub> / N<sub>2</sub> / H<sub>2</sub>O).

<b>Nitrogen flow</b> <b>[mln/min]</b>	<b>Feed flow</b> <b>[mln/min]</b>
20	17.24
15	12.90
10	8.61
5	4.32

The set-up is build within a box of Macrodon<sup>®</sup> (plexi glas) and PU insulation, heated to 373 K to prevent condensation of the water in the feed. The outlet of the reactors lead directly in to a second box heated to 423 K, to prevent condensation of oxidation products like acrylic acid. A 8-fold Valco valve was used to select the outlet of one reactor stream for GC analysis. The process flow diagram is shown in Figure 2.1.

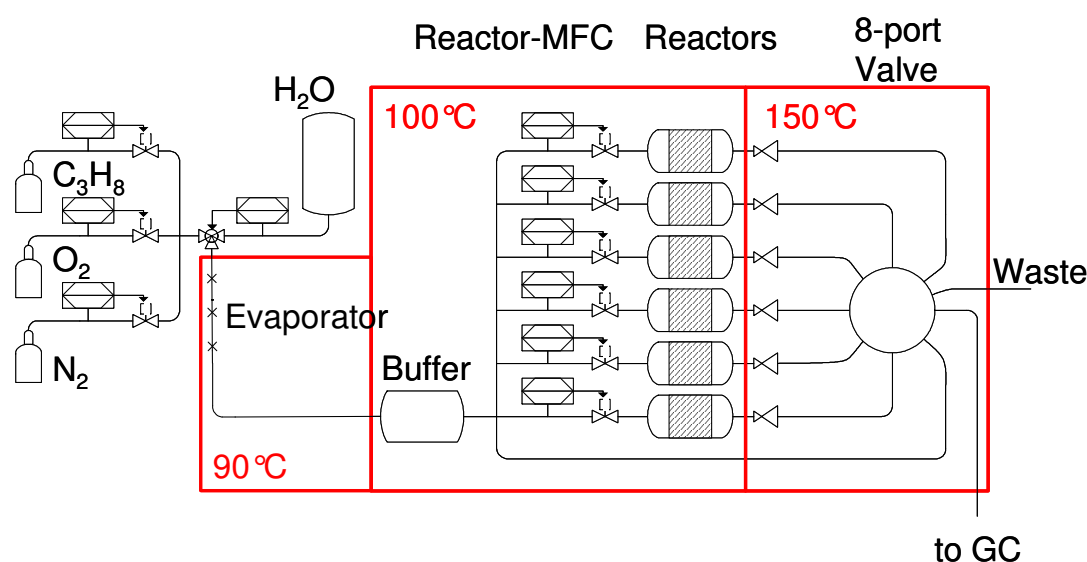


**Figure 2.1:** Process flow diagram of reaction set-up.

The GC sample loops were placed in an oven at 473 K and connected to the set-up by a heated 1/8 inch tube. The GC system was constructed by Shimadzu and is using two GCs for analysis. The first GC is equipped with a 25 m FFAP-Column and a flame ionization detector (FID). The high polarity of the column leads to a good separation of acetone, acrolein, acetic acid, propionic acid and acrylic acid.

The second GC is equipped with a precolumn with back flush using a 10-fold valve. In loading position the reactor flow is flushing to sample loop, carrier 1 goes onto the columns in the GC oven and carrier 2 back-flushes the precolumn (2 m HayeSep Q 60/80 mesh). When switching to dosing position, carrier 2 transports the sample from the sample loop over the precolumn to the columns in the GC oven. When oxygen, nitrogen, CO, CO<sub>2</sub>, propane and propene have passed the precolumn, the dosing valve is switched back to loading position and all components remaining on the precolumn are back-flushed. For the separation are used a 1.5 m silica column (800/100 mesh) and a 2 m molesieve column (60/80 mesh) that can be

connected in series to the silica column or bypassed. The analysis is performed by a TCD. The process flow diagram of the sample loops are shown in Figure 2.2.

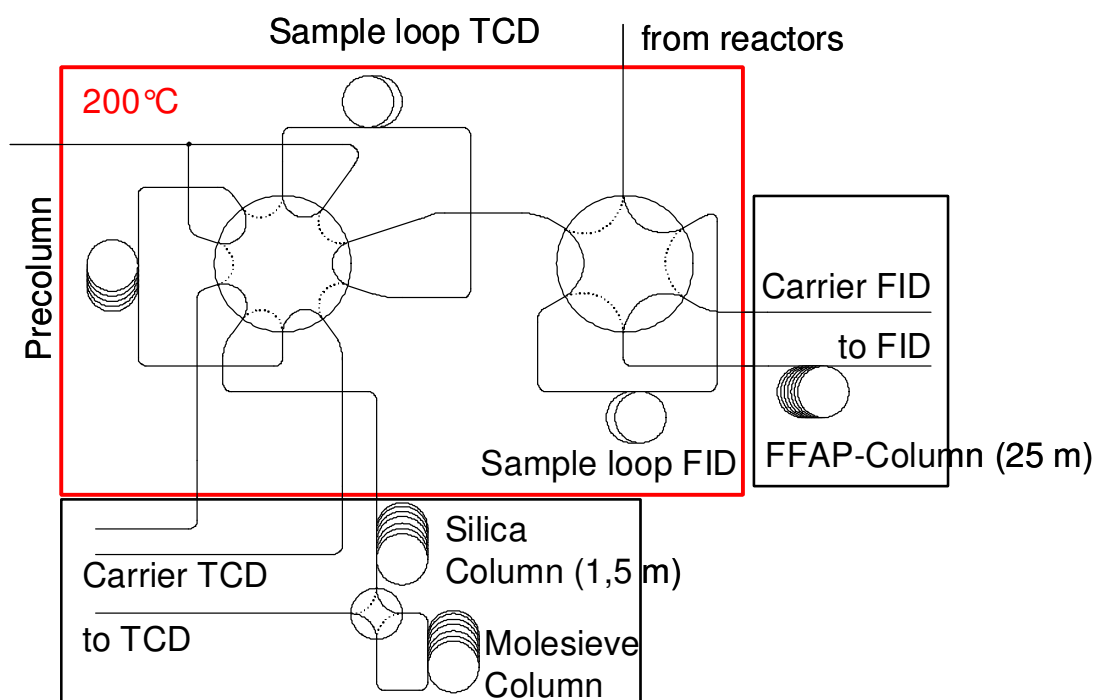


**Figure 2.2:** Flow scheme of GC analysis system.

The GC detectors were calibrated by using test gases with known compound concentrations. For the liquid compounds solutions with definite concentrations of acetone, acrolein, acetic acid, propionic acid and acrylic acid (fresh distilled) in pentane were evaporated in the analysis system. An important premise for achieving reproducibility for the GC runs is to stop the flow in the sample loops and waiting for 15 seconds before starting the GC run by switching the sample loop valves.

The temperatures of the reactors were controlled by *Eurotherm 2416* PID controller. The boxes and the connection to the GC oven were controlled by *Eurotherm 2131* PID controller. To achieve a constant temperature distribution over the whole box, three ventilators were built into the set-up. The MFCs are computer controlled with the interface program *Bronkhorst Flow DDE32*. The GC can be started by computer with a *Nudam relay device*. The *Eurotherm 2416* are also computer controlled. *Agilent VEE 8.0* was used as computer language for control of the set-up during experiment.

The reactors were filled with the catalysts in the following way: The bottom of the steel tube was closed with a 1 cm piece of quartz wool. A layer of 355 – 500  $\mu\text{m}$  silicon carbide was inserted, so that the catalyst layer starts at the bottom of the aluminum mantle. The sieved catalyst particles were mixed with a ten-fold amount of 210 – 355  $\mu\text{m}$  SiC and were covered with a second layer of 355 – 500  $\mu\text{m}$  SiC to the top of the reactor (Figure 2.3).

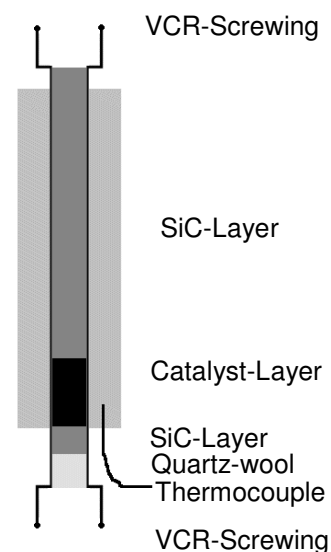


**Figure 2.3:** Reactor packing.

For testing of film diffusion all six reactors were filled with different amounts of catalysts and operated at same contact time and temperature. The results show that for flow rates higher than 4 mln/min no significant effects of mass transfer can be observed. Testing for pore diffusion can be neglected due to the absence of pores in mixed metal oxides.

### 2.2.2. Evaluation of kinetic data

In the oxidation reactions starting from propane, the mole number changes. Due to the fact that the sample loops of the GCs have a constant volume, measured concentrations have to be corrected by a normalizing factor. Because nitrogen is not involved in the reaction, the  $\text{N}_2$  concentration can be used as an internal standard to obtain the normalizing factor  $NF$  (Equation 2.1). Feed concentrations are marked with a subscript index  $0$ , concentrations from a reaction are marked with a subscript index  $R$ .

$$NF = \frac{[N_2]_0}{[N_2]_R} \quad (\text{Equation 2.1})$$

For low conversions and therefore small changes of the nitrogen concentration, the normalizing factor can also be calculated from the amount of products formed, based on the stoichiometry for each reaction (Equation 2.2).



$$NF = \frac{[O_2]_R + [N_2]_R + [CO]_R + [CO_2]_R + [Pr]_R + [Pe]_R + [Ace]_R + [Acr]_R + [AcA]_R + [Pr A]_R + [AA]_R}{100} \\ = \frac{\frac{[O_2]_R}{100} + \frac{[N_2]_R}{100} + \frac{[CO]_R}{100} \cdot \frac{9}{14} + \frac{[CO_2]_R}{100} \cdot \frac{6}{7} + \frac{[Pr]_R}{100} + \frac{[Pe]_R}{100} \cdot \frac{3}{4} + \frac{[Ace]_R}{100} + \frac{[Acr]_R}{100} \cdot \frac{5}{6} + \frac{[AcA]_R}{100} \cdot \frac{6}{5} + \frac{[Pr A]_R}{100} \cdot \frac{5}{4} + \frac{[AA]_R}{100}}{100}$$

(Equation 2.2)

The calculation from the nitrogen concentration is preferred for high conversions, because of high changes of the volume, whereas the second formula is more suitable for low conversions. The normalizing factor  $NF$  was used for normalizing the concentrations as shown by Equation 2.3. Normalized concentrations are marked with a subscript index  $N$ .

$$[component]_N = NF \cdot [component]_R \quad \text{(Equation 2.3)}$$

To verify the measurement the carbon-, hydrogen- and oxygen balance are calculated (Equation 2.4 – 2.6)

$$C - Balance = \frac{[CO]_N + [CO_2]_N + 3 \cdot [Ace]_N + 3 \cdot [Acr]_N + 2 \cdot [AcA]_N + 3 \cdot [Pr A]_N + 3 \cdot [AA]_N}{[CO]_0 + [CO_2]_0 + 3 \cdot [Pr]_0 + 3 \cdot [Pe]_0 + 3 \cdot [Ace]_0 + 3 \cdot [Acr]_0 + 2 \cdot [AcA]_0 + 3 \cdot [Pr A]_0 + 3 \cdot [AA]_0}$$

(Equation 2.4)

$$O - Balance = \frac{2 \cdot [O_2]_N + [CO]_N + 2 \cdot [CO_2]_N + [Ace]_N + [Acr]_N + 2 \cdot [AcA]_N + 2 \cdot [Pr A]_N + 2 \cdot [AA]_N + (100 - \sum components_N)}{2 \cdot [O_2]_0 + [CO]_0 + 2 \cdot [CO_2]_0 + [Ace]_0 + [Acr]_0 + 2 \cdot [AcA]_0 + 2 \cdot [Pr A]_0 + 2 \cdot [AA]_0 + (100 - \sum components_0)}$$

(Equation 2.5)

$$H - Balance = \frac{8 \cdot [Pr]_N + 6 \cdot [Pe]_N + 6 \cdot [Ace]_N + 4 \cdot [Acr]_N + 4 \cdot [AcA]_N + 6 \cdot [Pr A]_N + 4 \cdot [AA]_N + 2 \cdot (100 - \sum components_N)}{8 \cdot [Pr]_0 + 6 \cdot [Pe]_0 + 6 \cdot [Ace]_0 + 4 \cdot [Acr]_0 + 4 \cdot [AcA]_0 + 6 \cdot [Pr A]_0 + 4 \cdot [AA]_0 + 2 \cdot (100 - \sum components_0)}$$

(Equation 2.6)

All balances should be between 97% and 103%. Higher deviations indicate wrong component calibrations or errors during measurement.

The conversion is defined in the following way (Equation 2.7):

$$X = \frac{[Pr]_0 - [Pr]_N}{[Pr]_0} \quad \text{(Equation 2.7)}$$

For low conversions the determination of the difference of the propane concentration is getting difficult and therefore the conversion can also be calculated from the formation of the

formed products that can be measured with a higher accuracy. For this calculation Equation 2.8 is used:

$$X = \frac{\Delta[\text{CO}] + \Delta[\text{CO}_2] + 3 \cdot \Delta[\text{Pe}] + 3 \cdot \Delta[\text{Ace}] + 3 \cdot \Delta[\text{Acr}] + 2 \cdot \Delta[\text{AcA}] + 3 \cdot \Delta[\text{Pr A}] + 3 \cdot \Delta[\text{AA}]}{\Delta[\text{CO}] + \Delta[\text{CO}_2] + 3 \cdot [\text{Pr}]_N + 3 \cdot \Delta[\text{Pe}] + 3 \cdot \Delta[\text{Ace}] + 3 \cdot \Delta[\text{Acr}] + 2 \cdot \Delta[\text{AcA}] + 3 \cdot \Delta[\text{Pr A}] + 3 \cdot \Delta[\text{AA}]}$$

with  $\Delta[\text{component}] = [\text{component}]_N - [\text{component}]_0$  (Equation 2.8)

The selectivities are defined by Equation 2.9:

$$S = \frac{[\text{component}]_N - [\text{component}]_0}{[\text{Pr}]_0 - [\text{Pr}]_N} \cdot \frac{v_{\text{component}}}{3} \quad (\text{Equation 2.9})$$

with  $v_{\text{component}}$  is the number of carbon atoms of the component molecule

For low conversions the error of the propane measurement is higher, a calculation of the selectivity can also be done from the concentrations of formed products (Equation 2.10):

$$S = \frac{[\text{component}]_N - [\text{component}]_0}{\frac{\Delta[\text{CO}]}{3} + \frac{\Delta[\text{CO}_2]}{3} + \Delta[\text{Pe}] + \Delta[\text{Ace}] + \Delta[\text{Acr}] + \frac{2}{3} \cdot \Delta[\text{AcA}] + \Delta[\text{Pr A}] + \Delta[\text{AA}]} \cdot \frac{v_{\text{component}}}{3}$$

with  $\Delta[\text{component}] = [\text{component}]_N - [\text{component}]_0$  and (Equation 2.10)

$v_{\text{component}}$  is the number of carbon atoms of component

Yields are defined in the following way (Equation 2.11):

$$Y = \frac{[\text{component}]_N - [\text{component}]_0}{[\text{Pr}]_0} \cdot \frac{v_{\text{component}}}{3} \quad (\text{Equation 2.11})$$

with  $v_{\text{component}}$  is the number of carbon atoms of component molecule

Analog to the calculations of the selectivity for low propane conversions, yields can also be calculated from product formation (Equation 2.12):

$$S = \frac{[\text{component}]_N - [\text{component}]_0}{\frac{\Delta[\text{CO}]}{3} + \frac{\Delta[\text{CO}_2]}{3} + [\text{Pr}] + \Delta[\text{Pe}] + \Delta[\text{Ace}] + \Delta[\text{Acr}] + \frac{2}{3} \cdot \Delta[\text{AcA}] + \Delta[\text{Pr A}] + \Delta[\text{AA}]} \cdot \frac{v_{\text{component}}}{3}$$

with  $\Delta[\text{component}] = [\text{component}]_N - [\text{component}]_0$  and (Equation 2.12)

$v_{\text{component}}$  is the number of carbon atoms of component

### 2.3. Characterization of catalysts

X-ray diffraction patterns were collected on a Philips X'pert instrument at the energy of the Cu K $_{\alpha}$ -line. A Ni-filter was installed to remove the Cu K $_{\beta}$ -line. The XRD were measured between 2 $\theta$  angles of 5 and 70 ° with a step size of 0.017 ° and a scan speed of 115 s per step with a X'Cellerator semiconductor detector.

BET surface areas were determined by N $_2$  adsorption–desorption at 77 K using a Sorptomatic 1990 Series instrument after activation of the sample in vacuum at 523 K.

ICP-AES was measured with a Spectroflame Module. The samples were decomposed by heating 50 mg catalysts with 250 mg Soda – potash mixture in a ceramic crucible to red heat for 15 minutes. After cool down the melt is dissolved in water, 1 ml concentrated nitric acid and 1 ml 15% hydrofluoric acid and stirred for one hour. The solution is transferred to a 100 ml flask filled half with ultra pure water with an addition of 5 ml conc. HNO $_3$ . The crucible is rinsed again with 1 ml conc. HNO $_3$  and the flask is filled up with ultra pure water. Calibrations were done with commercial available ICP multi-element standard dilutions in 1 N HNO $_3$  with additional 0.15% HF.

Ammonia-TPD was measured with a six-fold vacuum TPD system, with one hour activation at 523 K, one hour ammonia loading at 1 mbar and two hour outgasing. TPD was carried out with a heating rate of 7 K/min up to 573 K for tellurium containing materials respectively 773 K for antimony containing materials. The desorbed species were detected by MS. A H-MFI zeolite with an acid site concentration of 360  $\mu\text{mol/g}$  was used as internal standard.



# Chapter 3

## *Phase Formation and selective Oxidation of Propane over MoVTeNbO<sub>x</sub> Catalysts with varying Compositions*

### *Abstract*

The selective oxidation of propane to acrylic acid on MoVTeNbO<sub>x</sub> catalysts with varying concentrations of vanadium, tellurium and niobium was investigated. Catalysts containing M1 phase were obtained over the compositional range of MoV<sub>0.14-0.22</sub>Te<sub>0.1-0.2</sub>Nb<sub>0.1-0.2</sub>O<sub>x</sub>. Vanadium containing sites in the M1 phase are drastically more active for propane activation than in other materials studied. The catalytic activity is directly correlated to its fraction in the overall material and in particular the M1 phase. High concentrations of tellurium induce the formation of the M2 phase decreasing so the overall activity of the catalysts. The intrinsic activity of the M1 phase is, however, independent of the tellurium concentration. Although the presence of the M1 phase is not a stringent requirement for the oxidative dehydrogenation of propane to propene, it is required to oxidize the intermediately formed propene with high selectivity to acrylic acid. The active sites for propane activation and propene oxidation are structurally coupled, because the ratio between the rates of the two reactions was always 1 : 25. Oxygen defect sites in mixed oxides seem to enhance interaction with acrylic acid and lead to decarboxylation and total oxidation.

### 3.1. Introduction

Acrylic acid is widely used as monomer for special application in polymers and its demand grows steadily at a high rate. A direct route from propane to acrylic acid is, therefore, of potential economic interest in order to replace the currently used two step oxidation from propene to acrylic acid.<sup>[1-3]</sup> The balance between high activity in the activation of the C-H bond of propane required for the transformation to propene and high selectivity in the conversion of propene to acrylic acid in order to prevent side product formation or deep oxidation to CO<sub>x</sub>, are the boundary conditions required for a catalyst in a process that has sufficient productivity and selectivity to compete with the current technology. In the conventional oxidation of propene to acrylic acid these demands are addressed by using a two-step process applying different catalysts and reaction temperatures for the oxidation of propene (BiMo oxide at 600 K) and the subsequent oxidation of acrolein into acrylic acid (MoVW oxide at 520 K).<sup>[2, 4]</sup>

Multi-component mixed metal oxides of the type MoVTeNbO<sub>x</sub> have been reported to be the most promising catalysts for the direct oxidation of propane to acrylic acid. Yields up to 48% at temperatures between 620 and 720 K have been documented in the open literature.<sup>[5, 6]</sup> Even considering that the yields could be significantly higher in proprietary industrial experiments, the productivity and yield are far below the current process. Thus, it is important to understand the kinetic limitations to envisage a catalyst design able to reach the required productivity for a single step process.

Two crystalline phases of MoVTeNbO<sub>x</sub> catalysts, known as M1 and M2 phases, are intensively discussed with respect to their rates in the oxidation of propane to acrylic acid.<sup>[7-9]</sup> Depending upon preparation conditions, the final catalyst crystallizes in the M1 or M2 phase or as a phase mixture.<sup>[9]</sup> The M1 phase consists of octahedra with molybdenum and vanadium centers connected via corner sharing oxygen atoms that form a structure with periodic layers and channels perpendicular to the *ab* plane (see Figure 3.1). Niobium is located inside the smallest channels, formed from five octahedra, whereas tellurium occupies channels formed from six or seven octahedra.<sup>[10]</sup> The existence of metals in a reduced oxidation state (V<sup>4+</sup> or Mo<sup>5+</sup>) in MoVTeNbO<sub>x</sub> crystallite appears to be essential for reaching a high activity for the propane activation.<sup>[11]</sup> It was shown that a catalyst (Mo-V-O) consisting of crystalline orthorhombic phase formed by molybdenum and vanadium is also able to activate propane.<sup>[12]</sup>

However, it is less selective for the formation of acrylic acid yielding large amounts of acetic acid and  $\text{CO}_x$ .

The M2 phase consists of periodic layers formed from oxygen terminated octahedra with molybdenum, vanadium and niobium centers. Tellurium occupies positions in the hexagonal channels. The stoichiometric composition of the M1 phase is  $\text{Te}_2\text{OM}_{20}\text{O}_{56}$  ( $\text{M} = \text{Mo}, \text{V}, \text{Nb}$ ) and of the M2 phase  $\text{TeM}_3\text{O}_9$  ( $\text{M} = \text{Mo}, \text{V}, \text{Nb}$ ). Details of the synthesis procedure and most suitable reactants/precursors for the synthesis are still under discussion.<sup>[13-17]</sup> The effects of each preparation step on the specific catalytic properties of the M1 and M2 phases and especially effects resulting from mixtures between both<sup>[18]</sup> as well as the details of the active sites and their reactivities have been discussed in the recent literature.<sup>[19]</sup>

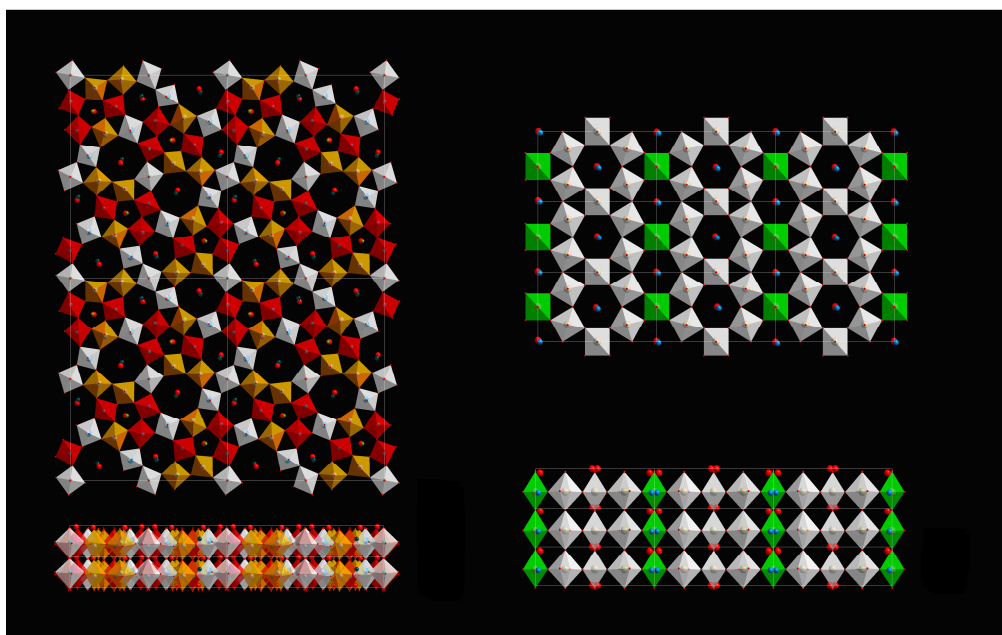
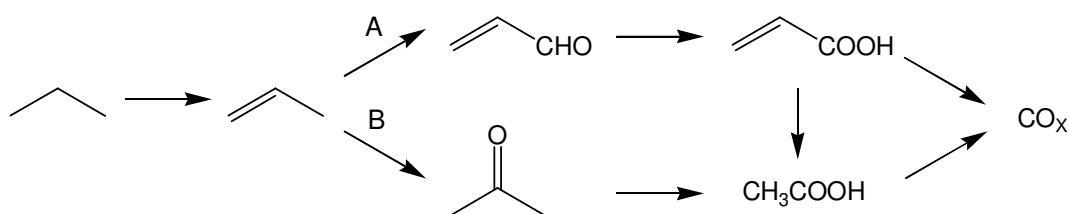


**Figure 3.1:** Structural models of orthorhombic M1 phase (left; red:  $\text{Mo}^{6+}$ , orange:  $\text{Mo}^{5+}$ , white: Mo or V) and pseudo hexagonal M2 phase (right; white: Mo/V, green: Mo/Nb) of  $\text{MoVTeNbO}_x$  catalysts.

The reaction network proposed for the oxidation of propane to acrylic acid is shown in Scheme 3.1.<sup>[20]</sup> Oxidative dehydrogenation of propane to propene is the first step followed by two parallel pathways. The first one (pathway A) proceeds over acrolein to acrylic acid, the second one (pathway B) over acetone to acetic acid. The final products of both pathways are the deep oxidation products  $\text{CO}$  and  $\text{CO}_2$  (denoted in the following with  $\text{CO}_x$ ). Acrylic acid can also be further oxidized to acetic acid and  $\text{CO}_x$  by functionalizing the  $\text{C}=\text{C}$  double bond

followed by elimination of CO or CO<sub>2</sub>. Note that direct reaction pathways to CO<sub>x</sub>, caused by the presence of unselective catalytic sites, also exist for propane and all intermediates (not shown in Scheme 3.1 due to clarity of the figure).



**Scheme 3.1:** Proposed reaction network in the selective oxidation of propane over MoVTenbO<sub>x</sub> catalysts.

As a first step towards understanding the kinetic limitations of the selective oxidation of propane to acrylic acid, we explore here the influence of vanadium, niobium and tellurium on the phase formation and the quantitative and qualitative aspects of the catalytic properties using a series of catalysts with a controlled variation of the composition.



## 3.2. Experimental

### 3.2.1. Catalyst preparation

Ammonium heptamolybdate,  $(\text{NH}_4)_6\text{Mo}_7\text{O}_{24} \cdot 4\text{H}_2\text{O}$ , was dissolved together with telluric acid,  $\text{H}_6\text{TeO}_6$ , in 50 ml bidistilled water and the solution was dried at 353 K for 24 h. The resulting white molybdotellurate complex was mixed with 50 ml water and heated to 353 K. A solution of vanadyl sulfate,  $\text{VO}_2\text{SO}_4 \cdot \text{H}_2\text{O}$ , (10 ml) was added drop wise within 30 min resulting in a black solution. Ammonium niobium oxalate  $(\text{NH}_4)_2\text{NbO}(\text{C}_2\text{O}_4)_2 \cdot x\text{H}_2\text{O}$  was added as solution and after 15 min of stirring the slurry was transferred to a PTFE lined autoclave and heated to 448 K under autogenous pressure. After 72 h the autoclave was removed from the oven and cooled with water to room temperature. The residue was filtered, washed five times with bidistilled water and dried at 353 K for 16 h. The material was calcined for 2 h at 523 K in static air and then for 2 h at 873 K in  $\text{N}_2$  (heating rate 10 K/min). Before reaction, the sample was ground and the fraction of particles with a size between 150 and 212  $\mu\text{m}$  was used. All precursors were obtained from Sigma-Aldrich or Fluka and were used without further purification.

### 3.2.2. Catalyst characterization

X-ray diffraction patterns were collected on a Philips X'pert instrument using the  $\text{Cu K}\alpha$ -line. A Ni-filter was installed to remove the  $\text{Cu K}\beta$ -line. XRD were measured between  $2\theta$  angles of 5 and 70 ° with a step size of 0.017 ° and a scan speed of 115 s per step. Phase formations were determined due to measured  $2\theta$  angles reflexes and relative signals. The fraction of M1 phase was calculated by integration of the major M1 reflexes using the concentration of the M1 phase in entry No. 4 of Table 1 as external standard (the composition in that sample has been determined by Rietveld analysis).

The BET surface areas were determined by  $\text{N}_2$  adsorption - desorption at 77 K using a Sorptomatic 1990 Series instrument after activation of the sample in vacuum at 523 K.

The chemical composition was measured by ICP-AES with a Spectroflame Instrument after decomposition of the materials by heating with Soda – potash.

The composition and structural properties of the catalysts are compiled in Table 3.1. In column Catalyst is shown the used metal composition in the synthesis mixture. It should be noted that the measured composition by ICP-AES are bulk composition and surface composition may differ, but changes metal ratios in the bulk material should also lead to changes of the metal ratios on the surface.

**Table 3.1:** Chemical compositions and characterizations of MoVTeNbO<sub>x</sub> catalysts.

No.	Fraction of metal cations in synthesis mixture	Fraction of metal cations in sample measured by ICP	Spec. surf. area [m <sup>2</sup> ·g <sup>-1</sup> ]	M1 Phase content [%]	Phases present
1	MoV <sub>0.07</sub> Te <sub>0.17</sub> Nb <sub>0.1</sub> O <sub>x</sub>	MoV <sub>0.13</sub> Te <sub>0.27</sub> Nb <sub>0.38</sub> O <sub>x</sub>	1.5	0	MoV <sub>0.22</sub> Nb <sub>0.1</sub> O <sub>x</sub> , V <sub>0.95</sub> Mo <sub>0.97</sub> O <sub>5</sub> , amorphous material
2	MoV <sub>0.14</sub> Te <sub>0.17</sub> Nb <sub>0.1</sub> O <sub>x</sub>	MoV <sub>0.16</sub> Te <sub>0.17</sub> Nb <sub>0.24</sub> O <sub>x</sub>	5.9	64	MoVTeNbO <sub>x</sub> -M1, amorphous material
3	MoV <sub>0.22</sub> Nb <sub>0.1</sub> O <sub>x</sub>	MoV <sub>0.21</sub> Nb <sub>0.11</sub> O <sub>x</sub>	18.8	0	MoV <sub>0.22</sub> Nb <sub>0.1</sub> O <sub>x</sub> , V <sub>0.95</sub> Mo <sub>0.97</sub> O <sub>5</sub>
4	MoV <sub>0.22</sub> Te <sub>0.1</sub> Nb <sub>0.1</sub> O <sub>x</sub>	MoV <sub>0.24</sub> Te <sub>0.09</sub> Nb <sub>0.11</sub> O <sub>x</sub>	10.2	88.4	MoVTeNbO <sub>x</sub> -M1
5	MoV <sub>0.22</sub> Te <sub>0.17</sub> Nb <sub>0.1</sub> O <sub>x</sub>	MoV <sub>0.20</sub> Te <sub>0.18</sub> Nb <sub>0.17</sub> O <sub>x</sub>	11.4	69	MoVTeNbO <sub>x</sub> -M1, amorphous material
6	MoV <sub>0.22</sub> Te <sub>0.2</sub> Nb <sub>0.1</sub> O <sub>x</sub>	MoV <sub>0.29</sub> Te <sub>0.15</sub> Nb <sub>0.10</sub> O <sub>x</sub>	9.7	52	MoVTeNbO <sub>x</sub> -M1, MoVTeNbO <sub>x</sub> -M2
7	MoV <sub>0.22</sub> Te <sub>0.2</sub> Nb <sub>0.2</sub> O <sub>x</sub>	MoV <sub>0.23</sub> Te <sub>0.17</sub> Nb <sub>0.22</sub> O <sub>x</sub>	12.4	78	MoVTeNbO <sub>x</sub> -M1, amorphous material
8	MoV <sub>0.22</sub> Te <sub>0.2</sub> Nb <sub>0.3</sub> O <sub>x</sub>	MoV <sub>0.17</sub> Te <sub>0.14</sub> Nb <sub>0.32</sub> O <sub>x</sub>	6.6	13	amorphous material, MoVTeNbO <sub>x</sub> -M1
9	MoV <sub>0.22</sub> Te <sub>0.3</sub> Nb <sub>0.1</sub> O <sub>x</sub>	MoV <sub>0.20</sub> Te <sub>0.31</sub> Nb <sub>0.19</sub> O <sub>x</sub>	9.8	24	MoVTeNbO <sub>x</sub> -M2, MoVTeNbO <sub>x</sub> -M1
10	MoV <sub>0.22</sub> Te <sub>0.5</sub> Nb <sub>0.1</sub> O <sub>x</sub>	MoV <sub>0.14</sub> Te <sub>0.50</sub> Nb <sub>0.12</sub> O <sub>x</sub>	1.5	1	MoVTeNbO <sub>x</sub> -M2, TeMo <sub>5</sub> O <sub>16</sub>

### 3.2.3. Catalytic activity

The catalytic activity was investigated in a six-fold parallel reactor using 100 mg of catalyst in all experiments. Reaction temperature was 653 K with the feed flow varied between 3.75 and 17.24 ml·min<sup>-1</sup> under standard temperature and pressure. Contact times were calculated by the quotient of catalyst mass to volume flow at reaction conditions. The flow of the gaseous components of the feed consisting of propane (5%), oxygen (10%) and nitrogen (65%) were controlled by Bronkhorst mass flow controllers, the fraction of steam (20%) was controlled with a Bronkhorst liquid water mass flow controller. A Wagner CEM system (controlled evaporator mixer) was used for the evaporation of the water. The four components were mixed and fed to the reactors using individual heated mass flow controllers for each reactor. The reactors were 1/4" stainless steel tubes. The products were analyzed using two gas chromatographs (Shimadzu) equipped with TCD (columns: silica/molsieve) and FID (column: FFAP) detectors. At the beginning of the analysis the silica and molsieve column were used in consecutive mode for the analysis of oxygen, nitrogen and carbon monoxide. For the analysis of carbon dioxide, propane and propene the molsieve column was bypassed and the separation was done on the silica column only. The silica and the molsieve column were protected from organic acids by a pre-column (HayeSep Q) using a back flush configuration. Acetic acid and acrylic acid were separated on the FFAP column and analyzed by FID. The average carbon balance was 99.9% with a deviation of 1% between single measurements.

### 3.3. Results

#### 3.3.1. Variation of tellurium content in the synthesis gel

The tellurium concentration of the catalysts was varied in the range of  $\text{MoV}_{0.22}\text{Te}_y\text{Nb}_{0.1}\text{O}_x$  with  $y = 0.0$  to  $0.5$ . The XRD patterns of the samples are shown in Figure 3.2, the chemical compositions and the specific surface areas are compiled in Table 3.1.

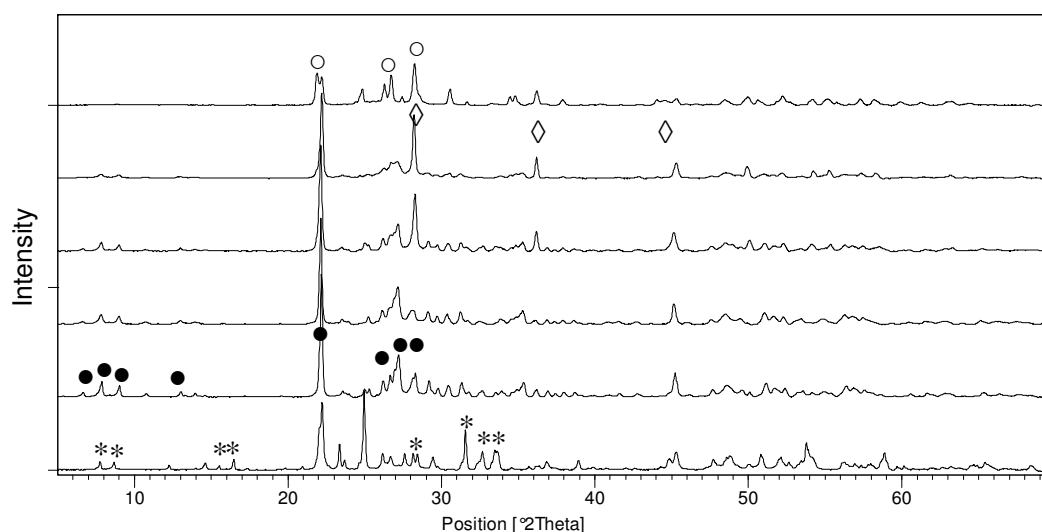


**Figure 3.2:** XRD of  $\text{MoV}_{0.22}\text{Te}_y\text{Nb}_{0.1}\text{O}_x$  with  $x = 0.0, 0.1, 0.17, 0.2, 0.3,$  and  $0.5$  (from bottom to top). M1 phase, indicated by (●), M2 phase indicated by (◇),  $\text{V}_{0.95}\text{Mo}_{0.97}\text{O}_5$  and  $(\text{Nb}_{0.09}\text{Mo}_{0.91})_5\text{O}_{14}$  indicated by (\*) and  $\text{TeMo}_5\text{O}_{16}$  indicated by (○).

The concentration of M1 phase was determined by integration of the XRD signals using entry 4 in Table 3.1 as standard. The tellurium free sample ( $\text{MoV}_{0.22}\text{Nb}_{0.1}\text{O}_x$ , Entry No. 3 in Table 3.1) consisted of the phases  $\text{V}_{0.95}\text{Mo}_{0.97}\text{O}_5$  and  $(\text{Nb}_{0.09}\text{Mo}_{0.91})_5\text{O}_{14}$  ( $2\theta = 7.8, 8.7, 25.1, 31.6, 32.7$  and  $33.7^\circ$ , marked with \* in Figure 3.2), while the presence of M1 phase was not observed. Addition of telluric acid into the synthesis gel led to the formation of  $\text{MoVTeNbO}_x$  M1 phase with peaks at  $2\theta = 7.9, 9.1$  and  $27.3$  (indicated by ●). For the synthesis compositions  $\text{MoV}_{0.22}\text{Te}_{0.1}\text{Nb}_{0.1}\text{O}_x$  (Entry No. 4) and  $\text{MoV}_{0.22}\text{Te}_{0.17}\text{Nb}_{0.1}\text{O}_x$  (Entry No. 5) 88.4 and 69% of M1 was observed. Other phases in  $\text{MoV}_{0.22}\text{Te}_{0.1}\text{Nb}_{0.1}\text{O}_x$  were M2 (6.7%),  $\text{Mo}_{18}\text{O}_{52}$  (3.1%) and  $\text{TeMo}_5\text{O}_{16}$  (1.8%). For the latter sample the remaining part was concluded to be amorphous mixed metal oxide phase. Higher concentrations of tellurium led to the formation of mixtures between the M1 and M2 phases ( $2\theta = 28.3$  and  $36.3$ , marked ◇ in Figure 3.2). With increasing tellurium concentrations the intensities of the M1 phase

decreased, until a mixture of the M2 phase and  $\text{TeMo}_5\text{O}_{16}$  ( $2\theta = 22.0, 24.9, 26.4, 26.8$ , indicated by  $\circ$  in Figure 3.2) was observed for the highest concentration of tellurium in the synthesis gel ( $\text{MoV}_{0.22}\text{Te}_{0.5}\text{Nb}_{0.1}\text{O}_x$ , Entry No. 10). The specific surface areas of these materials were between  $2$  and  $19 \text{ m}^2\cdot\text{g}^{-1}$  and decreased with increasing tellurium content.

Conversion levels of up to 55% were observed for the oxidation of propane. Due to the decrease of the surface areas with increasing tellurium concentration, the initial rates were normalized to the surface areas and plotted versus the tellurium concentration (Figure 3.3). The presence of Te leads to a sharp increase in the activity, which is attributed to the formation of the M1 phase. A further increase in the tellurium content results in a decrease of the activity due to the formation of the M2 phase and of  $\text{TeMo}_5\text{O}_{16}$ , which did not show activity in propane activation.

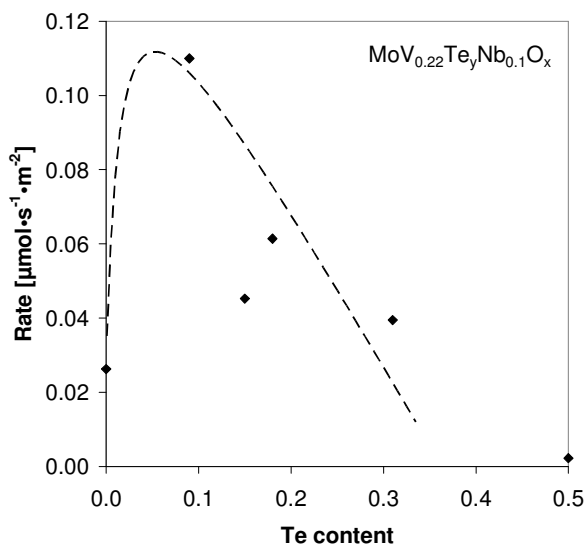


**Figure 3.3:** Normalized rates of propane conversion for  $\text{MoV}_{0.22}\text{Te}_y\text{Nb}_{0.1}\text{O}_x$ ,  $y = 0.0 - 0.5$ .

Propene yields as a function of the propane conversion are shown in Figure 3.4 (black labels) for  $\text{MoV}_{0.22}\text{Te}_y\text{Nb}_{0.1}\text{O}_x$  catalysts with  $y = 0.0 - 0.5$ . As expected propene is an intermediate product, which reacts further in a reaction with a higher rate constant and the yields are constant over a large range of conversion. At extremely short contact times (0.2% propane conversion) propene selectivities up to 95% were observed proving that propene is the major primary product of propane. Interestingly, the propene selectivities did not depend on the catalyst composition even for the material  $\text{MoV}_{0.22}\text{Nb}_{0.1}\text{O}_x$  (Entry No. 3 in Table 3.1), which does not contain the M1 phase, whereas the yields to acrylic acid show large differences between the catalysts (Figure 3.4, grey labels). Acrylic acid yields of 15 - 30% were observed for the catalysts containing M1 phase, whereas the other materials showed poor yields (< 5%). The decrease of the yields to acrylic acid indicates that it is a secondary, but instable product that can be further oxidized to  $\text{CO}_x$ . The yields of the main products (propene, acrylic acid and  $\text{CO}_x$ ) as function of the propane conversion for  $\text{MoV}_{0.22}\text{Te}_{0.17}\text{Nb}_{0.1}\text{O}_x$  (Entry No. 5 in Table 3.1) are shown in Figure 3.5.

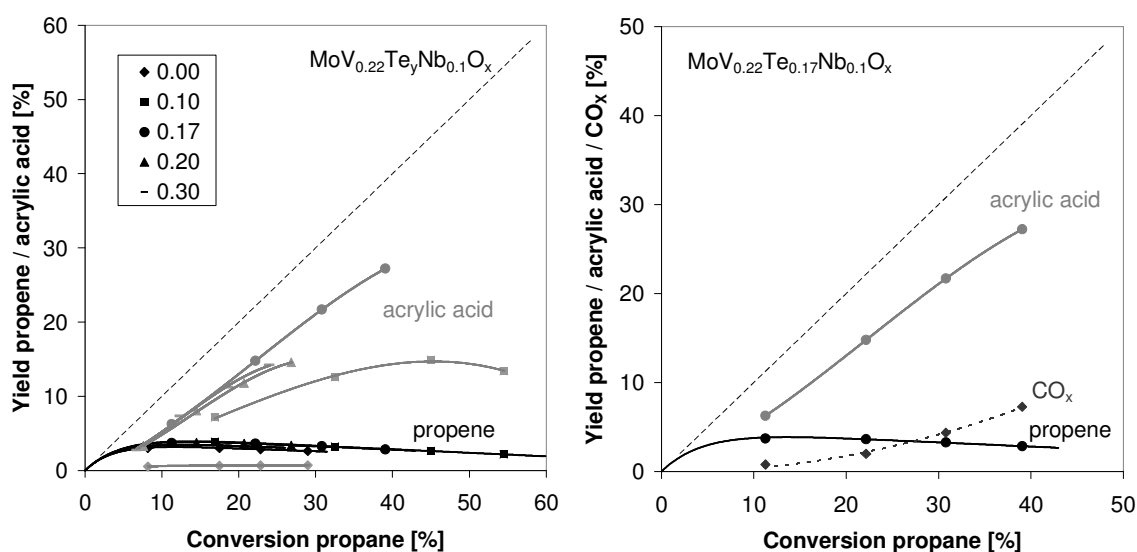


**Figure 3.4 (left):** Yield to propene (black labels) and acrylic acid (gray labels) for MoV<sub>0.22</sub>Te<sub>y</sub>Nb<sub>0.1</sub>O<sub>x</sub>, y = 0.0-0.5.

**Figure 3.5 (right):** Yield of propene, acrylic acid and CO<sub>x</sub> as function of conversion for MoV<sub>0.22</sub>Te<sub>0.17</sub>Nb<sub>0.1</sub>O<sub>x</sub>.

As carbon oxides are the final product of the reaction network (Scheme 3.1), their yield increased with increasing conversion of propane. Selectivities to acetic acid were between 2 - 12% for the M1 phase containing catalysts and increased with conversion of propane, whereas MoV<sub>0.22</sub>Nb<sub>0.1</sub>O<sub>x</sub> (Entry No. 3) showed 18% acetic acid selectivity at low conversion, which decreased with conversion (Figure sup 3.1f in the Supplementary Material).

### 3.3.2. Variation of the vanadium content in the synthesis gel

Catalysts of the formulations MoV<sub>y</sub>Te<sub>0.17</sub>Nb<sub>0.1</sub>O<sub>x</sub> with y = 0.07, 0.14 and 0.22 were studied for the effect of the vanadium concentration on the catalytic properties. The chemical compositions and specific surface areas are compiled in Table 3.1.

For the catalyst with lowest vanadium content (MoV<sub>0.07</sub>Te<sub>0.17</sub>Nb<sub>0.1</sub>O<sub>x</sub>, Entry No. 1 in Table 3.1) only weak peaks of (Nb<sub>0.09</sub>Mo<sub>0.91</sub>)<sub>5</sub>O<sub>16</sub> (2θ = 7.9, 8.7, 25.1) were observed, while the catalysts with higher concentration of vanadium (y= 0.14 and 0.22) consisted of M1 phase (See Figure sup 3.2 in the Supplementary Material). The specific surface areas increased with

the concentration of vanadium in the synthesis gel. It is interesting to note that for a synthesis gel mixture corresponding to  $\text{MoV}_{0.07}\text{Te}_{0.17}\text{Nb}_{0.1}\text{O}_x$  the final material had a composition of  $\text{MoV}_{0.13}\text{Te}_{0.27}\text{Nb}_{0.38}\text{O}_x$  indicating that a significant fraction of molybdenum is not incorporated in the final material, which consists mostly of amorphous material without  $\text{MoVTeNbO}_x$  M1 phase.

The activity of these catalysts for propane conversion increased linearly with the vanadium content (Figure 3.6), which indicates that vanadium is the key element for propane activation. It should be mentioned at this point, however, that the intersection of this linear relation with the x-axis indicates that not all vanadium cations contribute to the catalytic activity.

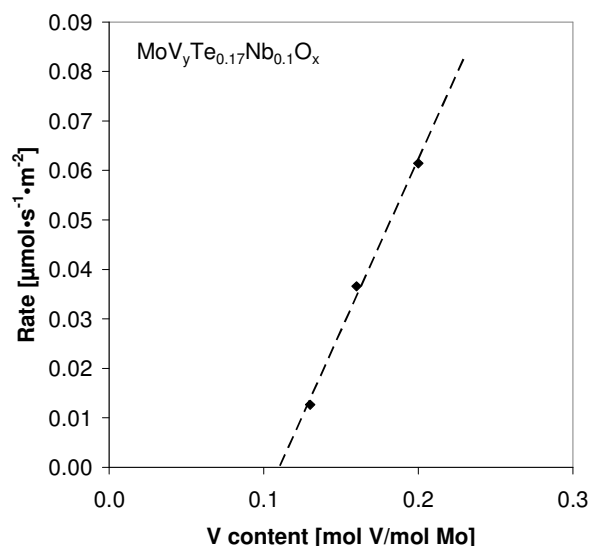


**Figure 3.6:** Surface normalized rates for propane conversion of  $\text{MoV}_y\text{Te}_{0.17}\text{Nb}_{0.1}\text{O}_x$ ,  $y = 0.07 - 0.22$ .

Comparable to the results of the tellurium content variation, the selectivities to propene of all catalysts reached identical

values at same propane conversion (see Figure sup 3.3 in the Supplementary Material). Sympathetically, the selectivities to the products with inserted oxygen, i.e., acrylic and acetic acid also increased and are on the same trend lines for all catalysts. Differences between the catalysts are only observed in the selectivity-conversion plot of  $\text{CO}_x$ , showing a higher selectivity to  $\text{CO}_x$  for the catalysts with the lowest vanadium content (Figure sup 3.3e).

### 3.3.3. Variation of niobium-content in the synthesis gel

The influence of the niobium concentration on the catalytic properties was studied with catalysts of the formulations  $\text{MoV}_{0.22}\text{Te}_{0.2}\text{Nb}_y\text{O}_x$  ( $y = 0.1, 0.2$  and  $0.3$ ). Specific surface areas and chemical compositions are compiled in Table 3.1. All samples showed only XRD peaks of the M1 phase, but quantitative analysis indicates that its concentration varied between 13 and 78% (Figure sup 3.4). Therefore, a large fraction of material is concluded to be X-ray

amorphous. For  $\text{MoV}_{0.22}\text{Te}_{0.2}\text{Nb}_{0.3}\text{O}_x$  (Entry No. 8 in Table 3.1) the concentration of M1 phase is the lowest, (see the weak signals and the peak broadening in the region from 22 - 30 °) indicating the presence of small crystalline domains of the M1 phase. Interestingly, the specific surface areas were higher for the samples containing a higher fraction of M1 phase, i.e., 9.7 and 12.4  $\text{m}^2\cdot\text{g}^{-1}$  compared to the samples with a larger fraction of X-ray diffraction amorphous material having only 6.6  $\text{m}^2\cdot\text{g}^{-1}$ . The chemical compositions of the material with the highest content of M1 phase agrees best with the composition of the synthesis mixture, whereas the differences between the compositions of the synthesis mixture and the final catalysts increased for the materials with lower content of M1 phase. Especially the concentration of vanadium in the final materials decreased with higher niobium concentration in the synthesis mixture.

All catalysts showed similar activities and selectivities to propene. The selectivities to acrylic acid for  $\text{MoV}_{0.22}\text{Te}_{0.2}\text{Nb}_{0.1}\text{O}_x$  (Entry No. 6) and  $\text{MoV}_{0.22}\text{Te}_{0.2}\text{Nb}_{0.2}\text{O}_x$  (Entry No. 7) were both in the range of 50 - 70%, whereas the selectivity to acrylic acid of  $\text{MoV}_{0.22}\text{Te}_{0.2}\text{Nb}_{0.3}\text{O}_x$  (Entry No. 8) was much lower (< 40%). In contrast, high selectivities to  $\text{CO}_x$  and acetic acid were observed for the catalysts that showed lower selectivity to acrylic acid (Figure sup 3.5).

### **3.4. Discussion**

#### **3.4.1. Influence of chemical composition upon phase concentrations**

The resulting phase composition depends on the concentration of tellurium in the synthesis mixture. Mainly M1 phase is formed with low concentrations of tellurium, whereas high concentrations lead to the formation of M2 phase in accordance with the literature.<sup>[21]</sup> Note that this is also in line with the composition of the pure phases (M1:  $\text{Te}_2\text{OM}_{20}\text{O}_{56}$ ; M2:  $\text{TeM}_3\text{O}_9$ ) indicating that excess of tellurium cannot be accommodated in the M1 phase. Theoretically the M1 phase can contain up to 27 at.% tellurium compared to molybdenum, assuming that half of the tetrahedral sites (available for V or Mo) are occupied by Mo (see also Figure 3.1). However M2 phase is formed in samples with a tellurium concentration higher than 20 at.%, showing that M2 phase formation is initiated before the M1 phase is saturated with tellurium. A minimum concentration of vanadium is, however, required for the formation of the M1 phase. The M1 phase was formed with V : Mo ratios higher than 0.14, while with lower concentrations of vanadium only led to  $(\text{Nb}_{0.09}\text{Mo}_{0.91})_5\text{O}_{16}$ . For all niobium



concentrations explored the M1 phase was formed. For the highest concentration of niobium the concentration of M1 phase is lower, while the concentration of X-ray amorphous materials higher than in the other materials of the series. Thus, the concentration of niobium in the synthesis mixture is not relevant for the formation of the M1 phase, as long as a minimum of niobium is contained in the synthesis mixture ( $\text{Nb} : \text{Mo}$  ratio  $\geq 0.1$ ). Synthesis without niobium did not show M1 phase (results not included here). It is also interesting that too high or too low concentrations of tellurium and vanadium led to the formation other phases than M1, whereas in the case of niobium the M1 phase is partly substituted by amorphous material.

Differences in the chemical compositions of the synthesis mixtures and in the final materials were observed for catalysts with lower content of M1 phase. Therefore, during M1 formation all metals are incorporated into the solid phase according to their concentration in the synthesis mixture over the compositional range of  $\text{MoV}_{0.14-0.22}\text{Te}_{0.1-0.2}\text{Nb}_{0.1-0.2}\text{O}_x$ . For the synthesis composition  $\text{MoV}_{0.07}\text{Te}_{0.17}\text{Nb}_{0.1}\text{O}_x$  the final material showed the composition of  $\text{MoV}_{0.13}\text{Te}_{0.27}\text{Nb}_{0.38}\text{O}_x$ , with only weak signals of  $(\text{Nb}_{0.09}\text{Mo}_{0.91})_5\text{O}_{16}$  in the XRD indicating that also a high amount of non-crystalline amorphous material is present with an enriched concentration of vanadium, tellurium and especially niobium compared to the synthesis mixture. Even for the synthesis composition  $\text{MoV}_{0.14}\text{Te}_{0.17}\text{Nb}_{0.1}\text{O}_x$  showing 64% M1 phase for the final material, the observed composition was  $\text{MoV}_{0.16}\text{Te}_{0.17}\text{Nb}_{0.24}\text{O}_x$ . The deviation of the final material from the synthesis composition is much lower, but still the niobium concentration is higher in the final material. Thus, we conclude that niobium is preferential incorporated into amorphous material. Also for the synthesis compositions  $\text{MoV}_{0.22}\text{Te}_{0.2}\text{Nb}_{0.3}\text{O}_x$  and  $\text{MoV}_{0.22}\text{Te}_{0.3}\text{Nb}_{0.1}\text{O}_x$  higher concentrations of niobium are found in the final material supporting the conclusions on preferred niobium incorporation.

The M1 phase is constructed from octahedra with molybdenum or vanadium surrounded by oxygen. Niobium is located in channels constructed from five octahedra and is not in the center of the octahedra. The amorphous material should, therefore, consist of octahedra without sufficient long range order. More sites comparable to the small channels in the M1 phase will be present to host niobium and will lead to higher niobium concentration in the material. This might also be the reason that high niobium concentrations cause the formation of a higher fraction of amorphous material, but do not change the relative composition of the other phases. The high concentrations of niobium favor the formation of such host ensembles and disrupt formation of the M1 structure.

### 3.4.2. Catalytic activity, phase composition and chemical composition

For materials containing M1 phase up to five times higher activities were observed than with other materials. The initial addition of tellurium, for example, leads to the formation of M1 phase causing a strong increase in activity. Further increase of the tellurium concentration, however, leads to the formation of the less active M2 phase and to  $\text{TeMo}_5\text{O}_{16}$  inducing a decrease in activity. Note in this context that the activity normalized to the surface area and the fraction of M1 phase varies only slightly (shown in Figure 3.7), indicating that lower activities are associated with the dilution of the M1 phase with less active. The rate of propane conversion increases with increasing concentration of vanadium suggesting that vanadium is a key element in the active sites of the M1 phase.<sup>[22]</sup> The reason why vanadium is so efficient in this phase remains unclear.

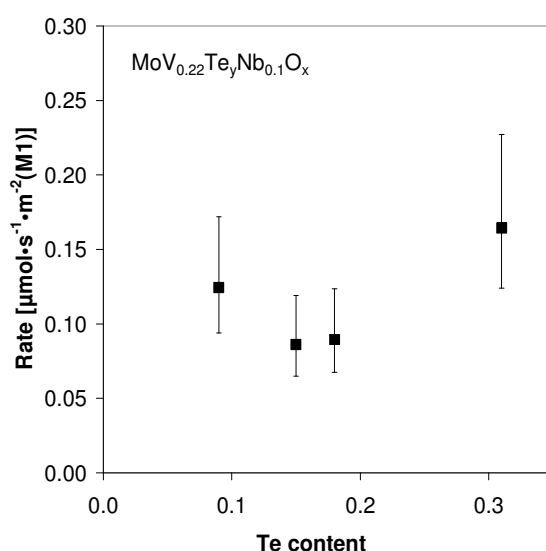


**Figure 3.7:** Rates of propane activation of  $\text{MoV}_{0.22}\text{Te}_y\text{Nb}_{0.1}\text{O}_x$  containing mixtures of M1 and M2 phase corrected to surface area and M1 phase content.

The content of niobium did not affect the catalyst activity (see also ref. <sup>[23]</sup>), which indicates that niobium is not part of an active site, but a crucial concentration ( $\text{MoVTenb}_y\text{O}_x$ ;  $y \geq 0.1$ ) is needed for formation and stabilization of the M1 phase. It has also been suggested that Nb does not play a significant role in propane activation, but helps stabilizing the acrylic acid formed on the catalyst surface and/or preventing further oxidation by weakening the interaction between the oxide surface and the product and reactant molecules.<sup>[24]</sup>

The yields to propene show a maximum for all catalysts and stay on a constant level at higher conversions. This is typical for a primary product, which is rapidly converted in a subsequent reaction. The activation of propane can be described by a first order reaction equation.<sup>[25]</sup> For propene also a first order reaction (Equation 3.1) is used, which permits to estimate the pseudo first order rate constants consisting of the product of the adsorption and the reaction constant using the variation in the overall rate of formation of propene.

$$\frac{d[\text{propene}]}{dt} = k_1 \cdot [\text{propane}] - k_2 \cdot [\text{propene}] \quad (\text{Equation 3.1})$$

Remarkably, the concentration of propene in the products varied in an identical way with the conversion for all catalysts regardless of metal and phase composition (see Figure 3.8). This agrees with the proposed reaction orders, because the path in the yield-conversion plot for a first order reaction only depends on the ratio of  $k_1 : k_2$ . In the proposed reaction network propene is formed by oxidative dehydrogenation (ODH) of propane, which is followed by oxidation of the allyl-position to acrolein or by oxo-insertion to acetone (Scheme 3.1). The similar propene yields for all catalysts indicates that the ratio of the kinetic constant for the first C-H abstraction ( $k_1$ , in general assumed to be the rate determining step of the ODH reaction) and the first addition of oxygen into the propyl cation ( $k_2$ , generally assumed to be the rate determining step in the oxygen addition processes) is constant for all catalysts. The fact that  $k_1 : k_2$  is 1 : 25 indicates that the oxygen addition to propene is a drastically more facile reaction than the oxidative dehydrogenation. This is tentatively explained by the fact that the presence of a double bond leads to weaker C-H bonds in propene than in propane.<sup>[26]</sup>

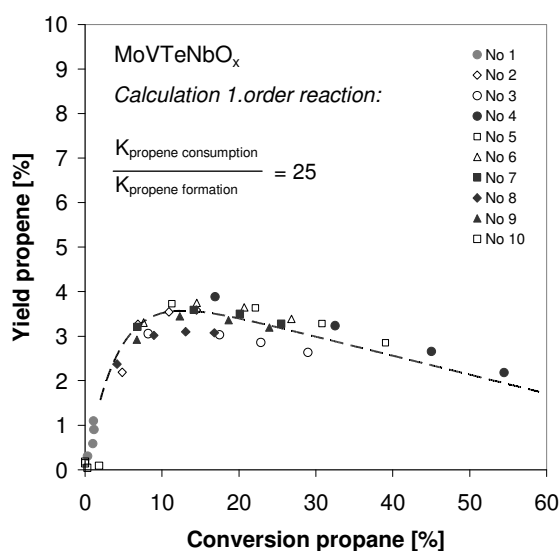


**Figure 3.8:** Observed propene yields as a function of propane conversion on MoVTeNbO<sub>x</sub> catalysts. The dashed line indicates the results of the kinetic fit; all points are experimental results.

It is important to note that also MoV<sub>0.22</sub>Nb<sub>0.1</sub>O<sub>x</sub> (Entry 3 in Table 3.1), which does not contain the M1 phase obeys this correlation. Its rate of propane activation was very low, but the ratio

of propene formation and propene consumption was also 1 : 25. This indicates that the relative concentration of active sites for the oxidative dehydrogenation of propane and propene oxidation is constant for the catalysts, regardless the selectivity in propene oxidation. In consequence, we conclude that the active sites for propane activation and oxo-functionalization are structurally linked to the extent that the concentration of both sites varies sympathetically. In turn the selectivity depends markedly on different properties of the catalysts among which the weak interaction between the formed products and the catalyst surface seems to be the most important one. Note that it also indicates that the sites for propane activation are not exclusive to the M1 phase, but that the M1 phase has a particularly high concentration of it.

Only for materials containing the M1 phase yields higher than 40% of acrylic acid were observed. To understand this, let us discuss the possible reaction pathways after propene is formed. Acrylic acid is formed from propene with acrolein as intermediate. However, propene can also be oxidized to acetone, leading to acetic acid. Therefore, the obtained yield of acrylic acid depends on the ratio of the reaction pathways A : B (Scheme 3.1). With  $k_1 : k_2$  being constant,  $k_2$  is higher for the M1 phase containing materials. Thus, the increase of the acrylic acid yield is attributed to the fact that on the M1 phase the rate on pathway A is selectively more increased than pathway B. It is speculated that it is associated with the lower stabilization of a propyl carbenium ion on the M1 phase as well as with the enhancement of the rate of  $\alpha$ -H abstraction. The latter reaction step is to be promoted in the presence of tellurium cations, as the  $\text{Te}^{4+}$ -O site is suggested to be the active for the  $\alpha$ -H abstraction and acrolein/acrylic acid formation.<sup>[27]</sup>

The  $\text{MoV}_{0.22}\text{Te}_{0.17}\text{Nb}_{0.1}\text{O}_x$  catalyst showed a higher yield to acrylic acid than the  $\text{MoV}_{0.22}\text{Te}_{0.1}\text{Nb}_{0.1}\text{O}_x$  catalyst although the phase purity is higher for the latter one. This is attributed to the fact that a full saturation of the M1 phase with tellurium was not achieved for  $\text{Mo}_{0.22}\text{Te}_{0.1}\text{Nb}_{0.1}\text{O}_x$  reducing the rate of  $\alpha$ -H abstraction and consequently the acrylic acid formation.

The role of amorphous mixed oxide phases can best be illustrated through the materials with varying niobium content. The variation of niobium showed the formation of M1 phase for all catalysts, but also a fraction of material without long range order for the materials with the highest concentration of niobium in the synthesis mixture (Entry 8, Table 3.1). The catalysts

with higher concentration of M1 phase showed selectivities to acrylic acid between 50 and 60%, whereas the catalyst with the highest fraction of amorphous mixed oxides shows only selectivity to acrylic acid of 30 to 40%. This indicates that the amorphous phase contains sites that increase the oxidation of the acrylic acid. We speculate at present that these sites are Lewis acid sites, which are able to strongly bind propene and the polar products and intermediates resulting in a higher residence that leads to an unselective conversion of the polar products.

### **3.5. Conclusions**

The M1 phase possesses by far the most efficient catalytically active surface. Synthesis of mainly M1 phase was possible in the range of  $\text{MoV}_{0.14-0.22}\text{Te}_{0.1-0.2}\text{Nb}_{0.1-0.2}\text{O}_x$ . Without vanadium, tellurium or niobium in the synthesis mixture formation of M1 phase was not observed, while too high concentration of tellurium led to the substitution of M1 by inactive M2 phase. High concentrations of niobium in synthesis still lead to M1 phase, but with an increased amount of amorphous material, because niobium changes the arrangement of the octahedra in the structure to increase the formation of small channels for hosting niobium.

The catalytic activity was proportional to the concentration of vanadium incorporated in the catalysts proving that vanadium is a key element in the activation of propane, but the results also show that not all vanadium atoms are active in the M1 phase.

Analysis of the kinetic data shows that the cleavage of the first C-H bond is the rate determining step, i.e., the reaction step has the slowest rate constant in the forward direction. It should be noted again that we compare here only pseudo rate constants that contain a contribution of the adsorption constants. A simple model of the reaction network shows that the ratio between propene formation and the oxygen insertion is 1 : 25. It is important to note that this ratio holds true for all tested catalysts, i.e., the reaction rate of the first oxygen insertion was indifferent between selective and unselective catalysts despite the fact that very

different rate determining steps could be involved. In the absence of a fortuitous compensation, it shows that the ratio of the sites active for C-H cleavage and the oxygen insertion is constant. We speculate at present that this is achieved as both functions are part of the same site or the sites are structurally coupled.

In all cases in which a significant fraction of an X-ray amorphous phase is present, the selectivities to acrylic acid was lower. The lower selectivity is attributed to the presence of distorted octahedra and higher concentration of metals cations not surrounded by oxygen (mainly niobium) leading to increased surface residence time with these materials caused by the strong interactions with the reacting molecules.

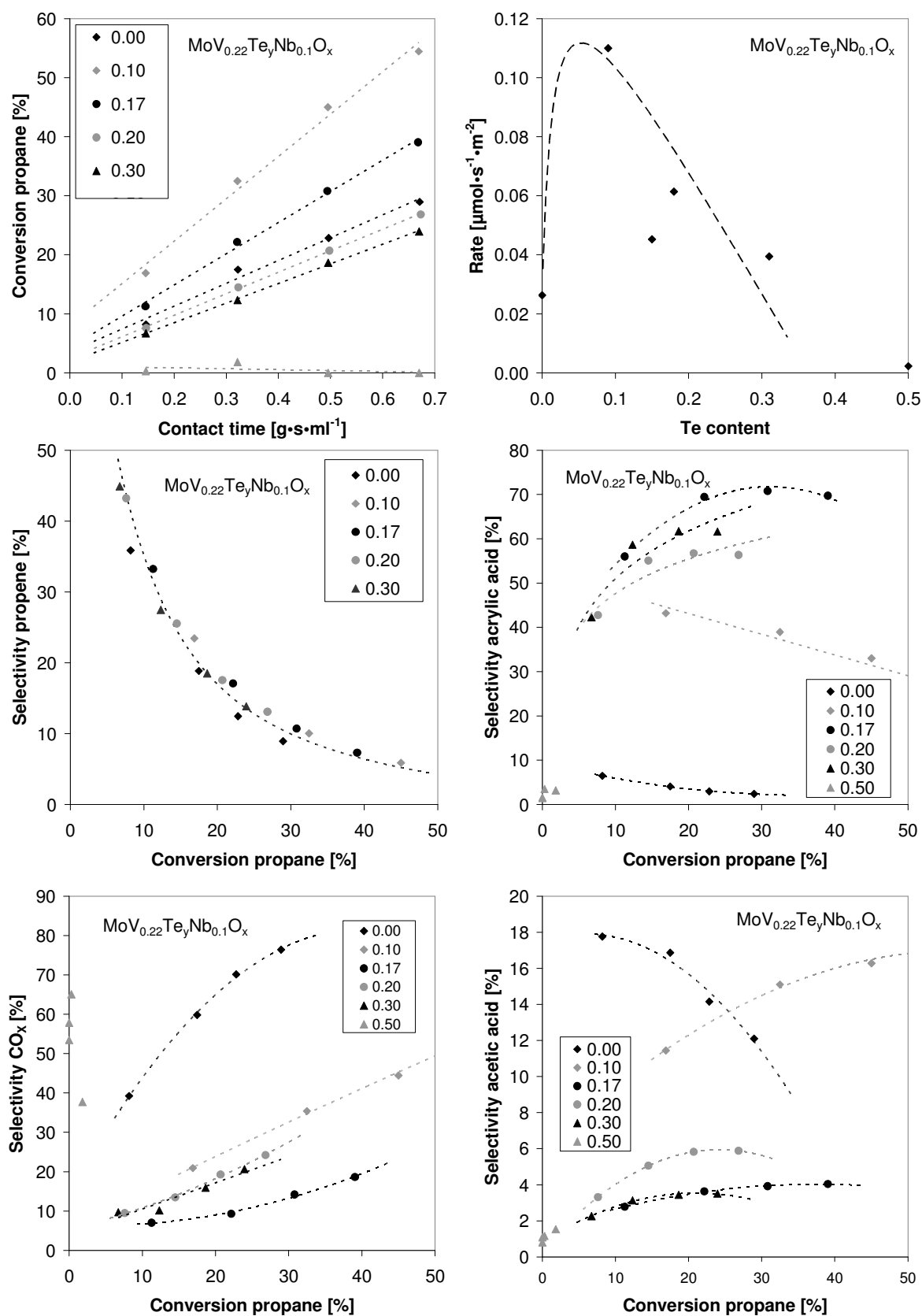
### **3.6. Acknowledgements**

The authors are grateful for the financial support from the European Union in the framework of the Integrated Project TOPCOMBI (NMP2-CT-2005-515792-2) and from the Bayerisches Staatsministerium für Wissenschaft, Forschung und Kunst within the NanoCat project. Ch.P.K. is grateful to the Alexander von Humboldt Foundation for a postdoctoral research fellowship. Discussions within the network of excellence IDECAT are also gratefully acknowledged.

### 3.7. References

- [1] M. M. Bettahar, G. Costentin, L. Savary, J. C. Lavalley, *Applied Catalysis A* **1996**, 145, 1.
- [2] W. Nojiri, Y. Sakai, Y. Watanabe, *Catalysis Reviews Science and Engineering* **1995**, 37, 145.
- [3] D. Vitry, J. L. Dubois, W. Ueda, *Journal of Molecular Catalysis A* **2004**, 220, 67.
- [4] A. Tenten, H. Hibst, F.-G. F.-G. Martin, L. L. Marosi, V. Kohl, DE Patent 4405514, **1994**.
- [5] M. M. Lin, *Applied Catalysis A* **2001**, 207, 1.
- [6] T. Ushikubo, H. Nakamura, Y. Koyasu, S. Wajiki, US Patent 5,380,933, **1995**.
- [7] P. Botella, E. Garcia-Gonzalez, J. M. L. Nieto, J. M. Gonzalez-Calbet, *Solid State Sciences* **2005**, 7, 507.
- [8] P. Botella, J. M. L. Nieto, B. Solsona, *Catalysis Letters* **2002**, 78, 383.
- [9] R. K. Grasselli, J. D. Burrington, D. J. Buttrey, P. DeSanto, C. G. Lugmair, A. F. Volpe, T. Weingand, *Topics in Catalysis* **2003**, 23, 5.
- [10] P. DeSanto, D. J. Buttrey, R. K. Grasselli, C. G. Lugmair, A. F. Volpe, B. H. Toby, T. Vogt, *Zeitschrift Für Kristallographie* **2004**, 219, 152.
- [11] P. DeSanto, D. J. Buttrey, R. K. Grasselli, C. G. Lugmair, A. F. Volpe, B. H. Toby, T. Vogt, *Topics in Catalysis* **2003**, 23, 23.
- [12] E. M. Thorsteinson, T. P. Wilson, F. G. Young, J. Kasai, *Journal of Catalysis* **1978**, 52, 116.
- [13] P. Botella, B. Solsona, A. Martinez-Arias, J. M. L. Nieto, *Catalysis Letters* **2001**, 74, 149.
- [14] M. M. Lin, *Applied Catalysis A* **2003**, 250, 287.
- [15] J. M. L. Nieto, P. Botella, B. Solsona, J. M. Oliver, *Catalysis Today* **2003**, 81, 87.
- [16] X. L. Tu, N. Furuta, Y. Sumida, M. Takahashi, H. Niiduma, *Catalysis Today* **2006**, 117, 259.
- [17] H. Watanabe, Y. Koyasu, *Applied Catalysis A* **2000**, 194, 479.
- [18] M. Baca, M. Aouine, J. L. Dubois, J. M. M. Millet, *Journal of Catalysis* **2005**, 233, 234.
- [19] E. Balcells, F. Borgmeier, I. Grissted, H. G. Lintz, F. Rosowski, *Applied Catalysis A* **2004**, 266, 211.
- [20] M. H. Lin, T. B. Desai, F. W. Kaiser, P. D. Klugherz, *Catalysis Today* **2000**, 61, 223.
- [21] M. Baca, A. Pigamo, J. L. Dubois, J. M. M. Millet, *Topics in Catalysis* **2003**, 23, 39.
- [22] Z. Zhao, X. T. Gao, I. E. Wachs, *Journal of Physical Chemistry B* **2003**, 107, 6333.
- [23] D. Vitry, Y. Morikawa, J. L. Dubois, W. Ueda, *Applied Catalysis A* **2003**, 251, 411.
- [24] W. Ueda, D. Vitry, T. Katou, *Catalysis Today* **2005**, 99, 43.
- [25] D. Vitry, Y. Morikawa, J. L. Dubois, W. Ueda, *Topics in Catalysis* **2003**, 23, 47.
- [26] A. Costine, B. K. Hodnett, *Applied Catalysis A* **2005**, 290, 9.
- [27] R. K. Grasselli, *Catalysis Today* **2005**, 99, 23.

## 3.8. Supplementary material

Figure sup 3.1 a-f: Conversion of propane and product selectivities over  $\text{MoV}_{0.22}\text{Te}_y\text{Nb}_{0.1}\text{O}_x$ ,  $y = 0.0 - 0.5$ .



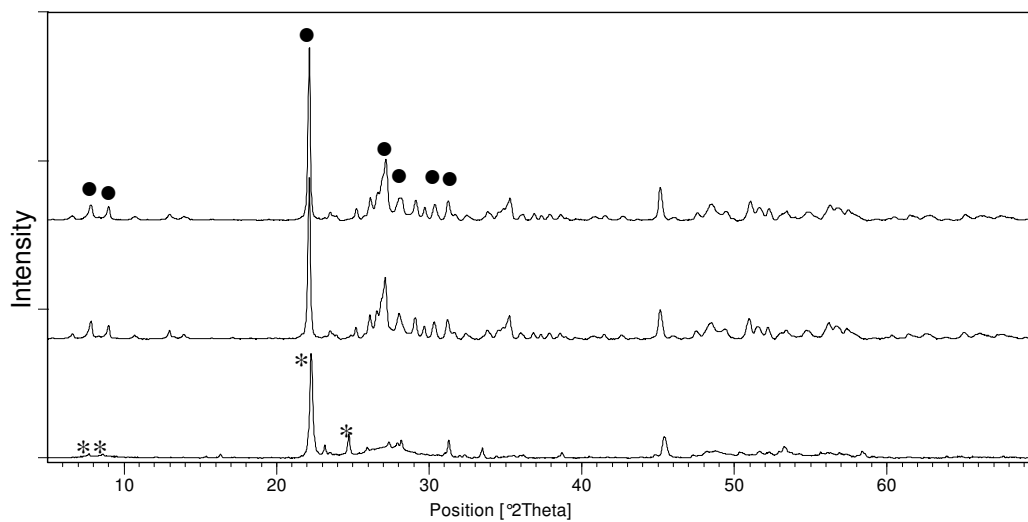


**Figure sup 3.2:** XRD of  $\text{MoV}_y\text{Te}_{0.17}\text{Nb}_{0.1}\text{O}_x$  with  $y = 0.07, 0.14$  and  $0.22$  (from bottom to top)

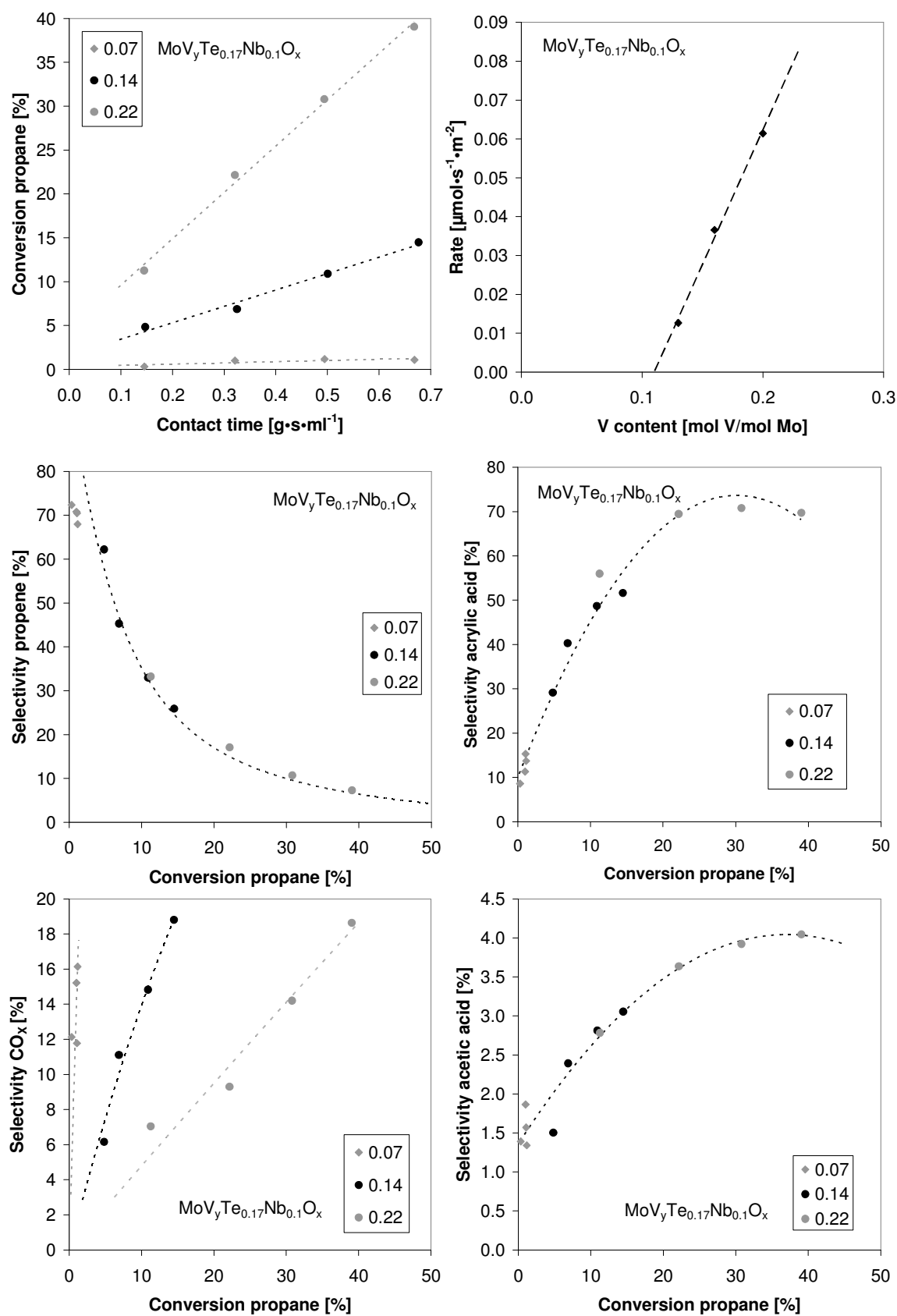
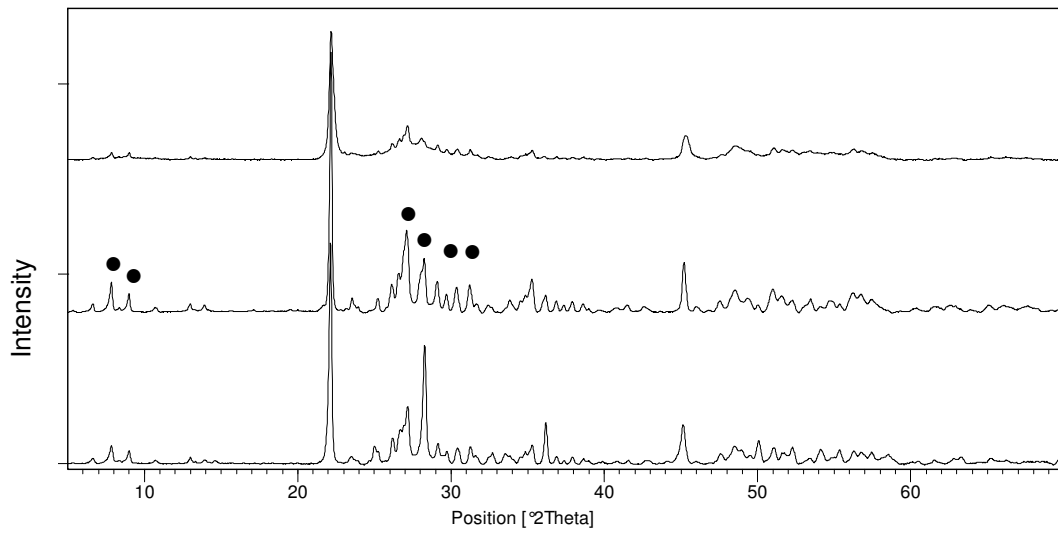


Figure sup3.3 a-f: Conversion of propane and product selectivities over  $\text{MoV}_y\text{Te}_{0.17}\text{Nb}_{0.1}\text{O}_x$ ,  $y = 0.07 - 0.22$ .



**Figure sup 3.4:** XRD of  $\text{MoV}_{0.22}\text{Te}_{0.2}\text{Nb}_y\text{O}_x$  with  $y = 0.1, 0.2$  and  $0.3$  (from bottom to top).

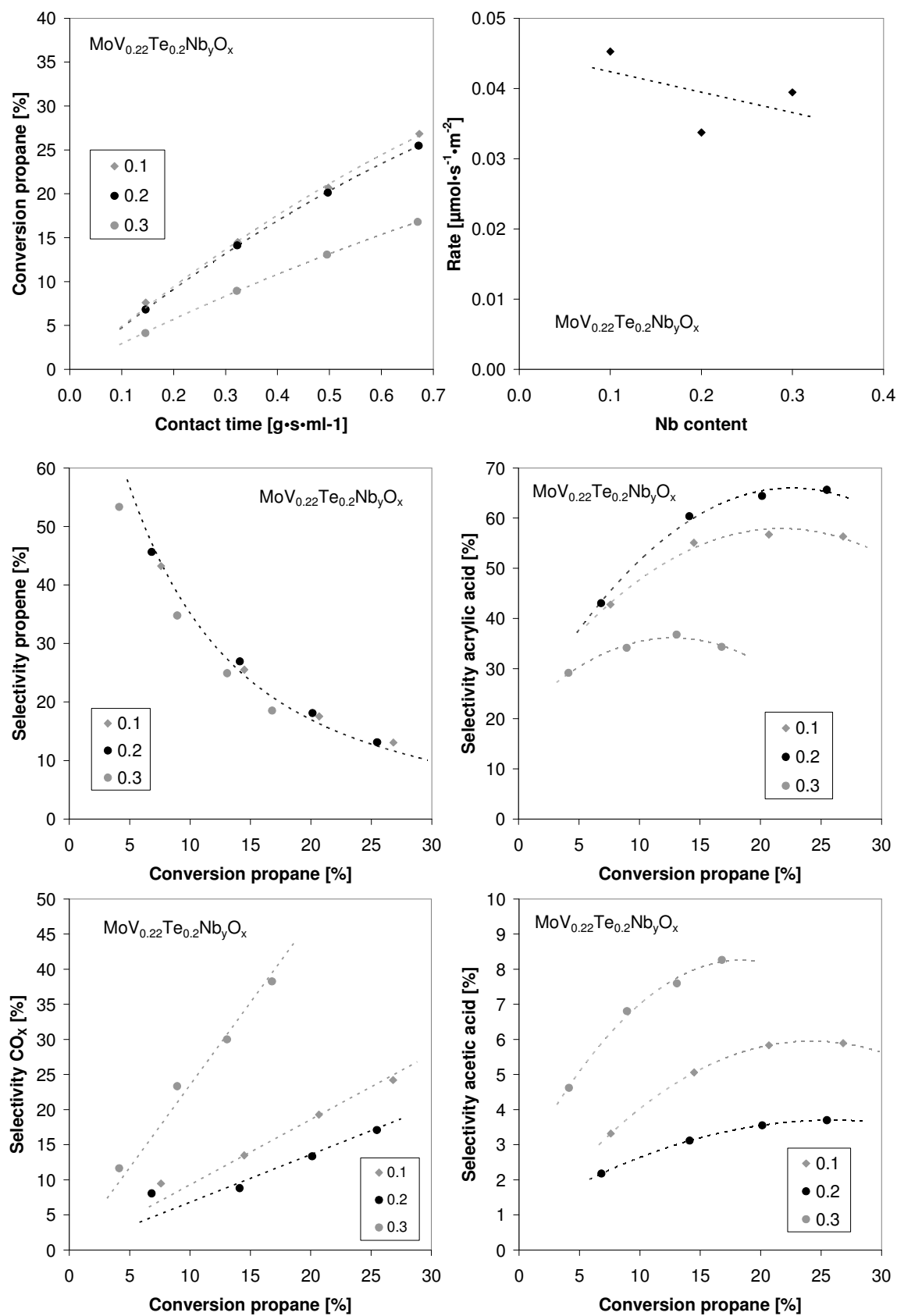


Figure sup 3.5 a-f: Conversion of propane and product selectivities over  $\text{MoV}_{0.22}\text{Te}_{0.2}\text{Nb}_y\text{O}_x$ ,  $y = 0.1 - 0.3$ .

# Chapter 4

## *On the Role of the Vanadium Distribution in MoVTeNbO<sub>x</sub> mixed Oxides for the selective catalytic Oxidation of Propane*

### *Abstract*

The selective oxidation of propane to acrylic acid is studied over a series of nearly pure *M1*-phase MoVTeNbO<sub>x</sub> catalysts. Quantitative analysis of the reaction network shows that the ratio of the rate constants for propane oxidative dehydrogenation to propene and for the further oxidation of propene is constant. The rates towards acrylic acid and acetone, however, vary subtly with the concentration of vanadium and the location of its substitution. The reaction of acrylic acid to acetic acid and carbon oxides, associated with accessible metal cations, contributes two thirds towards the non-selective pathway. The other third is associated with acetone formation. Vanadium is first substituted selectively at sites that are inactive for propane activation. Depending on the selectivity of this substitution two groups of materials have been identified, which show a distinctly different dependence on the concentration of vanadium. Statistic distribution of vanadium in the *M1* phase appears to be the most promising strategy to improve the performance of MoVTeNbO<sub>x</sub> catalysts for a given vanadium concentration.

## 4.1. Introduction

The selective oxidation of alkanes such as ethane and propane to alkenes or acrylic components as well as the oxidation of *n*-butane to maleic anhydride are conceptually economically favorable routes to oxygenates. Among these reactions only the oxidation of *n*-butane is used on an industrial scale, whereas all other processes are still not competitive to conventional processes, such as the two step oxidation of propene to acrylic acid.<sup>[1-4]</sup> The two major challenges are related to the fact that the alkanes are species difficult to activate and that the target molecules are thermodynamically metastable, while the most stable product is carbon dioxide.

For the oxidation of propane to acrylic acid multicomponent molybdates of the compositional type  $\text{MoVTeNbO}_x$  have been introduced by Mitsubishi in the early 90s allowing up to 48% yield of acrylic acid. Also the ammoxidation is catalyzed by these mixed oxides with yields of 58%.<sup>[5, 6]</sup> Such materials have the potential to replace the currently used two step oxidation process using propene as feed material.<sup>[7-14]</sup> Two crystallographic phases containing all four metals, named *M1* and *M2* phase, were reported for these oxides<sup>[15, 16]</sup> and it is generally accepted that only the *M1* phase is active for the C-H activation of propane.<sup>[17, 18]</sup> The stoichiometric composition of the *M1* phase is  $(\text{Te}_2\text{O})_2\text{M}_{20}\text{O}_{56}$  with  $\text{M} = \text{Mo}, \text{V}, \text{Nb}$ . It consists of molybdenum and vanadium octahedra with corner sharing oxygen atoms containing channels of five, six and seven octahedra perpendicular to the *ab* plane. The structure is periodically repeated along the *c* axis. Niobium is located in the pentagonal channels, whereas tellurium occupies the hexagonal and heptagonal channels. The *M2* phase  $(\text{TeO})_2\text{M}_6\text{O}_{18}$  contains only hexagonal channels, formed from octahedra with molybdenum, vanadium and niobium centers. Tellurium is occupying position in the hexagonal channels.<sup>[19-21]</sup>

While the presence of the *M1* phase appears to be essential for alkane activation, the effect of mixtures between the *M1* and *M2* phase on the catalytic activity is still under discussion. It was reported that the *M2* phase enhances the selectivity to oxygenates, while it is not able to catalyze the oxidation of propane to propene. The *M2* phase was also reported to serve as a tellurium reservoir for the *M1* phase.<sup>[22, 23]</sup> The effects of different preparation methods,<sup>[12-14]</sup> synthesis conditions<sup>[24-26]</sup> and precursors used<sup>[27-29]</sup> are also only fragmentary known. Well-defined synthesis procedures allow the synthesis of materials with reproducible catalytic

properties, but variations in the procedure still lead to catalysts with so far unpredictable catalytic properties.

One approach to better understand the impact of these subtle variations is to analyze the individual reaction steps of the network in relation to the composition of the M1 phase, i.e., the phase that is able to characterize all reaction steps. The reaction network for the oxidation of propane to acrylic acid, containing possible side reactions to acetic acid and  $\text{CO}_x$  was first reported on a qualitative level by Lin et al. (Figure 4.1).<sup>[30]</sup> Propene was found as the only primary product from propane oxidation, which is subsequently oxidized either to acrolein and subsequently to acrylic acid, or to acetone, followed by acetic acid formation. Both pathways lead to CO and  $\text{CO}_2$  (in the following summed up as  $\text{CO}_x$ ) as products of the total oxidation.<sup>[31, 32]</sup> In addition, the oxidation of acrylic to acetic acid and the deep oxidation of propane and all other intermediates to  $\text{CO}_x$  was observed.

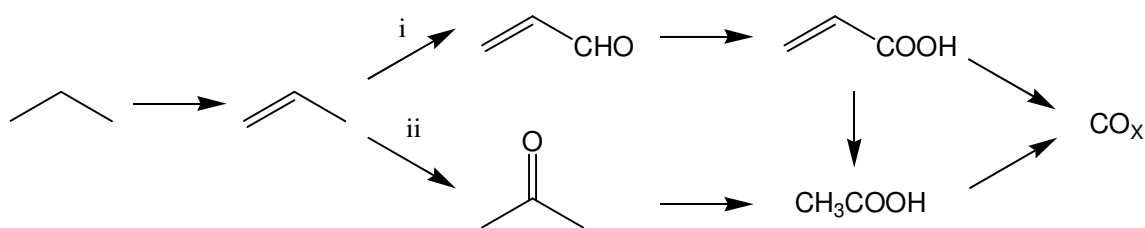


**Figure 4.1:** Reaction network of propane oxidation over MoVTaNb oxides.

The first quantitative kinetic description of the reaction network was reported by Luo et al. with an initial selectivity of propene to acrylic acid of 67% (pathway i) and to acetone of 17% (pathway ii).<sup>[33]</sup> In 2004 Balcells reported the kinetics of a simplified network containing propane, propene, acrylic acid and other by-products. The results reported indicated that the oxidative dehydrogenation is the slowest reaction and, therefore, the rate determining step for the acrylic acid formation, while the rate for the oxidation of acrylic acid is comparable to the oxidative dehydrogenation.<sup>[31-33]</sup>

In the *M1* structure a total number of 36 octahedrons are present. 24 of them are occupied by molybdenum, whereas 12 could be occupied by vanadium or molybdenum.<sup>[20]</sup> Therefore, the maximum possible V/Mo ratio is 0.5. The ratio between V/Mo may vary, but it is in most cases close to 0.3, whereas the Nb/Mo ratio is typically 0.1.<sup>[11, 12]</sup>

Vanadium sites adjacent to heptagonal channels are proposed to be the active sites for the oxidative dehydrogenation of propane.<sup>[34, 35]</sup> This is in agreement with the activity of an *M1* phase consisting only of  $\text{MoVO}_x$ , which is active for propane conversion. However, it should also be noted that only the *M1* phase contains adjacent vanadium octahedra, which have been shown to be the site of alkane activation in supported vanadium oxides.<sup>[36]</sup> DFT calculations suggest that the activation of propane occurs on vanadyl centers via a radical mechanism.<sup>[35, 37]</sup> Sequential steps such as the oxo-insertion of propene to acetone, in turn, is proposed to be catalyzed by Brønsted acid sites, which was confirmed by temperature programmed desorption of ammonia and sorption of pyridine on  $\text{MoVTeNbO}_x$  and  $\text{MoVSbNbO}_x$  catalysts.<sup>[38]</sup>

As described before vanadium is the key element for propane activation,<sup>[39]</sup> while the effect of tellurium and niobium is still under discussion.<sup>[40-42]</sup> It appears that tellurium plays an important role in the oxidation of propene to acrylic acid and in the stabilization of acrylic acid against further oxidation, as only for tellurium containing catalysts high selectivities to acrylic acid were observed, whereas tellurium-free catalysts with *M1*-phase showed mainly  $\text{CO}_x$  as product. Niobium, on the other hand, stabilizes the formation of the *M1*-phase,<sup>[39]</sup> and in addition, it enhances selectivity to acrylic acid, but the effect is not so strong as for tellurium.

In this work, we address, therefore, the synthesis of  $\text{MoVTeNbO}_x$  catalysts consisting mainly of *M1* phase with variations of the vanadium to molybdenum ratio and the catalytic properties of these materials for the oxidation of propane to acrylic acid. We use a detailed kinetic analysis of the reaction network to identify the reaction pathways and relate them to two apparent modes of vanadium substitution in the *M1* phase.



## 4.2. Experimental

### 4.2.1. Catalyst preparation

The catalysts were prepared by hydrothermal synthesis, the composition of the precursor mixtures and the conditions of the hydrothermal treatment are shown in Table 4.1. Ammonium para molybdate  $(\text{NH}_4)_6\text{Mo}_7\text{O}_{24} \cdot 4 \text{H}_2\text{O}$  was dissolved in 50 ml bidistilled water at 353 K in a Teflon tube followed by the addition of telluric acid dissolved in water. Vanadyl sulfate  $\text{VOSO}_4 \cdot x \text{H}_2\text{O}$  was added as aqueous solution drop wise within 30 min, resulting in a black solution. Ammonium niobate oxalate  $(\text{NH}_4)\text{NbO}(\text{C}_2\text{O}_4)_2 \cdot x \text{H}_2\text{O}$  was added as solution and after 10 min further stirring the mixture turned olive green. All precursors were purchased from Sigma-Aldrich or Fluka and were used without further purification. Oxygen dissolved in the mixture was removed by bubbling nitrogen through the liquid for 5 min. The tube was closed with a Teflon cap and mounted into a steel autoclave. Hydrothermal synthesis was carried out at 448 K under autogenous pressure for the duration given in Table 4.1. The autoclave was cooled with water to room temperature. The residue was filtered, washed five times with bidistilled water and dried 16 h at 353 K. The material was calcined for 2 h at 523 K in static air and then for 2 h at temperatures up to 873 K in nitrogen (heating rate 10 K/min). Before reaction, the sample was ground and pressed to a particle size 150 – 212  $\mu\text{m}$ .

**Table 4.1:** Composition and synthesis time for MoVTeNbO<sub>x</sub> catalysts.

No.	Synthesis Composition	AHM [g]	Te(OH) <sub>6</sub> [g]	VOSO <sub>4</sub> [g]	ANO [g]	Hydrothermal time [h]
1	MoV <sub>0,14</sub> Te <sub>0,17</sub> Nb <sub>0,1</sub> O <sub>x</sub>	8.63	1.86	1.59	2.24	72
2	MoV <sub>0,22</sub> Te <sub>0,17</sub> Nb <sub>0,1</sub> O <sub>x</sub>	8.26	1.78	2.29	2.14	72
3	MoV <sub>0,22</sub> Te <sub>0,2</sub> Nb <sub>0,2</sub> O <sub>x</sub>	7.58	1.97	2.10	3.93	72
4	MoV <sub>0,3</sub> Te <sub>0,1</sub> Nb <sub>0,1</sub> O <sub>x</sub>	8.74	1.14	3.58	2.27	24
5	MoV <sub>0,3</sub> Te <sub>0,1</sub> Nb <sub>0,1</sub> O <sub>x</sub>	8.74	1.14	3.58	2.27	48
6	MoV <sub>0,3</sub> Te <sub>0,1</sub> Nb <sub>0,1</sub> O <sub>x</sub>	8.74	1.14	3.58	2.27	120
7	MoV <sub>0,3</sub> Te <sub>0,17</sub> Nb <sub>0,1</sub> O <sub>x</sub>	8.26	1.78	3.58	2.14	72

AHM: Ammonium para molybdate  $(\text{NH}_4)_6\text{Mo}_7\text{O}_{24} \cdot 4 \text{H}_2\text{O}$

ANO: Ammonium niobat oxalat  $(\text{NH}_4)\text{NbO}(\text{C}_2\text{O}_4)_2 \cdot x \text{H}_2\text{O}$

**Table 4.2:** Characterization and catalytic activity for the MoVTeNbO<sub>x</sub> catalysts.

No.	Composition	BET surface area [m <sup>2</sup> ·g <sup>-1</sup> ]	Phase composition (XRD)	Rate constant propane activation [ml·g <sup>-1</sup> ·s <sup>-1</sup> ]	Initial rate of propane activation [μmol·m <sup>-2</sup> ·s <sup>-1</sup> (M1)]
1	MoV <sub>0,16</sub> Te <sub>0,17</sub> Nb <sub>0,24</sub> O <sub>x</sub>	5.9	M1 (97.8%) M2 ( 2.2%)	0.24	0.037
2	MoV <sub>0,20</sub> Te <sub>0,18</sub> Nb <sub>0,17</sub> O <sub>x</sub>	11.4	M1 (97.7%) M2 ( 2.3%)	0.75	0.063
3	MoV <sub>0,23</sub> Te <sub>0,17</sub> Nb <sub>0,22</sub> O <sub>x</sub>	12.4	M1 (94.1%) M2 ( 5.9%)	0.45	0.034
4	MoV <sub>0,23</sub> Te <sub>0,10</sub> Nb <sub>0,11</sub> O <sub>x</sub>	16.0	M1 (98.0%) M2 ( 2.0%)	1.36	0.081
5	MoV <sub>0,26</sub> Te <sub>0,11</sub> Nb <sub>0,10</sub> O <sub>x</sub>	18.1	M1 (97.2%) M2 ( 2.8%)	1.31	0.070
6	MoV <sub>0,28</sub> Te <sub>0,10</sub> Nb <sub>0,10</sub> O <sub>x</sub>	17.0	M1 (96.5%) M2 ( 3.5%)	1.45	0.082
7	MoV <sub>0,27</sub> Te <sub>0,17</sub> Nb <sub>0,12</sub> O <sub>x</sub>	11.4	M1 (90%) M2 (10%)	0.55	0.050

#### 4.2.2. Catalyst characterization

X-ray diffraction patterns were collected on a Philips X'pert instrument using the Cu K<sub>α</sub>-line. (A Ni-filter was installed to remove the Cu K<sub>β</sub>-line). XRD were measured between 2θ angles of 5 and 70 ° with a step size of 0.017 ° and a scan speed of 115 s per step. The phase composition was determined by Rietveld analysis using Bruker TOPAS 3.0 software.

The BET surface areas were determined by N<sub>2</sub> sorption at 77 K using a Sorptomatic 1990 Series instrument after activation of the sample in vacuum at 523 K. The chemical composition was measured by ICP-AES with a Spectroflame Instrument after decomposition of the materials by heating with soda – potash. The composition and structural properties of the catalysts are compiled in Table 4.2.

### 4.2.3. Catalytic activity

The catalytic activity was investigated in a six-fold parallel reactor using 100 mg of catalyst diluted with silicon carbide. The reaction temperature was 653 K at atmospheric pressure. The total feed flow was varied between 3.75 and 17.24 ml·min<sup>-1</sup>. The composition of the feed was 5% propane or propene, 10% oxygen and 65% nitrogen (controlled with Bronkhorst mass flow controller) and of 20% steam (controlled with a Bronkhorst liquid mass flow controller). A Wagner CEM system (controlled evaporator mixer) was used for evaporating and adding water. The four components were mixed and fed to the 1/4" stainless steel tube reactors using individually heated mass flow controllers for each reactor. The products were analyzed using two gas chromatographs (Shimadzu) equipped with TCD (columns: silica/molsieve) and FID (column: FFAP) detectors. At the beginning of the analysis, the silica and molsieve column were used in consecutive mode for the analysis of oxygen, nitrogen and carbon monoxide. For the analysis of carbon dioxide, propane, and propene, the molsieve column was bypassed and the separation was done on the silica column only. The silica and the molsieve columns were protected from organic acids by a pre-column (HayeSep Q) using a back flush configuration. Acetic acid and acrylic acid were separated on the FFAP column and analyzed by FID. The average carbon balance was 99.9% with a deviation of 1% between single measurements.

Reactions with intermediates including acetone, acetic acid, and acrylic acid were carried out on a single reactor. The organic component was mixed with water and evaporated. The feed compositions were: acetone (4%); acetic acid (4%) or acrylic acid (0.5%), oxygen (10%), steam (20%) and nitrogen as balance. The average carbon balance for acetone and acetic acid were 99% and for acrylic acid 90% with a deviation of 2% for a single measurement.

The rate of propane activation was described by a first order reaction with respect to the propane concentration  $c_{propane}$ <sup>[43]</sup> (Equation 4.1) with  $t$  being the contact time of the reactant over the catalyst.

$$dc_{propane} = -k_1 \cdot c_{propane} \cdot dt \quad (\text{Equation 4.1})$$

The contact time was calculated by the quotient of the catalyst weight [in g] and the feed flow [in ml/s] resulting in a unit for  $k$  of  $ml \cdot g^{-1} \cdot s^{-1}$ . Rate constants for reactions with acetone, acetic acid and acrylic acid were calculated analogously. For comparison between different

catalysts, the calculated rate constant  $k$  was normalized to the surface area and to the fraction of M1 phase present in the catalysts.

For propene, acrylic acid, acetone, acetic acid and carbon oxides analogous kinetic equations were used (Equation 4.2 – 4.6):

$$dc_{propene} = k_1 \cdot c_{propane} \cdot dt - (k_2 + k_3) \cdot c_{propene} \cdot dt \quad (\text{Equation 4.2})$$

$$dc_{acrylic\ acid} = k_2 \cdot c_{propene} \cdot dt - (k_4 + k_5) \cdot c_{acrylic\ acid} \cdot dt \quad (\text{Equation 4.3})$$

$$dc_{acetone} = k_3 \cdot c_{propene} \cdot dt - (k_6 + k_7) \cdot c_{acetone} \cdot dt \quad (\text{Equation 4.4})$$

$$dc_{acetic\ acid} = k_4 \cdot c_{acrylic\ acid} \cdot dt + k_6 \cdot c_{acetone} \cdot dt - k_8 \cdot c_{acetic\ acid} \cdot dt \quad (\text{Equation 4.5})$$

$$dc_{CO_x} = (k_4 + 3 \cdot k_5) \cdot c_{acrylic\ acid} \cdot dt + (k_6 + 3 \cdot k_7) \cdot c_{acetone} \cdot dt + 2 \cdot k_8 \cdot c_{acetic\ acid} \cdot dt \quad (\text{Equation 4.6})$$

### 4.3. Results

Based on X-ray diffraction, the catalysts 1 – 6 showed mainly diffraction peaks of the *M1* phase (Figure 4.2). In catalysts 7 the largest concentration of *M2* phase (~10 %) was present besides the *M1* phase. The fractions of *M1* and *M2* phases, determined by Rietveld analysis, are compiled in Table 4.2.

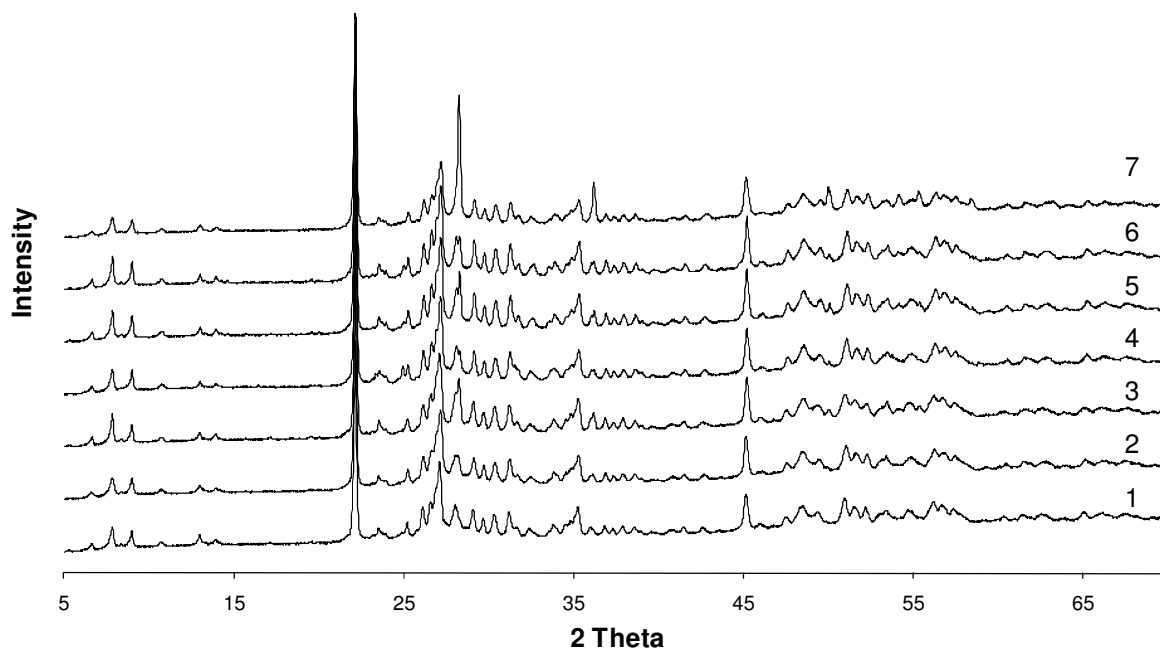


**Figure 4.2:** XRD from catalysts no. 1 – 7.

The chemical compositions of all samples are in good agreement with the composition used in the synthesis of the catalysts. The BET surface areas were between 6 and 18  $\text{m}^2\cdot\text{g}^{-1}$  and increased with the vanadium concentration of the samples.

The quantitative reaction network at 653 K of catalyst 7 was determined using each intermediate of the reaction network proposed by Lin et al. (see Fig. 4.1) <sup>[30]</sup> as feed molecule. The kinetics was modeled using first order rate equations for all reactants. The order was experimentally verified (reaction order with respect to propane was 0.88 and with respect to  $\text{O}_2$  0.06 ) and agrees well with results from literature.<sup>[43]</sup>

Starting with the reaction leading to  $\text{CO}_x$  formation, i.e., the oxidation of acetic and acrylic acid, and following the pathway towards the reactant (propane), the rate constants were derived for each step experimentally and calculated using the rates of the previously measured

reaction step for the further reactions of the intermediates formed. The rate constant for the conversion of acetic acid to  $\text{CO}_x$  was determined to be  $k_8 = 3.2 \text{ ml}\cdot\text{g}^{-1}\cdot\text{s}^{-1}$ .

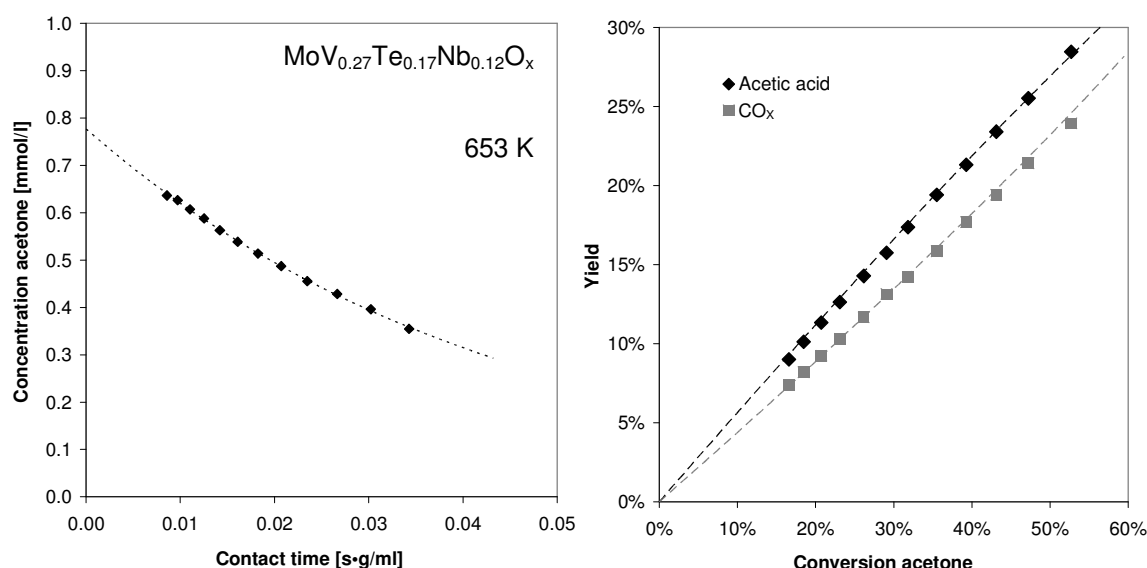


**Figure 4.3:** Concentration as function of contact time (left) and yield as function of conversion (right) of the acetone oxidation over  $\text{MoV}_{0.27}\text{Te}_{0.17}\text{Nb}_{0.12}\text{O}_x$ .

Following the same procedure the rate constants for the oxidation of acetone (Figure 4.3) to acetic acid ( $k_6 = 19.2 \text{ ml}\cdot\text{g}^{-1}\cdot\text{s}^{-1}$ ) and carbon oxides ( $k_8 = 3.6 \text{ ml}\cdot\text{g}^{-1}\cdot\text{s}^{-1}$ ) as well as for the oxidation of propene to acrylic acid ( $k_2 = 8.9 \text{ ml}\cdot\text{g}^{-1}\cdot\text{s}^{-1}$ ) and to acetone ( $k_3 = 2.2 \text{ ml}\cdot\text{g}^{-1}\cdot\text{s}^{-1}$ ) were derived. For the initial step, the oxidative dehydrogenation of propane to propene, a rate constant of  $k_1 = 0.57 \text{ ml}\cdot\text{g}^{-1}\cdot\text{s}^{-1}$  was obtained.

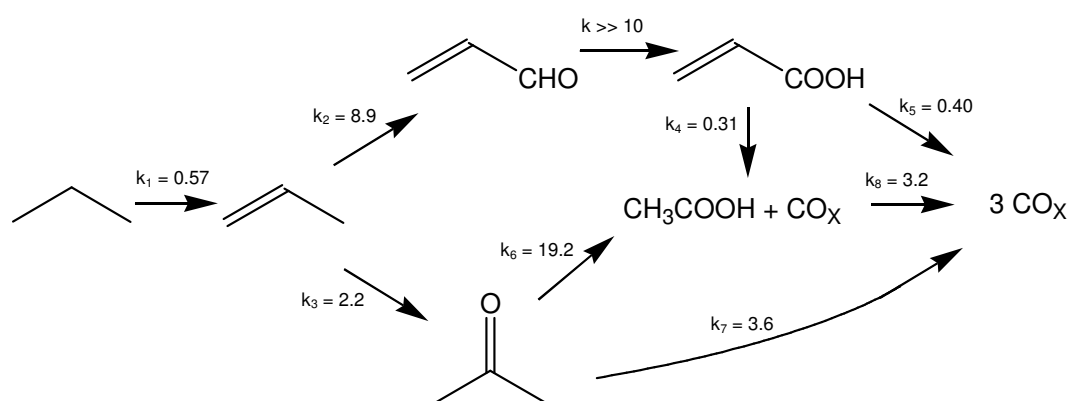


**Figure 4.4:** Reaction network and rate constants for  $\text{MoV}_{0.27}\text{Te}_{0.17}\text{Nb}_{0.12}\text{O}_x$  at 653 K derived from experiments with single reactants. (rate constants in  $\text{ml}\cdot\text{g}^{-1}\cdot\text{s}^{-1}$ ).

Using the rate constants derived from the individual reactions with propene and the reaction intermediates to calculate the kinetic network of parallel and consecutive reactions a fair

agreement between the calculated concentrations (solid lines Fig. 4.5 left) and the measured concentrations of reactor educts was reached. Using these values to start, a simultaneous fit of all rate constants was performed in order to better adapt the derived values to the experimentally determined concentrations. This resulted in a very good agreement of the experimental and fitted data points (Figure 4.5 right). While the number of constants to be fitted is large, the deviation from the rate constants determined experimentally with the individual reactants allows estimating the impact of the reaction conditions for the individual reaction steps in the sequential reaction. Table 4.3 compiles the comparison of rate constants from single experiments and from the fitting. The differences are attributed to the variations in the state of the surface between the situation of a single reactant and the complex reaction mixture as well as the simultaneous presence of a larger variety of molecules at once.

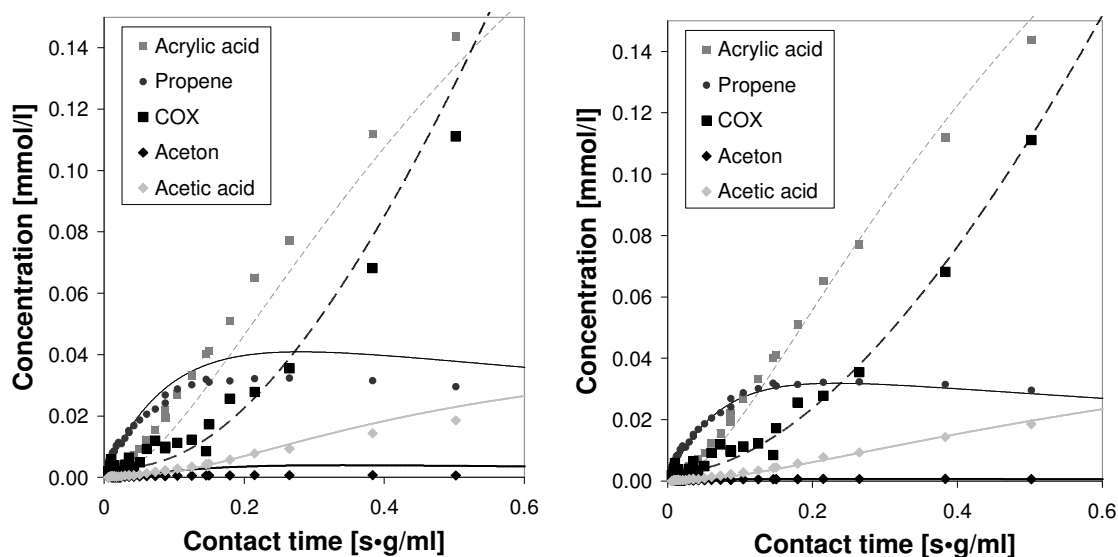


**Figure 4.5:** Concentration of products as function of contact time for propane oxidation over  $\text{MoV}_{0.27}\text{Te}_{0.17}\text{Nb}_{0.12}\text{O}_x$  (left: rate constants from single experiments; right: simultaneous fit).

**Table 4.3:** Comparison of rate constants from single experiments and simultaneous fit.

Rate constant	Rate constants single experiments [ml·g <sup>-1</sup> ·s <sup>-1</sup> ]	Rate constant simultaneous fit [ml·g <sup>-1</sup> ·s <sup>-1</sup> ]	Difference [%]
k <sub>1</sub>	0.57	0.56	-1.8
k <sub>2</sub>	8.9	12.6	+57.5
k <sub>3</sub>	2.2	1.9	-13.6
k <sub>4</sub>	0.31	0.41	+32.3
k <sub>5</sub>	0.40	0.25	-37.5
k <sub>6</sub>	19.2	57.5	+200
k <sub>7</sub>	3.6	23.6	+555
k <sub>8</sub>	3.2	3.00	-6.3

While the rate constant for the oxidative dehydrogenation of propane to propene was fairly constant in both approaches, the rate constant for the oxidation of propene to acrolein ( $k_2$ ) was markedly higher, whereas the rate constant for the parallel oxidation to acetone ( $k_3$ ) was lower. The reactions to acetic acid ( $k_4$  and  $k_6$ ) were much faster than observed in the individual reactions indicating that under the chosen reaction conditions the oxidative decarbonylation is a more substantial reaction than the full oxidation. Notably, however, also the total oxidation of acetone ( $k_7$ ) is enhanced suggesting that it is bound stronger than in the case of the reaction with the single components.

On the basis of the kinetic model presented, the maximum yield of acrylic acid and the main pathways for lowering the acrylic acid yield can be calculated. For the catalyst described the highest possible yield of acrylic acid is 26% at a conversion of propane of 63%. At this point yields are as follow: propene: 2%, acetic acid: 3%, CO<sub>x</sub>: 32%. From the yield data only, it is not possible to determine the loss by each pathway. Integral calculations, however, show that 11% of all molecules are converted along the propene – acetone – acetic acid - CO<sub>x</sub> reaction path and are, therefore, lost for acrylic acid formation. The same calculation indicates that 22% of all molecules converted to acrylic acid are further oxidized to carbon oxides.

The yields of propene and acrylic acid in the oxidation of propane at 653 K over MoVTeNbO<sub>x</sub>-M1 catalysts observed for the series of phase pure catalysts 1 – 6 are shown in Figure 4.6. Remarkably, the yields of propene show the same trend for all six catalysts, whereas the yields for acrylic acid differ significantly at high conversions.



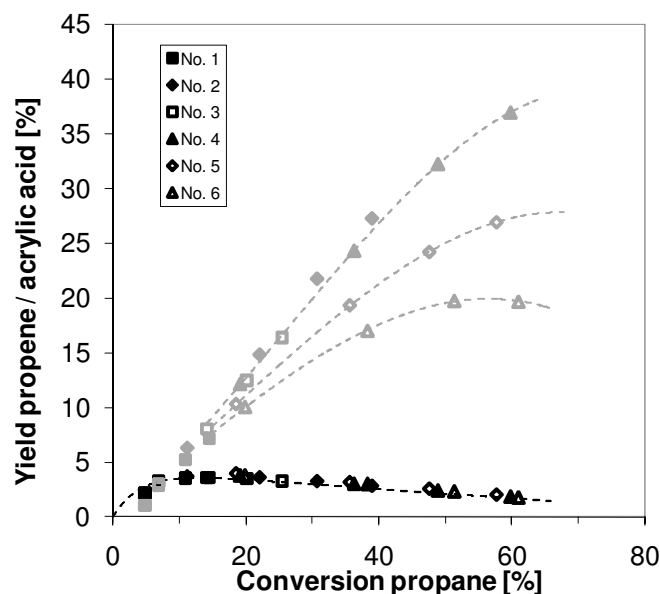


**Figure 4.6:** Propene (black) and acrylic acid yields (gray) of catalysts no. 1 – 6.

The initial rates of propane conversion (normalized to surface area and to the concentration of M1 phase present) as function of the vanadium fraction substituted for catalysts 1-6 are shown in Figure 4.7. Within each group, the activity appears to be a linear function of the vanadium concentration substituted for molybdenum, but none of the two functions passes through the origin.

These two subgroups of catalysts seem also to have distinctively different catalytic properties. The yields of acrylic acid at high conversions obtained for the first group of catalysts, i.e., catalysts 2 and 4, are much higher than those of the second group, i.e., 5 and 6. Note that for catalysts 1 and 3 the relative yield conversion curve cannot be assessed with certainty, because of the low activity of the material.

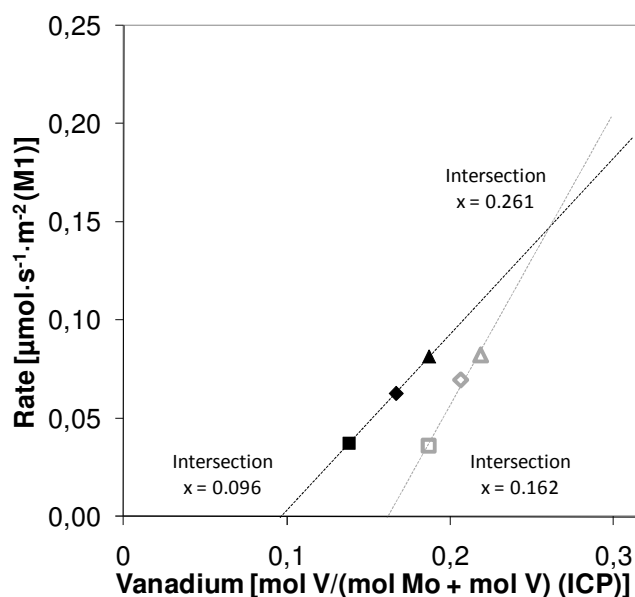


**Figure 4.7:** Initial rates of propane conversion normalized to surface area and fraction of M1 phase (same markers used as in Figure 4.3).

#### 4.4. Discussion

The catalytic conversion of propane to acrylic acid is one of the most complex reactions that are intended to be implemented on a large scale over one type of catalyst. Neither the type of active site nor the complete mechanism is currently unequivocally accepted despite 15 years of intense experimental and theoretical research. This is related to the complex nature of the catalysts, the not less complex transformations, these catalysts undergo when in operation and a network of parallel and sequential reaction that inevitably take place, which are markedly influenced by the local concentrations of reactants and products. This complexity in mind, we limit the present contribution to establishing a network of kinetic equations and to show how the concentration of vanadium substituted into positions of molybdenum in the lattice changes the activity and selectivity of the catalysts.

Let us first discuss the relative rates of the reaction steps in the overall sequence by exploring the intermediates in the overall network. Using propene, acetone, acrolein, and acrylic acid as the most abundant reactive intermediates, we have completed the reaction network of Lin et al.<sup>[30]</sup> by two additional pathways, i.e., the oxidation of acetone and the conversion of acrylic acid to acetic acid, which contribute markedly to the overall reaction. All reactions are first order with respect to the carbon species and zero order with respect to oxygen, which is typical for a Mars-van-Krevelen mechanism with a fast re-oxidation step of the surface.<sup>[44]</sup>

In agreement with the literature,<sup>[31]</sup> the oxidative dehydrogenation of propane is found to be the slowest step in the reaction path. The yield conversion plot shows that propene (see Fig. 4.5) is the only primary product, while the direct oxidation of propane to carbon oxides is hardly observed (< 1%). Surprisingly, the overall rate of the propene oxidation via the two parallel pathways to acrolein and subsequently acrylic acid and to acetone was approximately 19 times higher than the rate for propane conversion to propene, which is slightly lower than the value of 25 reported by us in ref.,<sup>[45]</sup> but the ratio increased to 26 for the simultaneous fit of all reactions. This constant ratio has two kinetic consequences, i.e., it indicates that that the two reaction channels complement and compensate each other and that also for the second step the adsorption of propene must be primarily controlled by dispersion forces and is hence independent of the nature of the specific surface.

The relative rates to acrolein and acetone depend upon the presence of Brønsted acid sites.<sup>[46]</sup> The importance of the latter pathway is proportional to the concentration of Brønsted acid

sites, which form a secondary propyl carbenium ion from propene. The ground state of this carbenium ion, the alkoxy group, is able to donate a proton to another oxygen atom, while maintaining and strengthening the C-O bond. The required ability to donate a proton (stabilization of at least the transition state to a carbenium ion) and the ability to accept the proton suggests that the reaction will occur with the highest rate on a material with modest Brønsted acid strength. Without being able to determine the concentration of Brønsted acid sites under reaction conditions, the selectivity to acrolein was higher for materials with lower concentrations of vanadium or with the vanadium being substituted more selectively into positions contributing to the alkane activation (see below).

Acetone formed, reacts with the by far highest rate to acetic acid and  $\text{CO}_x$ . It is speculated that this occurs by cleavage of the C-C bond and full oxidation of the surface methoxy group. This cleavage must be preceded by a strong interaction of the basic surface oxygen with the carbon atom of the carbonyl group generating a carboxylate precursor. Similar surface species have been spectroscopically observed in mixed oxides by IR spectroscopy.<sup>[47]</sup>

Acrolein was clearly identified as intermediate, but even at short contact times, it was not possible to achieve selectivities to acrolein higher than 17% and the rates and their variations will not be discussed in detail. Like acetone, acrylic acid reacted in parallel to acetic acid and  $\text{CO}_x$  with comparable rates. Materials that showed an enhanced conversion of propene to acetone also showed a higher rate from acrylic acid to acetic acid and to full oxidation, lowering so the overall achievable yield to acrylic acid.

The much higher stability of acrylic acid (and also of acetic acid) points to the pronounced surface cracking of acetone as one of the major reasons for its high reactivity. In contrast, the decarboxylation of the acid involves a more demanding oxygen insertion for further oxidation. It is interesting to note that deep oxidation to  $\text{CO}_x$  observed for acrylic acid and for acetone is associated with a higher polarity of the partly oxidized molecules, which enhances the interaction with mixed oxide surface. This stronger adsorption also increases the effective residence time in the reactor, enhancing in this way the probability to react. We would like to exclude “strongly adsorbing unselective sites” as the reason for total oxidation, because in such a scenario a pronounced concentration of such sites should also catalyze the total oxidation of propane and propene.

Because of its higher abundance, the sequential oxidation of acrylic acid to  $\text{CO}_x$  is twice as negative as the formation of acetone for the overall yield. For optimizing the catalyst, enhancing the rate of propane conversion to acrylic acid relative to the rate of the further conversion of acrylic acid has, therefore, a higher priority than decreasing the acetone formation rate. If propene oxidation and the further oxidation of acrylic acid are catalyzed by the same active site, an improvement of the catalytic properties is very challenging, while improvements are more feasible, if the reactions are catalyzed by different sites.

It is interesting to note, that the oxygen concentration does not influence the rate, as long as it does not fall below 1 vol.%. In this case the rate of re-oxidation becomes very low and the overall rate starts to depend on the oxygen concentration. Under such conditions also the formation of  $\text{CO}_x$  and acetic acid was enhanced indicating that accessible Lewis acid sites may be the reason for the enhanced adsorption of intermediates and total oxidation. It should also be noted that under these conditions the concentration of vanadyl groups will be lower than in the presence of a high partial pressure of oxygen. This should in turn decrease the oxidative dehydrogenation of propane to propene.

Overall, literature suggests that the presence of vanadium substituted for molybdenum in the mixed oxide is responsible for the activation of the alkane and for the oxygen insertion. A comparison of the catalytic activity for materials studied in the present paper shows that this is not the case despite the fact that all samples consisted predominantly of the M1 phase. Assuming that the materials contain a surface concentration of vanadium, which is similar to the concentration of bulk, we rule out that only one active site associated with vanadium exists. In the present case two groups of mixed oxides appear to be clustered, if the concentration of vanadium substituted into molybdenum sites of the M1 phase is used as a basis for comparing the overall activity (see Figure 4.7). For both groups of mixed oxides separate linear correlations between the overall rate of the catalytic conversion and the vanadium concentration were found. Both correlations do not pass through the origin indicating that not all vanadium is part of the catalytically active sites.

In order to better understand the possible nature of active and inactive sites containing vanadium let us consider the structure of the  $\text{MoVTeNbO}_x$ -M1 phase (see Figure 4.8), which consists of metal-oxygen octahedra linked via oxygen atoms. The octahedra marked in red contain in their center molybdenum in the oxidation state +VI and the orange octahedra molybdenum in the oxidation state +V. Each unit cell contains 36 octahedra out of which twelve contain molybdenum or vanadium in their center (indicated as white octahedra). These can be further grouped into four types characterized by their local surrounding. Note that only these octahedra are located between the 7 and 6 membered ring channels, while all other octahedra are part of at least one 5 membered ring channel.

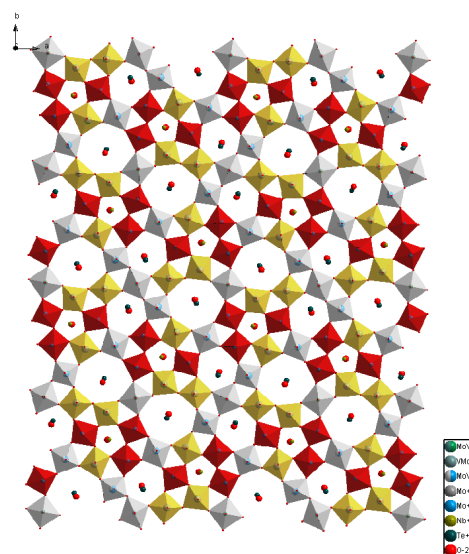


**Figure 4.8:** Structure of  $\text{MoVTeNbO}_x$ -M1 phase (red octahedra  $\text{Mo}^{+VI}$ , orange octahedra  $\text{Mo}^{+V}$  and white octahedra molybdenum or vanadium).

The four different molybdenum/vanadium centers are marked with circles in Figure 4.9. The sites marked with dashed circles (Type 1) are located between two six ring channels. Each unit cell contains two centers of this type. Those marked with a dotted line (Type 2) are located between six and seven ring channels and are in direct proximity to the vanadium centers of Type 1. Each unit cell contains four centers of this type. The centers marked with a triple line (Type 3) are also located between a six and a seven ring channel, but these are isolated from other vanadium centers. The vanadium centers marked with a full line (Type 4) are also isolated and located between two seven ring channels with two centers per unit cell.

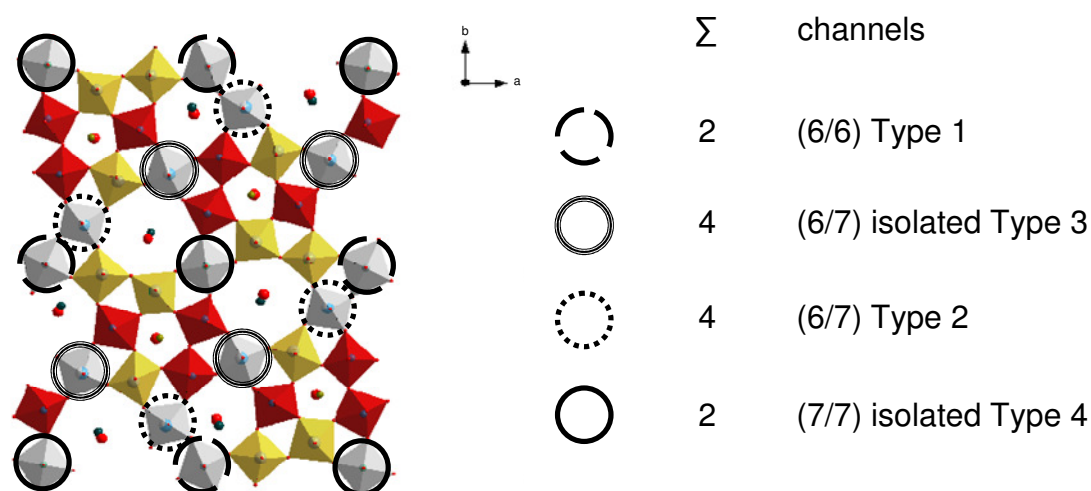


**Figure 4.9:** Number of vanadium centers in MoVTeNbO<sub>x</sub>-M1 phase.

Assuming that the activity of the vanadium sites depends on the surrounding structure, we speculate that each of these types of sites shows a different activity. Not all potentially exchangeable sites are occupied with vanadium at the ratio of vanadium to molybdenum between 0.16 - 0.28 (all sites would be occupied at a V/Mo ratio of 0.5). It is likely that the substitution energy for vanadium into these sites will vary leading to a preferential occupation with the different sizes of vanadium and molybdenum ions (Pauling radii are 59 pm vs. 62 pm) should have a significant effect on the substitution energy.

The surface and structural models of Grasselli et al. and Ueda et al. <sup>[34, 35]</sup> suggest that vanadium atoms located in octahedra adjacent to a seven-membered channel are active in propane activation. If the larger ring is more flexible, the larger metal cations (i.e., Mo) will be preferentially incorporated. Thus, we speculate that the structurally more confined Mo positions at the six ring channels having low (or no) catalytic activity will be substituted first by vanadium. This renders a substantial fraction of sites at low vanadium concentrations to be (nearly) inactive. In case of small differences in substitution energy at the different sites vanadium will be randomly distributed, which should lead to a linear correlation through the origin.

The data presented in Fig. 4.7 suggest that two groups of materials exist, which contain different fractions of vanadium in position leading to low catalytic activity. More specific, the offset at the x-axis at  $V/(Mo+V) = 0.096$  can be related to the incorporation of the first four

vanadium atoms per unit cell into sites having no activity for the propane activation (i.e., 4:36 = 0.111) followed by the occupation of active sites. For the other series of catalysts (trend line crossing the x-axis at  $V/(Mo+V) = 0.162 \approx 0.167 = 6:36$ ) six vanadium centers per unit cell showing no significant activity were occupied first. The two trend lines intersect at  $V/(Mo+V) = 0.261$ , which is close to  $0.278 = 10:36$ , indicating that two sites will not be occupied with vanadium. It should be noted that within the present accuracy an intersection at  $0.33 = 12:36$  can also be assumed, which can be related to the maximum concentration of vanadium in the *M1*-structure, i.e., a situation in which all potentially substitutable molybdenum sites are occupied by vanadium.

Combining the classification of vanadium sites on the basal plane of the *M1* phase with the attributions of active sites by Grasselli et al. and the probability to substitute molybdenum with vanadium, it appears tempting to suggest that first the sites of Type 1 and Type 2 are occupied first by vanadium. We would like to emphasize at this moment, however, that such an attribution would be premature.

It is interesting to note however, that the materials with the higher fraction of vanadium substituted into inactive sites show a higher tendency towards formation of acetone and acetic acid as well as towards full oxidation. As we have associated this with a higher degree of accessibility of metal cations, we would like to speculate that substitution into the inactive locations results also in a tendency to a lower oxidation state (partial reduction).

For a given vanadium concentration the constituents of group A (filled marks in Figure 4.7) show higher activities in propane oxidative dehydrogenation and selective oxidation than those of group B. Also the rates for oxygen insertion differ between group A and B type catalysts (for a comparison of the rate constants between group A and B see Table 4.4). The formation rate constant towards acetone was higher for group B type catalysts and increased within a group of catalysts with the concentration of vanadium. Similarly, the formation rate constant for acetic acid from acrylic acid (oxygen insertion at the acrylic acid double bond) with subsequent decarboxylation and the total oxidation to  $CO_x$  increased in that order.

**Table 4.4:** Comparison of rate constants from simultaneous fit for catalysts of group A and B.

	Catalyst Nr 4	Catalyst Nr 5	Catalyst Nr 6
Group	A	B	B
Theoretical yield [%]	38	26	20
Observed yield [%]	37	27	20
<b>Rate constants</b>			
<b>[ml·g<sup>-1</sup>·s<sup>-1</sup>]</b>			
k <sub>1</sub>	1.5	1.4	1.6
k <sub>2</sub>	29.5	26.6	28.4
k <sub>3</sub>	2.8	3.7	5.6
k <sub>4</sub>	0.5	1.4	2.3
k <sub>5</sub>	0.6	0.8	1.1
k <sub>6</sub>	~ 55	~ 55	~ 55
k <sub>7</sub>	~ 60	~ 60	~ 60
k <sub>8</sub>	~ 3	~ 3	~ 3

The model proposed here assumes that the mixed oxide crystal terminates with a well-defined crystalline surface. Such an assumption has been severely challenged by the results of electron microscopy as well as electron spectroscopy notably by Schlögl et al.<sup>[48]</sup> The authors present convincing evidence that an amorphous overlayer covers the crystalline phase, which has a distinctively different chemical composition than the bulk phase. It is important to note, however, that also in this case, the activities can be grouped into two clusters, which show a similar correlation with the vanadium concentration, as the materials discussed here. Further work is, however, needed to substantiate a correlation beyond this first attempt.



## 4.5. Conclusions

The analysis of the overall reaction network suggests that although the first C-H bond activation appears to be the most important effect determining the activity of the catalysts, subtle variations in the chemical composition and the location of the substitution of vanadium are able to exert an important influence on activity and selectivity. Two groups of mixed oxide catalysts have been identified that show two separate individual linear relations to the concentration of vanadium substituted for molybdenum. The grouping and the dependence on vanadium concentration in each group suggest that not only different substitution patterns for vanadium exist, but also that not all of these sites are catalytically active. We speculate that the preferential substitution and the inactivity of some substituted vanadium cations are related to their location at six membered rings on the basal plane of the M1 phase.

The constant ratio of propane oxidative dehydrogenation and the sum of the rates towards oxygenates suggest that not only propane, but also propene, adsorb mainly via dispersion forces. The selectivity to acrolein decreases from group A to B. The increased rates of acetone and acetic acid formation suggest a higher degree of accessibility of metal cations in the latter group of materials. These sites, not active in alkane activation, may contribute to oxygen insertion reactions and C-C bond cleavage.

The oxidation of acrylic acid to  $\text{CO}_x$  has been identified as the key factor limiting the yield of the selective oxidation of propane to acrylic acid. Approximately two-thirds of the losses in acrylic acid yields result from the oxidation and one third from acetone formation. The other possible side product, acetone, which subsequently oxidizes to acetic acid and finally to  $\text{CO}_x$  contributes only about one third towards lowering the yield of acrylic acid. This second pathway can be limited by the removal of all Brønsted acid sites in the catalysts.

As the current set of samples suggests that vanadium is first preferentially substituted into sites not active for the target reaction, statistical distributed of vanadium substitution is expected not only to lead to more active catalysts, but also to higher yields of acrylic acid.

#### **4.6. Acknowledgments**

The authors thank Daniela Hartmann for the Rietveld analysis of the catalysts and are grateful for the financial support from the European Union in the framework of the Integrated Project Topcombi (NMP2-CT-2005-515792-2) and from the from the Bayerisches Staatsministerium für Wissenschaft, Forschung und Kunst within the NanoCat project. Discussions within the network of excellence IDECAT are also gratefully acknowledged.

## 4.7. References

- [1] F. Cavani, F. Trifiro, *Catalysis Today* **1999**, 51, 561.
- [2] M. Baerns, O. Buyevskaya, *Catalysis Today* **1998**, 45, 13.
- [3] R. K. Grasselli, *Catalysis Today* **1999**, 49, 141.
- [4] J. M. L. Nieto, *Topics in Catalysis* **2006**, 41, 3.
- [5] T. Ushikubo, I. Sawaki, K. Oshima, K. Inumaru, S. Kobayakawa, K. Kiyono, US Patent 5,422,328, **1995**.
- [6] T. Ushikubo, K. Oshima, A. Kayo, T. Umezawa, K. Kiyono, I. Sawaki, EP Patent 529.853 A2, **1992**.
- [7] T. Ushikubo, H. Nakamura, Y. Koyasu, S. Wajiki, US Patent 5,380,933, **1995**.
- [8] T. Ushikubo, H. Nakamura, Y. Koyasu, S. Wajiki, EP Patent 608.838 A2, **1994**.
- [9] B. C. Zhu, H. B. Li, W. S. Yang, L. W. Lin, *Catalysis Today* **2004**, 93-95, 229.
- [10] B. Solsona, J. M. L. Nieto, J. M. Oliver, J. P. Gumbau, *Catalysis Today* **2004**, 91-92, 247.
- [11] P. Botella, E. Garcia-Gonzalez, J. M. L. Nieto, J. M. Gonzalez-Calbet, *Solid State Sciences* **2005**, 7, 507.
- [12] M. M. Lin, *Applied Catalysis A* **2003**, 250, 287.
- [13] H. Watanabe, Y. Koyasu, *Applied Catalysis A* **2000**, 194, 479.
- [14] P. Botella, B. Solsona, A. Martinez-Arias, J. M. L. Nieto, *Catalysis Letters* **2001**, 74, 149.
- [15] W. Ueda, D. Vitry, T. Katou, *Catalysis Today* **2005**, 99, 43.
- [16] M. M. Lin, *Applied Catalysis A* **2001**, 207, 1.
- [17] P. Botella, J. M. L. Nieto, B. Solsona, *Catalysis Letters* **2002**, 78, 383.
- [18] K. Oshihara, T. Hisano, W. Ueda, *Topics in Catalysis* **2001**, 15, 153.
- [19] M. Baca, J. M. M. Millet, *Applied Catalysis A* **2005**, 279, 67.
- [20] P. DeSanto, D. J. Buttrey, R. K. Grasselli, C. G. Lugmair, A. F. Volpe, B. H. Toby, T. Vogt, *Zeitschrift Für Kristallographie* **2004**, 219, 152.
- [21] P. DeSanto, D. J. Buttrey, R. K. Grasselli, C. G. Lugmair, A. F. Volpe, B. H. Toby, T. Vogt, *Topics in Catalysis* **2003**, 23, 23.
- [22] M. Baca, M. Aouine, J. L. Dubois, J. M. M. Millet, *Journal of Catalysis* **2005**, 233, 234.
- [23] R. K. Grasselli, J. D. Burrington, D. J. Buttrey, P. DeSanto, C. G. Lugmair, A. F. Volpe, T. Weingand, *Topics in Catalysis* **2003**, 23, 5.
- [24] F. Ivars, P. Botella, A. Dejoz, J. M. L. Nieto, P. Concepcion, M. I. Vazquez, *Topics in Catalysis* **2006**, 38, 59.
- [25] J. M. Oliver, J. M. L. Nieto, P. Botella, A. Mifsud, *Applied Catalysis A* **2004**, 257, 67.
- [26] G. Y. Popova, T. V. Andrushkevich, G. I. Aleshina, L. M. Plyasov, M. I. Khramov, *Applied Catalysis A* **2007**, 328, 195.
- [27] P. Botella, P. Concepcion, J. M. Lopez Nieto, Y. Moreno, *Catalysis Today* **2005**, 99, 51.
- [28] J. M. L. Nieto, P. Botella, B. Solsona, J. M. Oliver, *Catalysis Today* **2003**, 81, 87.
- [29] X. L. Tu, N. Furuta, Y. Sumida, M. Takahashi, H. Niiduma, *Catalysis Today* **2006**, 117, 259.
- [30] M. H. Lin, T. B. Desai, F. W. Kaiser, P. D. Klugherz, *Catalysis Today* **2000**, 61, 223.
- [31] E. Balcells, F. Borgmeier, I. Grisstede, H. G. Lintz, F. Rosowski, *Applied Catalysis A* **2004**, 266, 211.
- [32] E. Balcells, F. Borgmeier, I. Grisstede, H. G. Lintz, *Catalysis Letters* **2003**, 87, 195.

- [33] L. Luo, J. A. Labinger, M. E. Davis, *Journal of Catalysis* **2001**, 200, 222.
- [34] T. Katou, D. Vitry, W. Ueda, *Catalysis Today* **2004**, 91-92, 237.
- [35] R. K. Grasselli, D. J. Buttrey, J. D. Burrington, A. Andersson, J. Holmberg, W. Ueda, J. Kubo, C. G. Lugmair, A. F. Volpe, *Topics in Catalysis* **2006**, 38, 7.
- [36] M. D. Argyle, K. Chen, E. Iglesia, A. T. Bell, *Journal of Physical Chemistry B* **2005**, 109, 2414.
- [37] X. Rozanska, J. Sauer, *International Journal of Quantum Chemistry* **2008**, 108, 2223.
- [38] P. Concepcion, P. Botella, J. M. L. Nieto, *Applied Catalysis A* **2004**, 278, 45.
- [39] W. Ueda, D. Vitry, T. Katou, *Catalysis Today* **2004**, 96, 235.
- [40] M. Baca, A. Pigamo, J. L. Dubois, J. M. M. Millet, *Topics in Catalysis* **2003**, 23, 39.
- [41] P. Korovchenko, N. R. Shiju, A. K. Dozier, U. M. Graham, M. O. Guerrero-Perez, V. V. Gulians, *Topics In Catalysis* **2008**, 50, 43.
- [42] P. Botella, J. M. L. Nieto, B. Solsona, A. Mifsud, F. Marquez, *Journal of Catalysis* **2002**, 209, 445.
- [43] D. Vitry, Y. Morikawa, J. L. Dubois, W. Ueda, *Topics in Catalysis* **2003**, 23, 47.
- [44] J. L. Dubois, *Catalysis Today* **2005**, 99, 5.
- [45] F. N. Naraschewski, C. P. Kumar, A. Jentys, J. A. Lercher, *Applied Catalysis A*, doi:10.1016/j.apcata.2010.07.005.
- [46] A. Zecchina, C. Lamberti, S. Bordiga, *Catalysis Today* **1998**, 41, 169.
- [47] J. A. Lercher, *Z. Phys. Chemie NF* **129** **1982**, 209.
- [48] A. C. Sanfiz, T. W. Hansen, D. Teschner, P. Schnörch, F. Girgsdies, A. Trunschke, R. Schlögl, M. H. Looi, S. B. A. Hamid, *Journal of Physical Chemistry C* **2010**, 114, 1912.

# Chapter 5

## *Synthesis and Acid Properties of MoVSb and MoVTeNb Oxides for the selective Oxidation of Propane to Acrylic Acid*

### *Abstract*

The synthesis of MoVSb oxides with *M1* phase and mixture of *M1* and *M2* phase are described. Pure *M1* phase was obtained with hydrogen peroxide treatment after calcination. Results in selective oxidation of propane showed highest yield of acrylic acid for the pure *M1* phase catalysts. Reactions with propene were used to determine the ratio between acrylic acid and acetone formation. Mixtures of *M1* and *M2* phase form a higher fraction of acetone than the phase pure catalyst. TPD techniques were used to determine the amount of Brønsted and Lewis acid sites. All MoVSb oxides contain mainly Brønsted acid sites, but the amount of acid sites is lowest for the pure *M1* phase catalysts. As it is already reported in literature, Brønsted acid sites catalyze the formation of acetone. For comparison the acid sites of a MoVTeNbO<sub>x</sub> *M1*-phase catalyst were also determined, showing besides Brønsted acid sites a high amount of Lewis acid sites.

## 5.1. Introduction

The selective oxidation of alkanes to oxygenates has been a topic of high interest for the last decades, nevertheless only the oxidation of *n*-butane to maleic anhydride has been developed into an industrial process.<sup>[1-3]</sup> For the oxidation of propane to acrylic acid complex multi metal oxides are promising catalysts. Especially MoVTeNb oxides that were developed in the 90s by Mitsubishi showed yields up to 48%.<sup>[4]</sup> On the technical scale, however, acrylic acid is still produced in a two step process starting from propene with acrolein as intermediate using molybdenum based catalysts. For both steps the catalysts are optimized and yields exceed 90%, which lead to an overall yield of acrylic acid of 87% based on propene.<sup>[5, 6]</sup> Economical estimations reveal that the direct process starting from propane might become favorable in costs when the yield exceeds 60%.

For MoVTeNb oxides two phases containing all four metals are known, called *M1* and *M2*. The *M1* phase is an orthorhombic structure with periodic layers, consisting of metal-oxygen octahedrons with molybdenum and vanadium centers. These octahedrons form channels perpendicular to the *ab* plane of the unit cell. The smallest channels consist of five octahedrons and accommodate niobium, whereas the larger channels of six or seven octahedrons host tellurium. The *M2* phase is a hexagonal structure with periodic layers consisting also of metal-oxygen octahedrons, but forming only channels from six octahedrons.<sup>[7-11]</sup> It is generally accepted that the *M1* phase contains the active centers for alkane activation. The proposed centers for alkane activation are vanadium sites located adjacent to a seven octahedron ring. This structure leads to distortion of the octahedron causing the activity for alkane activation and due to the missing of such a structural element the *M2* phase shows no activity in alkane activation.<sup>[12, 13]</sup>

Beside compositions containing molybdenum, vanadium, tellurium and niobium, several other metal mixtures have been tested for selective oxidation reactions.<sup>[14-16]</sup> Multi metal oxides from molybdenum, vanadium and antimony showed high activity in the oxidative dehydrogenation which is the first and rate determining step in the selective oxidation of propane.<sup>[17]</sup> It was reported that in MoVSb oxides the same structures are existent as in MoVTeNb oxides. The MoVSbO<sub>x</sub>-*M1* structure is analogous to the MoVTeNbO<sub>x</sub>-*M1* structure with Tellurium replaced by Antimony. The stoichiometry is (SbO)<sub>2</sub>M<sub>20</sub>O<sub>56</sub> (M = Mo, V). Antimony with an oxidation state of +V forms infinite [Sb-O]<sub>∞</sub> chains in the

hexagonal channels. The Sb-*M2* phase is also analogous to the Te-*M2* phase, a hexagonal layer structure. Here Antimony is located inside the channel with an oxidation state of +III and forms [Sb-O-Sb] dimmers. The stoichiometries for this phase is  $(\text{Sb}_2\text{O})\text{M}_6\text{O}_{18}$ .<sup>[18]</sup>

The reaction network and intermediates of propane oxidation over MoVTeNb oxides is well described<sup>[19-21]</sup> and from products observed over MoVSbNb oxides it appears that the reaction proceed via the same pathway (Figure 5.1).<sup>[22]</sup>

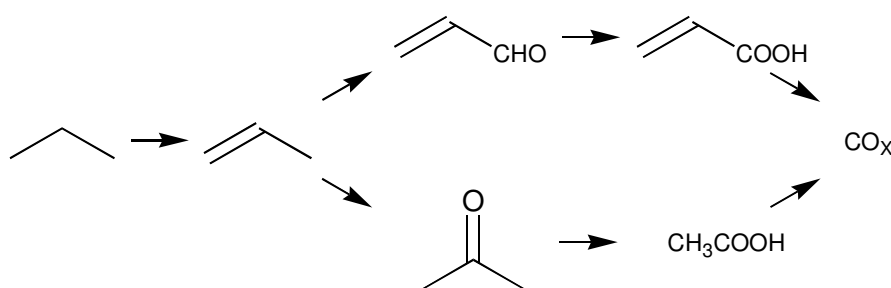


**Figure 5.1:** Reaction network of propane oxidation over MoVTe(Sb)Nb oxide catalysts.

The first step is the oxidative dehydrogenation of propane to propene, which can either be oxidized in ally position leading to acrolein or oxidized to acetone by oxo-insertion. Acetone is rapidly oxidized to acetic acid and carbon dioxide via C–C bond scission. Therefore, each molecule that undergoes the acetone pathway does not contribute to the yield of acrylic acid, because the C–C scission is irreversible. Oxo-insertion is catalyzed by Brønsted acid sites,<sup>[23]</sup> and it was reported several times that the yield of acrylic acid can be increased by potassium doping of MoVSb oxides,<sup>[24-26]</sup> which reduces the amount of Brønsted acid sites active for the oxo-insertion and acetone formation.

In this paper we present the preparation of MoVSbO<sub>x</sub> catalysts consisting of pure *M1* phase and *M1* / *M2* mixtures, followed by a correlation of the acid site concentration and type with the selectivity to acrylic acid in selective oxidation of propane. For comparison, acid site concentrations of MoVTeNb oxides were also determined.

## 5.2. Experimental

### 5.2.1. Catalyst preparation

Catalysts of the composition  $\text{MoV}_{0.26}\text{Sb}_{0.14}\text{O}_x$  were prepared by dissolving 9.28 g ammonium para molybdate in 30 ml ultra pure water at a temperature of 353 K in a Teflon tube. Antimony sulfate (1.06 g) was slowly added to the clear, colorless solution during a time period of 15 min. The color of the reaction mixture changed to dark green during this step. Stirring was continued for further 15 min. 3.46 g vanadyl sulfate hydrate was dissolved in 15 ml ultra pure water at 353 K and added to the reaction mixture within 20 minutes. During this step the mixture turned to black. After further stirring for 15 min the mixture was diluted with ultra pure water to 100 ml and the dissolved oxygen was removed by nitrogen flow through the solution for five minutes. The Teflon tube was closed and placed in a steel autoclave where the hydrothermal synthesis was carried out for 24 hour at a temperature of 448 K. After cooling, the black slurry was filtered, washed five times with water and dried at 353 K for 16 hours. The catalyst was calcined for 2 hours at 873 K in nitrogen.

To dissolve the *M2*-phase the catalysts were stirred in 15% hydrogen peroxide solution for four hours. This treatment was done before (named:  $\text{MoVSbO}_x\text{-H}_2\text{O}_2\text{-1}$ ) and after (named:  $\text{MoVSbO}_x\text{-H}_2\text{O}_2\text{-2}$ ) the calcination step.

$\text{MoVTeNbO}_x$  was prepared according to the following procedure. 8.74 g Ammonium para molybdate  $(\text{NH}_4)_6\text{Mo}_7\text{O}_{24} \cdot 4 \text{H}_2\text{O}$  was dissolved in 50 ml ultra pure water at 353 K in a Teflon tube followed by addition of 1.14 g telluric acid dissolved in water. 3.58 g Vanadyl sulfate  $\text{VOSO}_4 \cdot x \text{H}_2\text{O}$  was added as aqueous solution dropwise within 30 min, resulting in a black solution. 2.27 g Ammonium niobat oxalat  $(\text{NH}_4)\text{NbO}(\text{C}_2\text{O}_4)_2 \cdot x \text{H}_2\text{O}$  was added as solution and after 10 min further stirring the mixture turned olive green. Dissolved oxygen was removed by bubbling nitrogen through the mixture for 5 min. The tube was closed with a Teflon cap and mounted into a steel autoclave. Hydrothermal synthesis was done at 448 K for a duration of 48 hours. The autoclave was cooled with water to room temperature. The precipitate was filtered off, washed five times with water and dried 16 h at 353 K. The material was calcined 2 h at 523 K in static air and then 2 h at 873 K in nitrogen (heating rate 10 K/min).



## 5.2.2. Catalyst characterization

X-ray diffraction patterns were collected on a Philips X'pert instrument at the energy of the Cu  $K_{\alpha}$ -line. A Ni-filter was installed for removal of the Cu  $K_{\beta}$ -line. The XRD were measured between  $2\theta$  angles of 5 and 70 ° with a step size of 0.017 ° and a scan speed of 115 s per step. BET surface areas were determined by N<sub>2</sub> adsorption–desorption at 77 K using a Sorptomatic 1990 Series instrument after activation of the sample in vacuum at 523 K.

ICP-AES was measured with a Spectroflame Module after decomposition of the materials by heating with Soda – potash.

Ammonia-TPD was measured with a six-fold vacuum TPD system, with one hour activation at 573 K, one hour ammonia loading at 1 mbar and two hours outgasing. TPD was carried out with a heating rate of 7 K/min up to 873 K, using an mass spectrometer to detected the desorbing species. A H-MFI zeolite with an acid site concentration of 360  $\mu\text{mol/g}$  was used as standard. Brønsted acid sites were determined with TPD after ion exchange with ammonia nitrate (NH<sub>4</sub>NO<sub>3</sub>). Desorbed ammonia was detected with a mass spectrometer using M = 15.

The chemical compositions determined by ICP-AES, the specific surface areas and the yields from synthesis are presented in Table 5.1.

**Table 5.1:** Characterization data of MoV<sub>0.26</sub>Sb<sub>0.14</sub> oxide catalysts.

Catalyst	ICP-AES composition	BET surface area [m <sup>2</sup> /g]	Catalysts yield
MoV <sub>0.24</sub> Sb <sub>0.14</sub> O <sub>x</sub>	MoV <sub>0.27</sub> Sb <sub>0.06</sub> O <sub>x</sub>	8.7	87%
MoV <sub>0.24</sub> Sb <sub>0.14</sub> O <sub>x</sub> -H <sub>2</sub> O <sub>2</sub> _1	MoV <sub>0.27</sub> Sb <sub>0.06</sub> O <sub>x</sub>	14.0	54%
MoV <sub>0.24</sub> Sb <sub>0.14</sub> O <sub>x</sub> -H <sub>2</sub> O <sub>2</sub> _2	MoV <sub>0.26</sub> Sb <sub>0.03</sub> O <sub>x</sub>	19.0	39%
MoV <sub>0.3</sub> Te <sub>0.1</sub> Nb <sub>0.1</sub> O <sub>x</sub>	MoV <sub>0.26</sub> Te <sub>0.11</sub> Nb <sub>0.10</sub> O <sub>x</sub>	18.1	78%

### 5.2.3. Catalytic activity

Catalytic activity of the catalysts for propane and propene conversion was investigated in a six-fold-parallel reactor. The feed consisted of propane or propene (5%), oxygen (10%), nitrogen (65%) and steam (20%) and was controlled by Brookhorst mass flow controllers. The evaporation of water was done with a Wagner CEM system (controlled evaporator mixer). The four components were mixed and fed to the reactors using individual heated mass flow controllers for each reactor. The reactors were 1/4" stainless steel tubes. Products were analyzed using two gas chromatographs (Shimadzu) equipped with TCD (columns: silica/molsieve) and FID (column: FFAP) detectors. The average carbon balance was 99% with a deviation of 1% for a single measurement.

### 5.3. Results

XRD pattern of the  $\text{MoVSbO}_x$  samples are shown in Figure 5.2. The material synthesized without hydrogen peroxide treatment consists of a mixture of the *M1* and *M2* phase. Hydrogen peroxide treatment before calcination yields in a mixture of *M1* and *M2* phase with a lower amount of *M2* phase, clearly visible by the decrease of peak intensity at  $28^\circ$ . Only for the catalysts treated with  $\text{H}_2\text{O}_2$  after calcination ( $\text{MoVSbO}_x\text{-H}_2\text{O}_2\text{-2}$ ) pure *M1* phase was observed in the XRD.

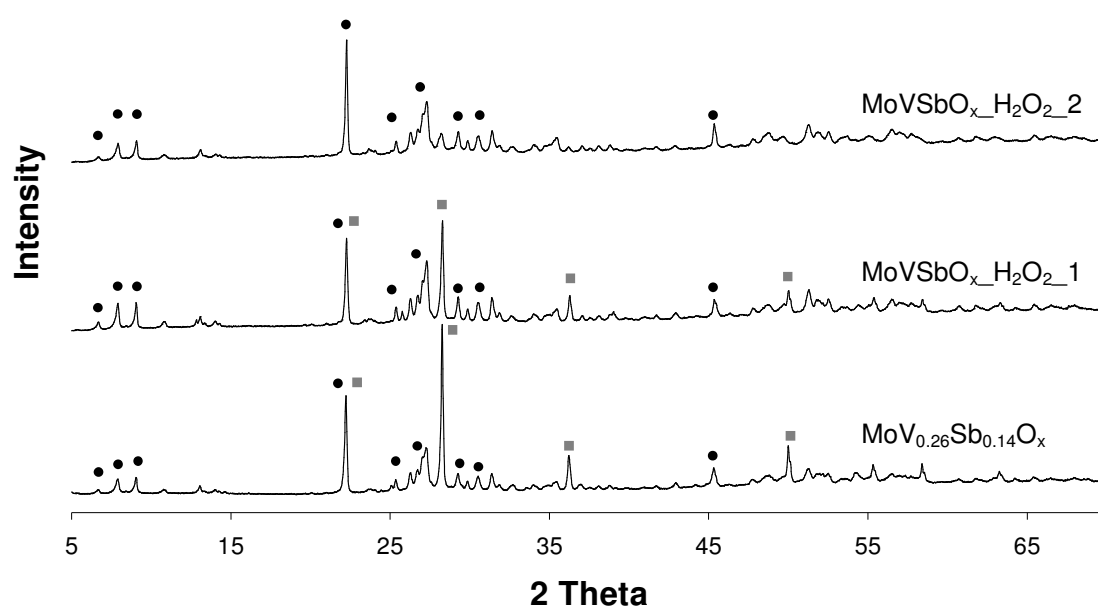


**Figure 5.2:** XRD of MoVSb oxide catalysts (M1: ●, M2: ■).

Temperature programmed desorption techniques were used for determination of acid site concentrations. While  $\text{NH}_3$ -TPD can be used to detect Brønsted and Lewis acid sites, a prior ion exchange with an ammonia salt ( $\text{NH}_4\text{NO}_3$ ) followed by a TPD without ammonia adsorption will only detect Brønsted acid sites. In Figure 5.3 is shown the recorded ion current of the mass spectrometer for both measurements with  $\text{MoVSbO}_x\text{-H}_2\text{O}_2\text{-1}$ . The results show nearly the same amount of acid sites after ion exchange with  $\text{NH}_4\text{NO}_3$  as with ammonia TPD, meaning that the majority of centers are Brønsted acid sites.

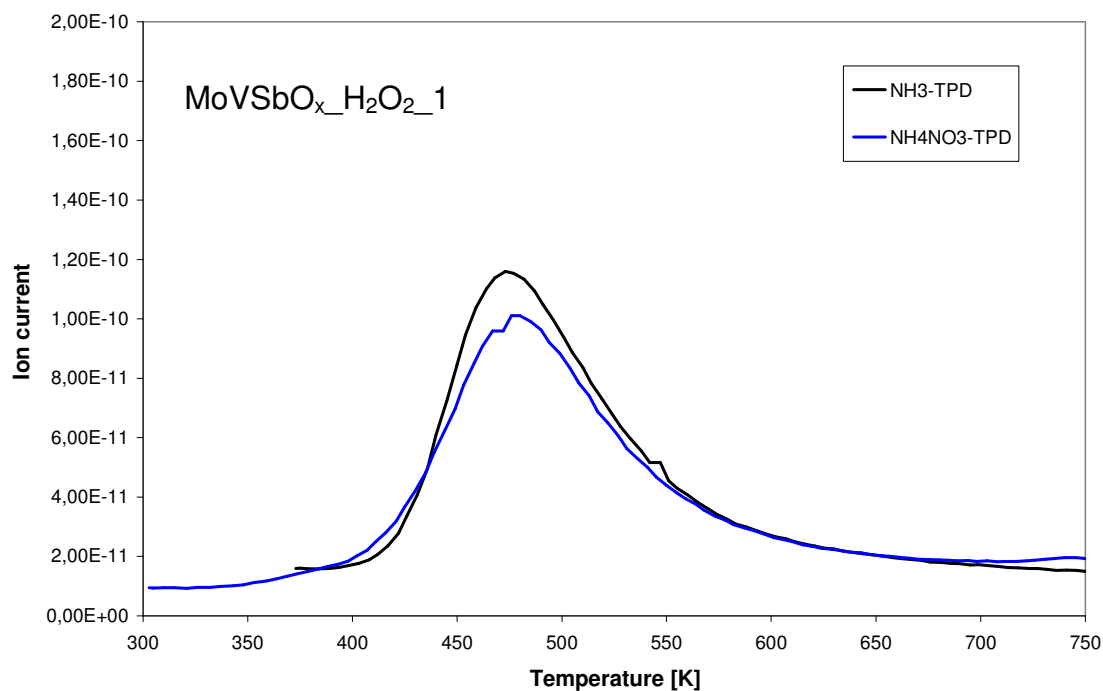


**Figure 5.3:** Results from TPD-Experiments for MoVSbO<sub>x</sub>-H<sub>2</sub>O<sub>2</sub>-1.

The concentrations of acid sites, measured by NH<sub>3</sub>-TPD (Brønsted + Lewis sites) are summarized in Table 5.2. Results from TPD after ion exchange are shown in Table 5.3 (only Brønsted sites). Calculation of Lewis acid sites from both TPD results are in Table 5.4.

**Table 5.2:** Results NH<sub>3</sub>-TPD measurements.

	Acid sites [ $\mu\text{mol/g}$ ]	Acid site concentration [ $\mu\text{mol/m}^2$ ]	Desorption peak maximum Temperature [K]
MoVSbO <sub>x</sub>	27.8	3.2	477
MoVSbO <sub>x</sub> -H <sub>2</sub> O <sub>2</sub> -1	45.4	3.2	473
MoVSbO <sub>x</sub> -H <sub>2</sub> O <sub>2</sub> -2	31.4	1.7	466
MoV <sub>0.3</sub> Te <sub>0.1</sub> Nb <sub>0.1</sub> O <sub>x</sub>	57.4	3.2	477

**Table 5.3:** Results TPD measurements with  $(\text{NH}_4)\text{NO}_3$  exchange (Bronstedt sites).

	Acid sites [ $\mu\text{mol/g}$ ]	Acid site concentration [ $\mu\text{mol/m}^2$ ]	Desorption peak maximum Temperature [K]
$\text{MoVSbO}_x$	25.5	2.9	484
$\text{MoVSbO}_x\text{-H}_2\text{O}_2\text{-1}$	41.4	3.0	478
$\text{MoVSbO}_x\text{-H}_2\text{O}_2\text{-2}$	22.0	1.2	467
$\text{MoV}_{0.3}\text{Te}_{0.1}\text{Nb}_{0.1}\text{O}_x$	24.2	1.3	478

**Table 5.4:** Calculated amount of Lewis acid sites.

	Acid sites [ $\mu\text{mol/g}$ ]	Acid site concentration [ $\mu\text{mol/m}^2$ ]
$\text{MoVSbO}_x$	2.4	0.3
$\text{MoVSbO}_x\text{-H}_2\text{O}_2\text{-1}$	4.0	0.3
$\text{MoVSbO}_x\text{-H}_2\text{O}_2\text{-2}$	9.4	0.5
$\text{MoV}_{0.3}\text{Te}_{0.1}\text{Nb}_{0.1}\text{O}_x$	33.2	1.8

For all MoVSb oxides mainly Bronstedt acid sites were observed. The total acid site concentration for mixtures of *M1* and *M2* phase is  $3.2 \mu\text{mol/m}^2$  for both catalysts, whereas for pure MoVSbO-*M1* phase only  $1.7 \mu\text{mol/m}^2$  is observed. For comparison, acid site concentrations of a *M1*-MoVTeNb oxide of the composition  $\text{MoV}_{0.3}\text{Te}_{0.1}\text{Nb}_{0.1}\text{O}_x$  were determined, showing  $3.2 \mu\text{mol/m}^2$  as total acid site concentration, but with a higher fraction (58%) of Lewis acid sites (Figure 5.4).

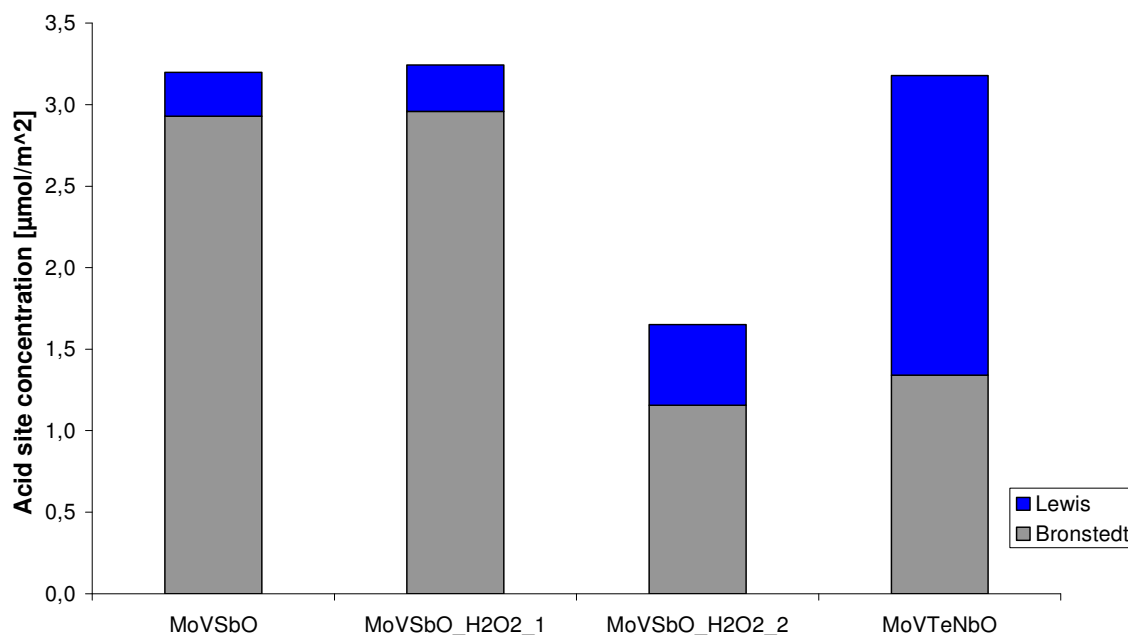


**Figure 5.4:** Acid site concentrations of MoVSbO<sub>x</sub> and MoVTenbO<sub>x</sub> by TPD techniques.

The product yields for the oxidation of propane are shown in Figure 5.5 a - d. No significant differences between propene yields were observed among the MoVSb and MoVTenb oxides, whereas the yields to acrylic acid, acetic acid and CO<sub>x</sub> depend on metal composition and on the catalysts phase composition for the MoVSb oxides. Both hydrogen peroxide treated catalysts showed higher yields to acrylic acid compared to the untreated catalyst and in particular, the pure MoVSb-*MI* catalyst showed the highest formation of acrylic acid among all MoVSb oxides. The yield to acrylic acid for MoVTenbO<sub>x</sub>-*MI* is much higher than for MoVSbO<sub>x</sub>-*MI*, but also at higher conversion. Therefore selectivities to acrylic acid of pure *MI* - MoVSb and MoVTenb oxides are comparable. For CO<sub>x</sub> and acetic acid, observed yields are lowest for the pure *MI*-MoVSbO<sub>x</sub> catalyst.

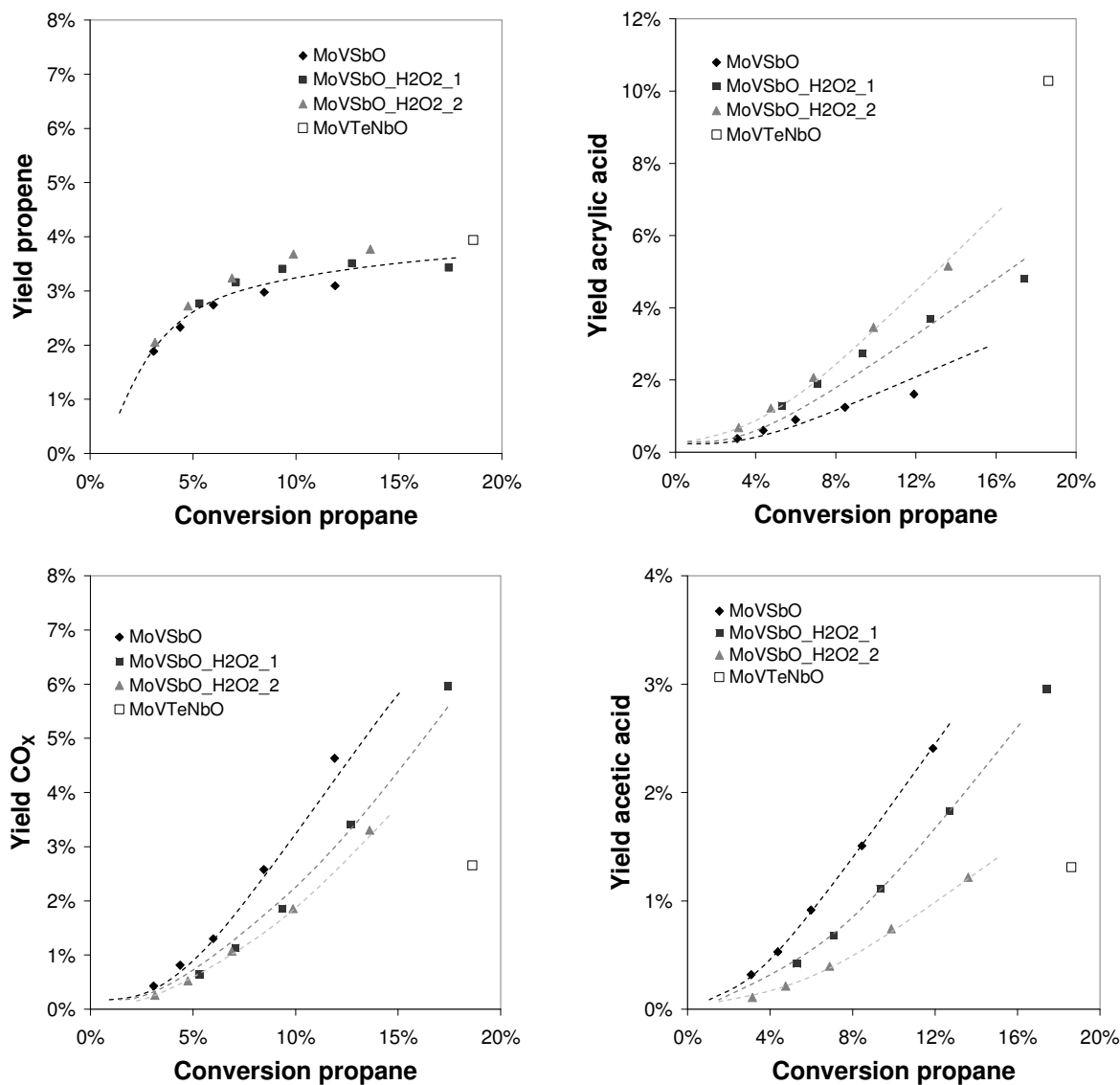
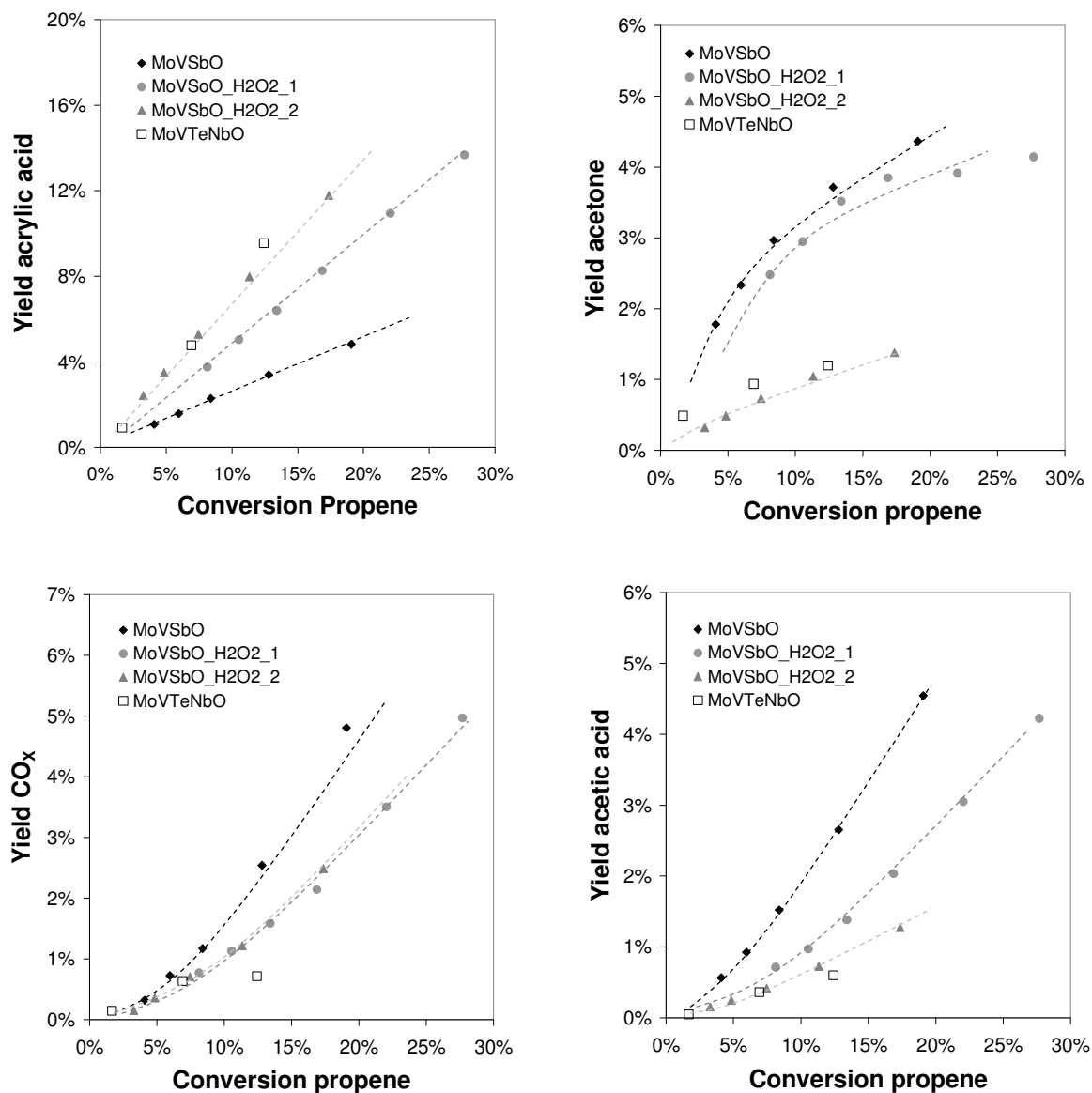


Figure 5.5 a-d: Product yields over MoVSb and MoVTeNb oxides in propane oxidation.

In agreement with the described reaction network propene is formed as a primary product, whereas acrylic acid, acetic acid and CO<sub>x</sub> are secondary products. To study the formation of these products in detail propene was used as reactant. Yields for propene oxidation are shown Figure 5.6 a - d. As expected acrylic acid and acetone are primary and acetic acid and carbon oxides are secondary products. For the pure *MI*-MoVSbO<sub>x</sub> (MoVSbO<sub>x</sub>\_H<sub>2</sub>O<sub>2</sub>\_2) and MoVTeNbO<sub>x</sub> selectivities of 70% acrylic acid were observed, whereas the untreated MoVSbO<sub>x</sub> catalyst shows only 25% selectivity to acrylic acid, but a higher selectivity to acetone.



**Figure 5.6 a-d:** Product yields over MoVSb and MoVTenb oxides in propene oxidation.

Between  $M1$ -MoVSbO<sub>x</sub> and  $M1$ -MoVTenbO<sub>x</sub> no significant differences in product yields of all intermediates were observed. Yield-Conversion-Plots are nearly identical, but the activity of MoVTenbO<sub>x</sub>- $M1$  is much higher. In contrast catalysts containing  $M2$ -MoVSbO<sub>x</sub> phase show higher selectivity to acetone and also to acetic acid, whereas the selectivity to acrylic acid is reduced.

The kinetics of the first three reactions in the network were fitted using first order kinetics (Equations 5.1 – 5.3). The contact times  $t$  were calculated using the quotient of catalyst mass [g] to feed flow in [ml · s<sup>-1</sup>]. Therefore the unit of the rate constant is [ml · g<sup>-1</sup> · s<sup>-1</sup>]. Acrolein



is neglected in this model because it is rapidly further oxidized and can only be observed in traces. The results of  $k_1$  show comparable values for all MoVSb oxides, whereas the activity of MoVTeNbO<sub>x</sub> is approximately three times higher (Table 5.5). For comparison of acrylic acid and acetone formation the dimensionless ratio of  $k_2/k_3$  is used. For MoVSbO<sub>x</sub> without H<sub>2</sub>O<sub>2</sub> treatment the ratio is 0.5, meaning that formation of acetone is twice as high as acrylic acid. For the catalysts with H<sub>2</sub>O<sub>2</sub> treatment the ratio increases up to 7.1 for the MoVSbO<sub>x</sub>-MI catalysts and is comparable to  $k_2/k_3 = 7.2$  observed for MoVTeNbO<sub>x</sub>.

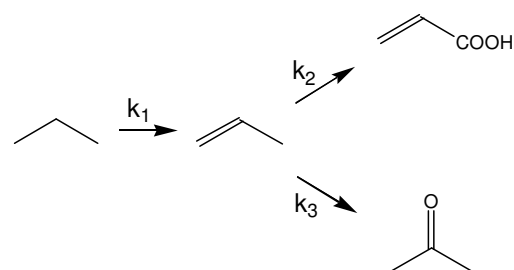
$$dc_{propane} = -k_1 \cdot c_{propane} \cdot dt \quad \text{Equation 5.1}$$

$$dc_{propene} = -(k_2 + k_3) \cdot c_{propene} \cdot dt \quad \text{Equation 5.2}$$

$$k_2 / k_3 = c_{acrylic\ acid} / c_{acetone} \quad \text{Equation 5.3}$$

**Table 5.5:** Rate constants for MoVSb and MoVTeNb oxide catalyst.

Catalysts	$k_1$	$k_2$	$k_3$	$k_2/k_3$
MoV <sub>0.26</sub> Sb <sub>0.14</sub>	0.44	4.5	8.2	0.5
MoV <sub>0.26</sub> Sb <sub>0.14</sub> _H <sub>2</sub> O <sub>2</sub> -1	0.37	5.0	4.5	1.1
MoV <sub>0.26</sub> Sb <sub>0.14</sub> _H <sub>2</sub> O <sub>2</sub> -2	0.36	7.1	1.0	7.1
MoVTeNbO	1.43	26.6	3.7	7.2



## 5.4. Discussion

As already reported in literature, the *M1* and *M2* phase of MoVTeNbO<sub>x</sub> can also be synthesized, with Antimony replacing Tellurium in the structure.<sup>[17]</sup> The synthesis of mixtures of *M1* and *M2* phase was successful with the described method, whereas the synthesis of phase pure *M1*-MoVSbO<sub>x</sub> was not possible, like it can be done for MoVTeNbO<sub>x</sub>. Phase pure *M1*-MoVSbO<sub>x</sub> can only be obtained by synthesis of a *M1/M2* phase mixture and removal of the *M2* phase by hydrogen peroxide treatment.<sup>[27]</sup> Hydrogen peroxide treatment after calcinations yields phase pure *M1*-MoVSbO<sub>x</sub>. The same treatment of the synthesis product followed by calcination at 873 K results in a *M1/M2* mixture, but with a decreased fraction of *M2* phase. This indicates that *M1* phase is partially transformed into *M2* phase during calcination and therefore, a phase pure catalyst can only be obtained by H<sub>2</sub>O<sub>2</sub> treatment after calcination.

Only the catalyst consisting of pure MoVSbO<sub>x</sub>-*M1* phase showed high selectivity to acrylic acid, whereas the presence of MoVSbO<sub>x</sub>-*M2* phase rapidly decreased selectivity. This behavior is different to catalysts of the composition MoVTeNbO<sub>x</sub>. In this system large *M2* fractions does not decrease the selectivity to acrylic acid and it was observed that mixtures of *M1* and *M2* phase resulted in higher selectivity than *M1* phase alone.<sup>[28]</sup> Two effects can decrease the yield of acrylic acid according to the reaction network (Figure 5.1): (1) Formation of acetone from propene instead acrolein/acrylic acid and (2) further oxidation of acrylic acid to carbon oxides.

Using propene as feed the ratio of acrolein/acrylic acid and acetone formation can directly be observed. The calculated rate constants and the ratio of acrylic acid to acetone formation are shown in Table 5.5. Acrolein is neglected in the fit of the reaction network, due to its high reactivity it will instantly be further oxidized and only traces can be observed. The rate constants were calculate assuming a first order reaction with respect to the carbon containing species as it is also reported in literature.<sup>[22]</sup>

Results with propene were used as feed confirmed the reaction network. Acrylic acid and acetone were formed as primary products for all catalysts, however, the initial selectivities (at 0% conversion) varied for the different H<sub>2</sub>O<sub>2</sub> treated catalysts. The reactivity in propane activation ( $k_1$ ) is similar for all three catalysts, but for the subsequent oxidation of propene

large differences were observed. The catalysts consisting of the MoVSbO<sub>x</sub>-*M1* phase only showed predominantly the formation of acrylic acid from propene and only small concentrations of acetone ( $k_2/k_3 = 7.1$ ), whereas for the H<sub>2</sub>O<sub>2</sub>-untreated catalyst containing MoVSbO<sub>x</sub>-*M1* and MoVSbO<sub>x</sub>-*M2* phase higher formation of acetone was observed ( $k_2/k_3 = 0.5$ ). The catalyst with the hydrogen peroxide treatment before calcination and therefore lower *M2* content shows a ratio of  $k_2/k_3 = 1.1$ . Therefore the effect of acetone formation in presence of *M2* phase is a continuous effect and higher contents of *M2* phase lead to higher selectivity of acetone.

Pure MoVSbO<sub>x</sub>-*M1* phase showed acrylic acid selectivity up to 35% and mixtures of *M1* and *M2* phase only 15%. Interestingly, mixtures of *M1* and *M2* phase of MoVTeNb oxides showed no significant effect on the selectivity on acrylic acid. In previous experiments phase mixtures of MoVTeNb oxides showed same selectivity and only activity of propane activation was reduced, due to the inability of the *M2* phase in propane activation.<sup>[29]</sup>

A significant difference between MoVSb and MoVTeNb oxides are the acidity and also the different types of acidity. The results from TPD experiments revealed that MoVSb oxides contain a high amount of Brønsted acid sites and hardly any Lewis acid sites. For the pure MoVSb-*M1* oxide the amount of Brønsted acid sites is decreased approximately by factor two in comparison to the mixture of *M1* and *M2* phase. In contrast, MoVTeNbO<sub>x</sub> contains a similar amount of Brønsted acid sites, but also a high amount of Lewis acid sites. A significant higher amount of acid sites is for MoVSbO<sub>x</sub> is already reported in literature,<sup>[30]</sup> but our results show that in MoVSbO<sub>x</sub> catalysts with *M2* phase Brønsted acid sites are the major fraction. Therefore we propose that the *M2* phase contains the major amount of Brønsted acid sites and is therefore selective for acetone formation.

Brønsted acid sites catalyze the oxo-insertion of propene to acetone.<sup>[23]</sup> Through hydrogen transfer a secondary carbenium ion is formed from propene, followed by an insertion of O<sup>2-</sup>, leading to acetone. As a result the antimony containing catalysts show higher selectivity to acetone. Treatment of MoVSb oxides with hydrogen peroxide dissolved the MoVSbO<sub>x</sub>-*M2* phase, thereby leading to lower amounts of Brønsted acid sites and improved catalytic performance. Therefore the MoVSbO<sub>x</sub>-*M2* phase is the major source of Brønsted acid sites.

MoVTeNbO<sub>x</sub>-*M1* phase showed a higher amount of Lewis acid sites and also a higher activity than MoVSbO<sub>x</sub> catalysts, but this is not proof that the activity is correlated to the amount of Lewis acid sites. If the amount of Lewis acid sites were be the key factor for propane activity, the activity of the MoVSbO<sub>x</sub> catalysts must be worse, in comparison to the observed results, due to their low amount of Lewis acid sites. Therefore it seems that Lewis acid sites are not involved in the C-H activation. This is also in line with DFT calculations of the C-H activation, showing vanadyl groups as the active center.

## 5.5. Conclusions

For MoVSb oxide phases with similar structure to *M1* and *M2* phases of MoVTeNb oxides can be synthesized, but pure *M1* phase for MoVSb oxides were only observed when the *M2* phase was dissolved in hydrogen peroxide as the last step of the synthesis. Calcination of a H<sub>2</sub>O<sub>2</sub> treated material lead to less *M2* phase than in the untreated material, but no phase purity was obtained. Therefore under calcination conditions (873 K in nitrogen) *M1* phase transforms partly to *M2* phase.

The catalysts consisting of pure *M1*-MoVSbO<sub>x</sub> phase showed up to 37% selectivity to acrylic acid, whereas for the mixture of *M1* and *M2* phase only 15% selectivity was observed. Detailed kinetics of the catalysts showed that the ability for propane activation is for all MoVSbO<sub>x</sub> catalysts similar, but the phase composition is important for the further oxidation of propene. Mixtures of *M1* and *M2* phase from preferentially acetone form propene, whereas for pure MoVSbO<sub>x</sub>-*M1* phase acrylic acid is the major product.

Reason for the changed selectivities are the acid sites of the material. MoVSb oxides mainly contain Brønsted acid sites that catalyze oxo-insertation to acetone, whereas the concentration of acid sites is lower for pure MoVSbO<sub>x</sub>-*M1* phase compared to the mixture of *M1* and *M2* phase. In comparison MoVTeNbO<sub>x</sub>-*M1* phase showed a Brønsted acid site concentration comparable to MoVSbO<sub>x</sub>-*M1* phase, but also a higher amount of Lewis acid sites, which have no function in the selective oxidation of propane.

## **5.6. Acknowledgements**

The authors thank Xaver Hecht and Florian Schuessler for the support with the BET and TPD measurements and are grateful for the financial support from the European Union in the framework of the Integrated Project Topcombi (NMP2-CT-2005-515792-2) and from the Bayerisches Staatsministerium für Wissenschaft, Forschung und Kunst within the Nanocat project. Discussions within the network of excellence IDECAT are also gratefully acknowledged.

## 5.7. References

- [1] F. Cavani, F. Trifiro, *Catalysis Today* **1999**, *51*, 561.
- [2] B. Grzybowska-Swierkosz, *Topics in Catalysis* **2000**, *11*, 23.
- [3] J. M. L. Nieto, *Topics in Catalysis* **2006**, *41*, 3.
- [4] T. Ushikubo, H. Nakamura, Y. Koyasu, S. Wajiki, US Patent 5,380,933, **1995**.
- [5] M. M. Lin, *Applied Catalysis A* **2001**, *207*, 1.
- [6] W. Nojiri, Y. Sakai, Y. Watanabe, *Catalysis Reviews Science and Engineering* **1995**, *37*, 145.
- [7] J. N. Al-Saeedi, V. K. Vasudevan, V. V. Guliants, *Catalysis Communications* **2003**, *4*, 537.
- [8] P. Botella, E. Garcia-Gonzalez, J. M. L. Nieto, J. M. Gonzalez-Calbet, *Solid State Sciences* **2005**, *7*, 507.
- [9] P. DeSanto, D. J. Buttrey, R. K. Grasselli, C. G. Lugmair, A. F. Volpe, B. H. Toby, T. Vogt, *Zeitschrift Für Kristallographie* **2004**, *219*, 152.
- [10] P. DeSanto, D. J. Buttrey, R. K. Grasselli, C. G. Lugmair, A. F. Volpe, B. H. Toby, T. Vogt, *Topics in Catalysis* **2003**, *23*, 23.
- [11] H. Murayama, D. Vitry, W. Ueda, G. Fuchs, M. Anne, J. L. Dubois, *Applied Catalysis A* **2007**, *318*, 137.
- [12] R. K. Grasselli, D. J. Buttrey, J. D. Burrington, A. Andersson, J. Holmberg, W. Ueda, J. Kubo, C. G. Lugmair, A. F. Volpe, *Topics in Catalysis* **2006**, *38*, 7.
- [13] T. Katou, D. Vitry, W. Ueda, *Catalysis Today* **2004**, *91-92*, 237.
- [14] S. Bergh, P. J. Cong, B. Ehnebuske, S. H. Guan, A. Hagemeyer, H. Lin, Y. M. Liu, C. G. Lugmair, H. W. Turner, A. F. Volpe, W. H. Weinberg, L. Woo, J. Zysk, *Topics in Catalysis* **2003**, *23*, 65.
- [15] V. H. Rane, U. Rodemerck, M. Baerns, *Journal of Molecular Catalysis A* **2006**, *245*, 161.
- [16] W. Ueda, K. Oshihara, *Applied Catalysis A* **2000**, *200*, 135.
- [17] W. Ueda, K. Oshihara, D. Vitry, T. Hisano, Y. Kayashima, *Catalysis Surveys from Japan* **2002**, *6*, 33.
- [18] J. M. M. Millet, M. Baca, A. Pigamo, D. Vitry, W. Ueda, J. L. Dubois, *Applied Catalysis A* **2003**, *244*, 359.
- [19] E. Balcells, F. Borgmeier, I. Grissted, H. G. Lintz, *Catalysis Letters* **2003**, *87*, 195.
- [20] E. Balcells, F. Borgmeier, I. Grissted, H. G. Lintz, F. Rosowski, *Applied Catalysis A* **2004**, *266*, 211.
- [21] M. H. Lin, T. B. Desai, F. W. Kaiser, P. D. Klugherz, *Catalysis Today* **2000**, *61*, 223.
- [22] E. K. Novakova, J. C. Vedrine, E. G. Derouane, *Journal of Catalysis* **2002**, *211*, 226.
- [23] M. M. Bettahar, G. Costentin, L. Savary, J. C. Lavalley, *Applied Catalysis A* **1996**, *145*, 1.
- [24] T. Blasco, P. Botella, P. Concepcion, J. M. L. Nieto, A. Martinez-Arias, C. Prieto, *Journal of Catalysis* **2004**, *228*, 362.
- [25] P. Botella, P. Concepcion, J. M. L. Nieto, B. Solsona, *Catalysis Letters* **2003**, *89*, 249.
- [26] W. Ueda, Y. Endo, N. Watanabe, *Topics in Catalysis* **2006**, *38*, 261.
- [27] M. Baca, J. M. M. Millet, *Applied Catalysis A* **2005**, *279*, 67.
- [28] M. Baca, M. Aouine, J. L. Dubois, J. M. M. Millet, *Journal of Catalysis* **2005**, *233*, 234.
- [29] F. N. Naraschewski, C. P. Kumar, A. Jentys, J. A. Lercher, *Applied Catalysis A* **2011**, *391*, 63.

- [30] M. Baca, A. Pigamo, J. L. Dubois, J. M. M. Millet, *Catalysis Communications* **2005**, *6*, 215.



# *Chapter 6*

## **Summary**

## 6.1. Summary

Selective oxidation of propane to acrylic acid is a promising route to convert an abundantly available feedstock within a single step into a highly demanded chemical. Multi mixed oxides of the composition  $\text{MoVTeNbO}_x$  have given up to 48% yield of acrylic acid in this reaction, but this is still not sufficient to be competitive with the conventional process of propene oxidation. For this reason there is great interest in understanding the processes and interactions within the catalytic reactions of the selective oxidation. This knowledge will help to synthesize improved catalysts that enable the use of propane as feedstock instead of propene.

The aim of this thesis was to gain detailed insights into the reaction processes and active center properties of mixed metal oxide catalysts for selective oxidation of propane. In the first chapter an introduction to acrylic acid production processes and selective oxidation over  $\text{MoVTeNbO}_x$  catalysts are given. Additionally, a review of C-H activation mechanisms over oxide catalysts presents details of various catalytic systems. The C-H activation of alkanes is the rate determining step in selective oxidation reactions and therefore of high importance for the design of highly active and selective catalysts. Experimental methods and synthesis procedures are described in detail in chapter 2.

In chapter 3, the phase formation and catalytic activity of  $\text{MoVTeNb}$  oxides with varying concentration of vanadium, tellurium and niobium in the synthesis mixture was investigated. Pure M1 phase catalysts were obtained with hydrothermal synthesis in the range of  $\text{MoV}_{0.14-0.22}\text{Te}_{0.1-0.2}\text{Nb}_{0.1-0.2}\text{O}_x$ . The materials were tested in selective oxidation of propane at 653 K in a plug flow reactor. Vanadium containing sites in the M1 phase are drastically more active for propane activation than in other materials studied. The catalytic activity is directly correlated to the fraction of vanadium in the overall material and in particular the M1 phase. High concentrations of tellurium induce the formation of the M2 phase, decreasing the overall activity of the catalysts. The intrinsic activity of the M1 phase is, however, independent of the tellurium concentration. Although the presence of the M1 phase is not a stringent requirement for the oxidative dehydrogenation of propane to propene, it is required to oxidize the intermediately formed propene with high selectivity to acrylic acid. The active sites for propane activation and propene oxidation are structurally coupled, because the ratio between

the rates of the two reactions was always 1 : 25. Oxygen defect sites in mixed oxides seem to enhance interaction with acrylic acid and lead to decarboxylation and total oxidation.

A detailed kinetic study on MoVTeNbO<sub>x</sub> M1-phase is described in chapter 4. The selective oxidation of propane to acrylic acid is studied over a series of nearly pure *M1*-phase MoVTeNbO<sub>x</sub> catalysts. Quantitative analysis of the reaction network shows that the ratio of the rate constants for propane oxidative dehydrogenation to propene and for further oxidation of propene is constant. The rates towards acrylic acid and acetone, however, vary subtly with the concentration of vanadium and the location of its substitution. The reaction of acrylic acid to acetic acid and carbon oxides, associated with accessible metal cations, contributes two thirds towards the non-selective pathway. The other third is associated with acetone formation. Vanadium is first substituted selectively at sites that are inactive for propane activation. Depending on the selectivity of this substitution two groups of materials have been identified, which show a distinctly different dependence on the concentration of vanadium. Statistic distribution of vanadium in the M1 phase appears to be the most promising strategy to improve the performance of MoVTeNbO<sub>x</sub> catalysts for a given vanadium concentration.

Catalysts of the type MoVSbO<sub>x</sub> and acid sites properties are discussed in chapter 5. Pure M1 phase of MoVSbO<sub>x</sub> was obtained by hydrogen peroxide treatment after calcination and showed higher yields of acrylic acid than mixtures of MoVSbO<sub>x</sub> *M1* / *M2* phase. Reactions with propene were used to determine the ratio between acrylic acid and acetone formation. Mixtures of *M1* and *M2* phase form more acetone than the phase pure catalyst. TPD techniques were used to determine the amount of Brønsted and Lewis acid sites. All MoVSb oxides contain mainly Brønsted acid sites, but the amount of acid sites is lowest for the pure *M1* phase catalysts, proving that acetone formation is catalyzed by Brønsted acid sites, as it is already reported in literature.

The presented results show that MoVTeNb and MoVSb oxides are interesting catalysts for the selective oxidation of propane to acrylic acid. The improved understanding of the kinetic network, the phase formation and metal distribution are important factors for new synthesis of high performance catalysts. Especially the distribution of vanadium seems to be one of the most important factors determining the achievable yield of acrylic acid. Further research in this area is needed to understand, how the vanadium distribution can be adjusted to control the

activity and selectivity of the material and finally to archive catalysts suitable for industrial usage.

## **6.2. Zusammenfassung**

Selektive Oxidation von Propan zu Acrylsäure ist ein vielversprechender Weg, um einen leicht verfügbaren Rohstoff in einem einzigen Prozessschritt zu einem dringend benötigten Zwischenprodukt der chemischen Industrie umzusetzen. Mischmetalloxide des Typs  $\text{MoVTaNbO}_x$  haben bereits bis zu 48% Ausbeute von Acrylsäure in dieser Reaktion gezeigt, jedoch ist diese Ausbeute noch nicht ausreichend, um den konventionellen zwei-stufigen Prozess der Propenoxidation, der aktuell in chemischen Industrie genutzt wird, zu ersetzen. Ein tiefgehendes Verständnis der Vorgänge am Katalysator ist daher von größtem Interesse, um mit diesem Wissen verbesserte Katalysatoren zu entwickeln und schließlich Propen durch Propan in der Acrylsäureproduktion ersetzen zu können.

Das Ziel dieser Arbeit war es, ein detailliertes Verständnis über die Vorgänge an der Katalysatoroberfläche und über die Natur der aktiven Zentren von Mischmetalloxiden für die Selektivoxidation von Propan zu erlangen. Das erste Kapitel gibt eine Einführung in die Verwendung und Produktion von Acrylsäure. Daneben wird eine Literaturübersicht über C-H Aktivierungsmechanismen verschiedener heterogener Katalysatoren gegeben. Die Aktivierung der C-H Bindung ist in Alkanen bei Selektivoxidationen der geschwindigkeitsbestimmende Schritt und daher von größter Bedeutung für die Entwicklung von aktiven und zugleich selektiven Katalysatoren. Genaue Beschreibungen der experimentellen Aufbauten und Synthesevorschriften sind in Kapitel 2 enthalten.

In Kapitel 3 wurde die Phasenbildung und katalytische Aktivität von MoVTeNb Oxiden mit variierendem Gehalt an Vanadium, Tellur und Niob untersucht. Reine *M1* Phase wurde mittels Hydrothermalsynthese innerhalb der Komposition  $\text{MoV}_{0.14-0.22}\text{Te}_{0.1-0.2}\text{Nb}_{0.1-0.2}\text{O}_x$  erzielt. Die Katalysatoren wurden in der Selektivoxidation von Propan bei 653 K im Festbettreaktor getestet. Vanadium ist in der *M1* Phase deutlich aktiver als in allen anderen untersuchten Materialien. Die katalytische Aktivität war dabei direkt abhängig vom Vanadiumgehalt. Hohe Konzentrationen an Tellur führten zur Bildung von *M2* Phase, wodurch die Gesamtaktivität der Katalysatoren verringert wurde. Die intrinsische Aktivität der *M1* Phase ist jedoch unabhängig vom Tellurgehalt. Obwohl die oxidative Dehydrierung von Propan auch ohne *M1* Phase beobachtet wird, ist diese zwingend erforderlich, um das Zwischenprodukt Propen mit großer Selektivität zu Acrylsäure umzusetzen. Weiterhin zeigte sich, dass die aktiven Zentren für die Propanaktivierung und die Propenoxidation strukturell gekoppelt sein müssen, da die Raten beider Reaktionen immer im festen Verhältnis 1 : 25 standen.

Eine detaillierte Kinetik an  $\text{MoVTeNbO}_x$  *M1*-Phase wird in Kapitel 4 vorgestellt. Die Selektivoxidation von Propan zu Acrylsäure wurde dafür mit phasenreinen *M1*- $\text{MoVTeNbO}_x$  untersucht. Die quantitative Analyse des Reaktionsnetzwerkes zeigte, dass das Verhältnis von Propanaktivierung zu Propenoxidation konstant ist. Die Weiteroxidation von Acrylsäure zu Essigsäure und  $\text{CO}_x$  ist verantwortlich für zwei Drittel der Nebenproduktbildung, während das letzte Drittel durch Acetonbildung aus Propene verursacht wird. Die Verringerung der Weiterreaktion von Acrylsäure ist daher ein wichtiger Ansatzpunkt für die Verbesserung der Katalysatorleistung. Bei der Verteilung des Vanadiums im Katalysator zeigt sich, dass zuerst die für Propanaktivierung inaktiven Zentren besetzt werden. Insgesamt wurden zwei verschiedenen Materialien identifiziert, die sich durch verschiedene Vanadiumverteilungen im Katalysator unterscheiden. Eine möglichst statistische Verteilung des Vanadiums scheint die beste Möglichkeit zu sein, die Aktivität der *M1*-Phase zu erhöhen.

Katalysatoren des Typs  $\text{MoVSbO}_x$  werden in Kapitel 5 diskutiert. Reine *M1* Phase von  $\text{MoVSbO}_x$  konnte nur durch eine Behandlung der Katalysatoren mit Wasserstoffperoxid nach dem Calcinieren gewonnen werden. Diese Katalysatoren zeigten deutlich größere Ausbeuten von Acrylsäure als Mischungen aus  $\text{MoVSbO}_x$  *M1* und *M2* Phase. Umsetzungen mit Propen wurden angewendet, um das Verhältnis zwischen Acrylsäure und Aceton Bildung direkt bestimmen zu können. Dabei zeigten *M1* / *M2* Mischungen eine deutlich höhere

Acetonbildung als die reine *MI* Phase. Die Anzahl Brønsted und Lewissäurezentren wurden mittels TPD Techniken bestimmen. Alle MoVSbO<sub>x</sub> Materialien besaßen vor allem Brønsted Säurezentren, wobei die Konzentration bei *MI*-MoVSbO<sub>x</sub> am niedrigsten war. Dies zeigt, dass Brønsted Säurezentren die Acetonbildung katalysieren, was zu einer Verringerung der Acrylsäureausbeute führt.

Die gezeigten Resultate belegen, dass MoVTeNb und MoVSb Oxide äußerst interessante Katalysatoren für die Selektivoxidation von Propan zu Acrylsäure sind. Das Verständnis der Kinetik, der Phasenbildung bei der Synthese und der Metallverteilung im Katalysator ist wichtig für die Synthese von verbesserten Materialien. Besonders die Vanadiumverteilung im Katalysator scheint ein entscheidender Faktor für die Aktivität und damit auch für die erzielbare Ausbeute an Acrylsäure zu sein. Weitere Forschung ist notwendig, um zu verstehen, wie die Vanadiumverteilung während der Synthese beeinflusst werden kann, um auf diese Weise die Aktivität und Selektivität der Materialien einstellen zu können und schließlich zu kommerziell nutzbaren Katalysator zu gelangen.

## *Curriculum vitae*

Frederik Nikolaus Naraschewski was born on August, 27<sup>th</sup> of 1979 in Wilhelmshaven, Germany. He attended the Gymnasium am Mühlenweg in Wilhelmshaven from 1992 to 1999, from which he graduated with the general qualification for university entrance (Abitur). After his military service in the German navy he started studying chemistry at the Technische Universität München in 2000. Additionally he began to study economics at the Fernuniversität in Hagen in 2003. During his studies he was working at Degussa AG in Shakopee, USA and Bain & Company Germany, Inc. in München, Germany.

He wrote his Diploma thesis at the chair of inorganic chemistry of Prof. Hermann in the group of Dr. Eppinger entitled „NMR-basierte Bestimmung von Enantiomerenüberschüssen in der asymmetrischen Katalyse am Beispiel von *NHC*-Komplexen“. After his graduation as „Diplom-Chemiker“ in 2005 he joined Prof. Lercher’s group (chair of technical chemistry II) at the Technische Universität München and started to work as a PhD student within the doctorate program „NanoCat: Nanodesign of High Performance Catalysts“ of the Elite Network of Bavaria. His work was focused on the selective oxidation of propane to acrylic acid over mixed metal oxides.

In 2008 he wrote his Diploma thesis in economics at the chair of Prof. Rödder with the title „IDA\* - Vorteile der iterativen Tiefensuche“ and graduated as „Diplom-Kaufmann“. In 2009 he started a position as “process unit engineer” at centrotherm SiTec GmbH in Burghausen.





## *List of Publications*

### *Refereed Journals / Book articles:*

1. D. Hartmann, F. N. Naraschewski, A. Jentys, J. A. Lercher; Synthesis and acid properties of MoVSb and MoVTeNb oxides for the selective oxidation of ethane and propane, in preparation.
2. F. N. Naraschewski, A. Jentys, J. A. Lercher; On the role of the vanadium distribution in MoVTeNbO<sub>x</sub> mixed oxides for the selective catalytic oxidation of propane, *Topics in Catalysis*, **2011**, DOI: 10.1007/s11244-011-9686-x.
3. J. A. Lercher, F. N. Naraschewski; C-H activation over solid oxide catalysts in *Nanostructured Catalysts: Selective Oxidation Reactions*, RSC Publishing, submitted.
4. F. N. Naraschewski, C. P. Kumar, A. Jentys, J. A. Lercher; Phase formation and selective oxidation of propane over MoVTeNbO<sub>x</sub> catalysts with varying compositions, *Applied Catalysis A*, **2011**, 391, 63-69.
5. T. Reiner, F. N. Naraschewski, J. Eppinger; <sup>31</sup>P NMR assays for rapid determination of enantiomeric excess in catalytic hydrosilylations and transfer hydrogenations, *Tetrahedron: Asymmetry*, **2009**, 20, 362-367.

---

## ***Presentations, Poster:***

1. F. N. Naraschewski, A. Jentys, J. A. Lercher; Factors limiting acrylic acid yield in the selective oxidation of propane over MoVTenb oxides (Talk), *42. Jahrestreffen Deutscher Katalytiker*, **2009**, Weimar, Germany.
2. F. N. Naraschewski, D. Hartmann, A. Jentys, J. A. Lercher; Catalytic properties and acid site concentration of MoVSb oxide catalysts (Poster), *42. Jahrestreffen Deutscher Katalytiker*, **2009**, Weimar, Germany.
3. F. N. Naraschewski, A. Jentys, J. A. Lercher; Influence of tellurium on the oxidation of propane to acrylic acid (Poster), *41. Jahrestreffen Deutscher Katalytiker*, **2008**, Weimar, Germany.
4. A. Jentys, F. N. Naraschewski, C. P. Kumar, J. A. Lercher; Direct oxidation routes from propane to acrylic acid (Talk), *1st International Symposium on Molecular Oxygen in Catalysis*, **2007**, Stuttgart, Germany.
5. F. N. Naraschewski, A. Jentys, C. P. Kumar, J. A. Lercher; Direct oxidation routes from propane to acrylic acid (Talk), *EuroCombiCat*, **2007**, Bari, Italy.
6. F. N. Naraschewski, C. P. Kumar, A. Jentys, J. A. Lercher; Direct routes from propane to acrylic acid (Poster), *40. Jahrestreffen Deutscher Katalytiker*, **2007**, Weimar, Germany.